Few-Cycle High-Repetition-Rate Optical Parametric Amplifiers And Their Synchronisation Schemes

von Diplom-Ingenieur Catherine Yuriko Teisset
aus Osaka, Japan

von der Fakultät V - Verkehrs- und Maschinensysteme
der Technischen Universität Berlin
zur Erlangung des akademischen Grades

Doktor der Ingenieurwissenschaften
- Dr.-Ing. -

genehmigte Dissertation

Berlin 2009

D83

Promotionsausschuss

Vorsitzender: Prof. Dr.-Ing. Henning Meyer (TU Berlin)
1. Gutachter: Prof. Dr. rer. nat. Heinz Lehr (TU Berlin)
2. Gutachter: Dr.-Ing. Alexander Binder (Ingenieurbüro Dr. Binder)

Tag der Eröffnung des Promotionsverfahrens: 16.10.2009
Tag der wissenschaftlichen Aussprache: 22.12.2009

Susanna:
Sotto i pini... del boschetto...

La Contessa:
Ei già il resto capirà.

Susanna:
Certo, certo il capirà.

Canzonetta sull'aria, Le nozze di Figaro.

Wolfgang Amadeus Mozart

Zusammenfassung

Hochenergetische ultrakurze Lichtpulse mit wenigen optischen Zyklen und vollständig kontrolliertem elektromagnetischen Feld sind Voraussetzung für die Erforschung von feldstärkeempfindlichen elektronischen Prozessen auf subatomarer Ebene. Insbesondere optische, parametrische Verstärker für gechirpte Pulse (OPCPA) haben sich als leistungsstarke Alternative zu herkömmlichen Titan:Saphir-Lasern erwiesen, um breitbandige Pulse mit wenigen optischen Zyklen und gleichzeitig hoher mittlerer Leistung zu generieren. Die entscheidenden Vorteile von OPCPAs sind neben der großen Verstärkungsbandbreite die geringe thermische Belastung der nichtlinearen Kristalle sowie die im Vergleich zu Lasermedien sehr hohe Verstärkung in einem Durchgang durch den Kristall.

Der Prozess der parametrischen Verstärkung in einem nichtlinearen optischen Kristall läuft ohne Zwischenspeicherung der Pumpenergie ab und benötigt, um Skalierbarkeit und praktische Anwendung einer OPCPA zu gewährleisten, hohe Anforderungen an die Synchronisation von Pump- und Seedpulsen. Parametrische Verstärker sind zur Zeit die einzige Methode, mit der hochenergetische, kohärente Lichtpulse weniger optischer Zyklen im vielfachen Milli-Joulebereich hergestellt werden können. Allerdings werden solche Systeme bisher nur im Bereich von wenigen Hertz Wiederholraten betrieben, da geeignete hochrepetitive Pumplaser bisher nicht existieren.

Diese Dissertation konzentriert sich auf die Entwicklung von robusten und leistungsstarken optischen parametrischen Verstärkern mit hohen Wiederholraten für die Erzeugung von Pulsen mit wenigen optischen Zyklen. Hierfür wurden im Rahmen dieser Arbeit zwei speziell für das Pumpen von parametrischen Verstärkern zugeschnittene effiziente Lasersysteme entwickelt mit Wiederholraten von 10 kHz und 10 MHz und Pulsenergien von 1.6 mJ beziehungsweise 6 µJ. Zusätzlich werden die in dieser Arbeit entwickelten Synchronisationstechniken zwischen der Femtosekundenseedquelle und den Pumplasern vorgestellt.

Abstract

High-energy few-cycle and carrier-envelope phase controlled laser sources are urgently required in many applications of high-intensity and laser field-sensitive physics. Optical parametric chirped pulse amplification (OPCPA) offers a particularly promising route toward compact ultrashort ultrahigh-peak-power laser systems because of its very broad gain bandwidth, negligible thermal load on the nonlinear crystal, and an extremely high single-pass gain as compared to amplifiers based on laser gain media. Due to the absence of energy storage in the nonlinear crystal, parametric amplification implies stringent requirements in terms of synchronisation between the pump and seed pulses which may hinders its scalability and its practical application. Synchronisation is thus of crucial importance for the generation of stable intense few-cycle pulses. Based on this technology terawatt-class multi-millijoule OPCPA systems were already reported at lower repetition-rates, typically of few Hz, due to power scaling issues of the pump source.

This thesis focuses on the realisation of robust high-power high-repetition-rate optical parametric chirped pulse amplifiers for the generation of few-cycle pulses. Within this work, two efficient picosecond pump sources were developed to amplify the output of a broadband seed oscillator. These laser sources operate at 10 kHz and approximately 10 MHz with pulse energies of 1.6 mJ and 6 µJ, respectively. In addition, two reliable and technologically attractive solutions for the synchronisation between a femtosecond seed oscillator and an external pump laser are presented. Broadband amplification of 7-fs pulses is demonstrated up to 700 nJ at MHz repetition rate. First compression experiments were undertaken with a pulse energy of 240 nJ and resulted in 10 fs pulses.

Contents

1 Introduction

Since the advent of the first ruby laser in 1960 [1], lasers have become a common tool for scientists and engineers for the study of natural phenomena and the development of new technologies. Owing to its unique characteristics (spatio-temporal coherence, brightness ...), lasers are routinely used in our daily life from optical telecommunication, material processing, surgery, data storage to detection. In particular the technology of ultrafast lasers has opened up new fields of investigation and application opportunities. Such lasers based on mode-locking techniques produce pulses with durations in the picosecond (1 ps=10^{-12} s) to the few-femtosecond (1 fs=10^{-15} s) range and are now commercially available with energies ranging from a few picojoule and to a few hundreds of nanojoule.

In an industrial context, femtosecond pulses are particularly attractive for their reduced thermal collateral damage through laser ablation. This permits high-quality machining of microstructures [2] and high-precision surgery with minimal invasive effects [3]. In fundamental research, ultrafast lasers can be implemented for the real-time observation of fast-evolving processes. In these experiments, the laser pulse performs as a "camera" with an extremely short exposure time by mapping the temporal evolution of the reaction. Using femtosecond lasers in pump-probe techniques, the intermediate states of a chemical reaction could be observed for the first time in 1987 [4]. The attribution in 1999 of the Nobel price to Prof. A. H. Zewail for his pioneer work in femtochemistry attests the relevance of this field of research [5].

Recent advances in the development of highly intense ultrashort laser sources have decreased the pulse duration close to its natural limit of one optical cycle of the electric field. For visible and near-infrared laser sources this corresponds to a minimum of approximately 2 fs, leaving sub-femtosecond time scale out of reach with conventional laser technology. Acceding to the attosecond regime (1 as=10^{-18} s) requires using much shorter optical cycles and hence shorter wavelengths. Through extreme nonlinear optical processes based on high harmonic generation, the optical spectrum of a high-energy ultrashort pulse can be shifted from the visible into the extreme ultraviolet. The resulting pulses, as short as 80 as [6], can be used as a probe for investigating ultrafast phenomena with an unprecedented time accuracy. While femtosecond lasers enabled the measurement of molecule dynamics, attosecond pulses allow for the first time direct exploration of electron dynamics.

1.1 Motivation for high-peak-power few-cycle pulses

Present-day ultrashort lasers are essentially based on Ti:Sapphire material for the very large gain bandwidth of its ions Ti^{3+} and the good thermal characteristics of the host [7]. Typically these lasers deliver output energies in the range of 5 nJ at a repetition rate of 80 MHz with a pulse duration of 6 fs. At a centre wavelength of 800 nm, this corresponds to approximately two optical cycles of the electric field.

Through the extreme temporal confinement of the light, optical peak power in the range of a megawatt can be obtained directly from such lasers of modest energy. Unfortunately, these peak powers are not sufficient for many high-field experiments which require electric field strengths comparable to that of the nuclear fields binding the electrons to the ionic core. Amplification schemes based on chirped pulse amplification (CPA) [8] and optical parametric amplification (OPA) [9] techniques were thus developed to perform energy-scaling of these ultrashort pulses.

With energetic pulses approaching two oscillations of the electric field, light-induced nonlinear effects in matter are temporally located around the peaks of the driving field. Indeed, in the presence of a few-cycle pulse, the electric field amplitude rather than the pulse envelope becomes the determining factor. Exploiting these circumscribed occurrences, few-cycle pulses can be employed to trigger more efficiently atomic processes in a controlled manner on a sub-femtosecond scale.

Such experiments need to be undertaken over multiple pulses to record the necessary data and achieve significant signal-to-noise ratio. Consequently, reproducible guiding of atomic processes demands that the electric field oscillation remains identical from shot to shot. Yet, due do environmental perturbations acting on the laser oscillator (temperature, air, vibrations ...), the phase of the electric field from successive pulses undergoes random fluctuations. This phase is usually referenced with respect to the the pulse envelope and is known as the carrier-envelope phase (CEP). The electrical fields of two pulses with identical pulse duration but with different carrier-envelope phases are shown in figure 1-1.

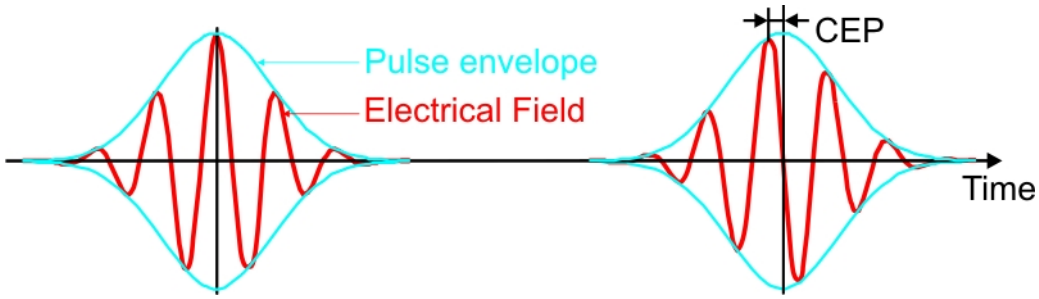

Figure 1-1 Pulse envelope and electrical field of two few-cycle pulses with an phase offset of $\frac{\pi}{2}$.

Thus controlling the carrier-envelope phase from shot to shot is a prerequisite for light-matter interactions featuring pulses approaching the single-cycle regime. With the introduction of phase stabilisation schemes [10, 11, 12], the synthesis of definite electric field waveform became possible. In particular the emerging field of attosecond science benefits from the development of CEP-stabilised pulsed source. Provided sufficiently short pulses ($\sim$5 fs), a single burst of high-energy photons may be emitted through high-harmonic generation when the peak of the oscillating electric field is made to coincide with that of the pulse envelope. This results in the generation of isolated attosecond pulses in the extreme ultraviolet as opposed to trains of attosecond pulses observed with longer driving pulses [13]. Based on these single attosecond signals, time-resolved spectroscopy and steering of electronic motions become possible with a never-before-achieved precision [14]. In conclusion, using high-peak-power CEP-stabilised few-

cycle pulses, attosecond science should allow for better understanding of natural processes in physics but also in biology and ultimately the development of new technologies. The bridge between attosecond science and technology could be realised by exploiting coherent X-rays pumped by intense few-cycle lasers for radiotherapy and diagnostics of cancer competing with synchrotron sources [15].

1.2 Comparison of pulse amplification techniques

Conventional amplification schemes based on chirped amplification were first established to overcome nonlinear effects and avoid the risk of optical damage with increasing pulse energy. In this approach, a temporally stretched pulse is amplified in a laser medium and subsequently compressed, as depicted in figure 1-2. Consequently, the peak power in the gain medium is reduced according to the stretching ratio of the pulse.

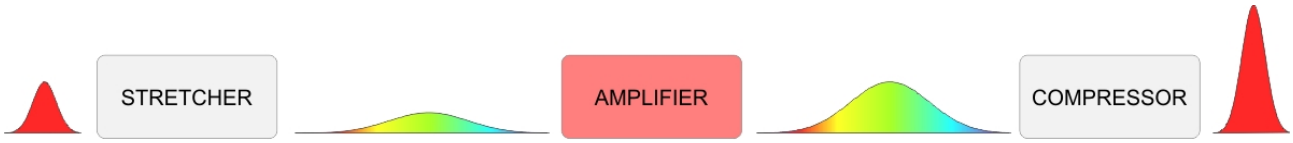

Figure 1-2 Principle of chirped pulse amplification.

Using CPA, petawatt (10^{15} W) level with 0.5-ps pulse duration could be reached for the first time in 1996 at the Lawrence Livermore National Laboratory [16]. Nonetheless, the finite gain bandwidth of the laser medium results in a narrowing of the amplified spectrum and ultimately sets a limit to the scaling of shorter pulses without additional gain narrowing compensating elements [17]. In order to obtain few-cycle pulses in CPA systems, post-amplification broadening techniques are commonly used. These techniques make use of self-phase modulation, commonly in noble gas-filled hollow-fibre or in bulk material, to generate new spectral components followed by pulse compression [18, 19, 20]. Often, these methods suffer usually from low throughput which make them less attractive for high-power systems.

While amplification in CPA systems relies on population inversion of a laser medium under excitation of a pump, parametric amplification originates from a three-wave mixing process inside a nonlinear crystal. Combined with the CPA approach, amplifiers based on parametric amplification should provide sufficient gain bandwidth for petawatt scale systems with sub-10-fs pulse duration [21]. This dual approach is known as optical parametric chirped pulse amplification (OPCPA).

The key to the success of the OPA technique is given by its large amplification bandwidth combined with extremely high single-pass gain even from few-millimetre-long nonlinear crystals. In contrast to CPA where the realisation of a population inversion leads to non radiative processes, there is no energy release in the crystal leading to negligible thermal effects. As a result, diffraction-limited beam quality is compatible with high pumping intensities enabling a straightforward scaling of the system. Finally, parametric amplification offers many degrees of

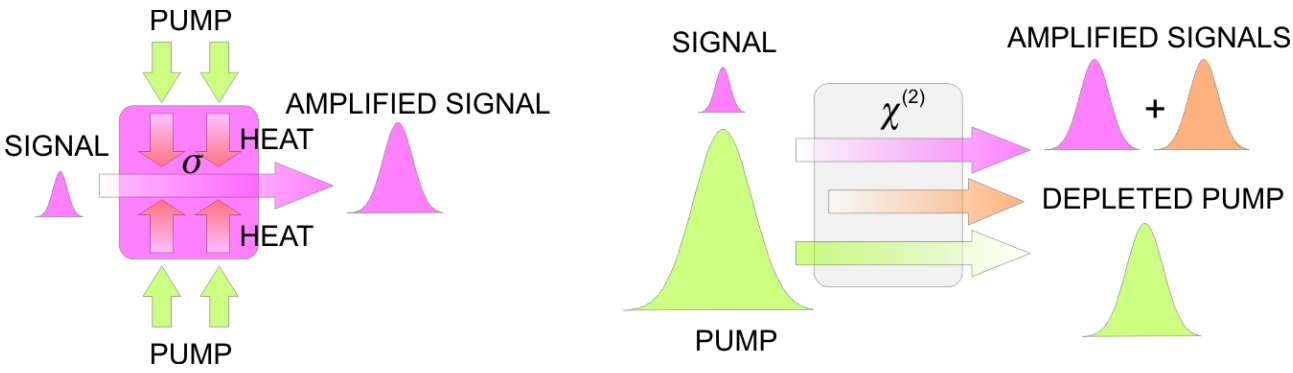

Figure 1-3 **Amplification based on laser material with transition cross section σ (left) and optical parametric amplification in a nonlinear material with second order susceptibility $\chi^{(2)}$ (right).**

freedom to obtain large amplification bandwidths such as the pump wavelength, the nonlinear crystal and the geometry of the nonlinear interaction. This allows for higher flexibility in the conception and optimisation of the amplifier design, as compared to CPA-based systems which are restricted to the laser amplifier medium. On the other hand, the absence of energy storage imposes temporal overlap of the pulses inside the crystal to ensure interaction between the pump and the signal pulses. Precise control over the pulse timing is hence required to achieve reasonable conversion efficiency. This issue clearly becomes especially severe with decreased pump pulse duration. Some of the main advantages and drawbacks of the two amplification approaches are summarised in table 1-1.

Amp. technique	CPA	OPA
Pulse duration (mJ level)	∼26 fs [22] ∼10 fs* [17]	∼8 fs [23]
Single-pass gain	∼10	up to 10^6
Amp. of pre-pulses	Yes	In the pump time-window
Background emission	Amp. spontaneous emission	Amp. superfluorescence
Thermal load	High	Negligible
Pump timing	Simple	Essential
Design flexibility	Fixed by the laser	Large

Table 1-1 **Comparison between CPA and OPA amplification schemes. *with gain shaping optical elements to compensate for the gain narrowing.**

It follows that the advantages of parametric amplification are primarily associated to the amplifier, whereas its drawbacks are related to the pump laser, for which the requirements are more severe than in the case of laser-medium based amplifiers.

1.3 Timing jitter

As mentioned earlier, a crucial point in OPAs is the timing between the pump and the seed laser pulses since amplification can only occur within the pump time window. In a pulsed laser, pulses are emitted essentially periodically. However, fluctuations of the pulse period are inevitable due to quantum noise, environmental perturbations and nonlinear processes. These

deviations of the pulse temporal localisation from an ideal periodic pulse train are known as timing jitter.

In the case of a parametric amplifier driven by an independent pump, the two interacting laser sources are subject to different vibrations and drifts of their resonator. These effects are translated into fluctuations of the laser repetition rates causing variations of the pulse arrival time on the OPA. Particularly, thermalisation of the laser optical components leads to a drift of the resonator length. Figure 1-4 illustrates the offset between two laser pulse trains in the presence of different resonator drifts.

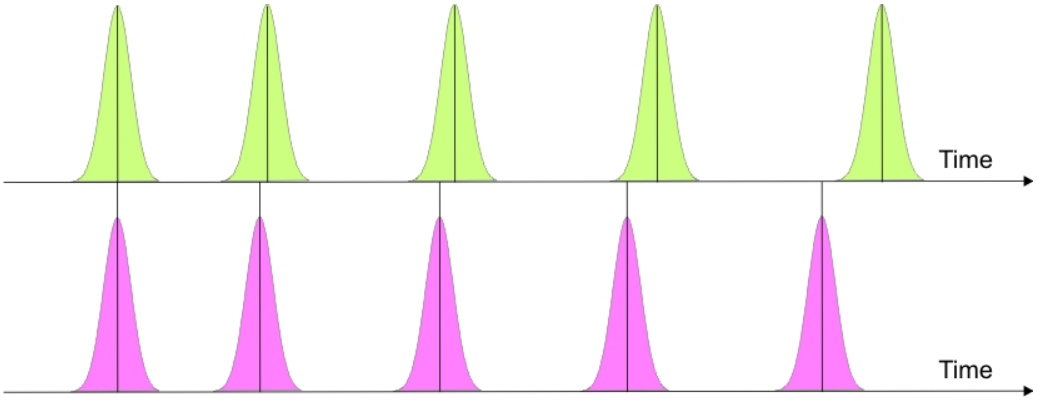

Figure 1-4 Drift of the pulse temporal positions for two lasers.

In order to make the pulses repetitively coincide on the nonlinear crystal, control of the pulse timing is essential. Synchronisation techniques define the different procedures used to coordinate the emitted pulse trains of different sources. The residual timing jitter will notably determine the performances of a parametric amplifier in terms of efficiency and stability. Indeed variations of the pump-seed temporal overlap cause a degradation of the amplified signal characteristics such as pulse energy and spectrum. For reliable parametric amplification, a timing jitter below a tenth of the pump pulse width is commonly required. Obviously, difficulties will increase with shorter pulse durations.

In OPCPA systems, active synchronisations are employed in the presence of independent lasers to discipline the repetition rate of one laser to the another one, or by locking both lasers to an external reference, usually a microwave source [24, 25]. Passive synchronisations rely on self-stabilisation mechanisms of the laser repetition rates [26] or an amplifier scheme where the pump and seed lasers are derived from a single source [27]. In this latter case, strict synchronisation is nevertheless not automatically guaranteed as the two interacting pulses do not usually follow the same optical path, resulting in the introduction of an additional source of timing jitter.

1.4 High-repetition-rate

Optical parametric chirped pulse amplification has proven to be a powerful alternative to conventional laser-amplification technologies for energy scaling of few-cycle pulses. Yet, optical

parametric amplifiers have been essentially demonstrated at low repetition rates or at low output energies as thermal management becomes more critical with increasing pump average power [28, 29, 30]. This is particularly true for Ti:Sapphire-based pump sources, where higher peak powers are usually reached at the cost of the pulse repetition rate. Only recently, the availability of robust high average power pump sources have opened the way towards multi-kHz and MHz high-energy parametric amplifiers [31, 32, 33, 34].

Because many interesting light-matter interactions are governed by low probabilities or low efficiency, characterisation of these processes requires repeating the measurement over a high number of laser shots. As a result, extensive recording times are necessary in order to achieve good signal statistics. Such measurements need to be commonly taken over several hours involving over millions of shots [13, 35] and conventionally using Ti:Sapphire CPA systems. Another problem rises from the extreme sensitivity of nonlinear processes to fluctuations of the optical intensity and in some cases even to the electrical field. External perturbations such as air turbulence, temperature, mechanical vibrations, electric noise may in return cause fluctuations in pulse energy, carrier-envelope phase, timing jitter, wave front or beam pointing. Hence, operating at low repetition rates sets accordingly severe criteria on the long-term and shot-to-shot stability of the laser source for the acquisition of relevant and accurate data. Increasing the repetition rate would permit to take faster measurements with an improved signal-to-noise ratio and open new fields of investigation of ultrafast phenomena.

1.5 Thesis outline

In this thesis, two approaches will be addressed for the amplification at 10-kHz and 10-MHz repetition rate of few-cycle pulses from a broadband seed. Both schemes rely on narrow-band synchronised pump sources optimised for the generation of high-energy pulses. The kHz-pump is based on a millijoule amplifier, while the MHz-pump consists of a high-energy oscillator delivering multi-microjoule output pulse energies.

In the second chapter of this thesis, the concept and realisation of optical parametric chirped pulse amplifiers are described. In the first section, the principles and challenges of broadband parametric amplification are reviewed. The dispersion management and characterisation of ultrashort pulses are introduced. Finally different approaches for the generation of high-energy pump pulses and solutions for the synchronisation between a femtosecond seed oscillator and an external pump laser are presented.

In chapter 3, an optical parametric chirped pulse amplifier system operating at kHz repetition rate is presented based on a Ti:Sapphire seed oscillator and an amplifier-type Nd^{3+}-pump. The two lasers are locked to each other using a passive all-optical synchronisation scheme with a timing jitter estimated to be below 30 fs. These results led to a publication in Optics Express [36].

The realisation of a 10-MHz optical parametric chirped pulse amplifier scheme is described in

chapters 4, 5 and 6. This work includes the development of a MHz high-energy pump source based on a thin-disk mode-locked oscillator (chapter 4), the design of an active synchronisation with an electronic-optical control loop (chapter 5), and the amplification-compression of ultrashort pulses (chapter 6). Part of this work was described in references [37, 97]. Using a high-energy Yb:YAG oscillator, few-nanojoule pulses delivered by a Ti:Sapphire oscillator are amplified in a single-stage optical parametric amplifier. The Yb:YAG laser delivers up to 6-µJ pulses at 11.5 MHz with a duration of 1 ps. After frequency doubling, up to 3.8-µJ pulses are generated at 515 nm for pumping a non-collinear optical parametric amplifier. After synchronisation of the two laser sources, a residual timing jitter of approximately 100 fs is measured. In a single-stage parametric amplifier, amplification of the broadband Ti:Sapphire seed is demonstrated up to 700 nJ. The amplified spectrum still supports pulse durations below 7 fs. First compression experiments are undertaken with 250-nJ pulses and result in 10-fs pulses.

2 Femtosecond optical parametric amplifiers

2.1 Phase-matching condition

Parametric amplification is a nonlinear optical phenomenon resulting from a three-wave mixing process in a nonlinear medium, where an initial high-energy photon splits into two photons of lower energies. In this instantaneous interaction, the generated photon frequencies are set by the energy conservation condition. For a pump wave of angular frequency ω_p, this implies

$$\omega_p = \omega_s + \omega_i, \tag{2-1}$$

where ω_s and ω_i are the signal and idler wave angular frequencies, respectively. The suffix p denotes the pump, while s and i refer to the signal and idler. Thus amplification of a low energy signal can be obtained through an energy transfer from an energetic pump source to the signal and its resulting idler. Ideally their corresponding wave-vectors $\mathbf{k_p}$, $\mathbf{k_s}$ and $\mathbf{k_i}$ should fulfil the phase matching condition:

$$\mathbf{k_p} = \mathbf{k_s} + \mathbf{k_i} \quad \text{with} \quad |\mathbf{k}| = n(\lambda)\frac{\omega}{c_0} = n(\lambda)\frac{2\pi}{\lambda}, \tag{2-2}$$

where $n(\lambda)$ is the refractive index of the nonlinear crystal for the wavelength λ and c_0, the velocity of light in vacuum. These two conditions are derived from the coupled three-wave equations [38]. The latter ensures that the generated waves are added constructively across the nonlinear crystal. Due to chromatic dispersion, this condition is usually not satisfied. Indeed, in a normal dispersive crystal, the refractive index of the pump $n(\lambda_p)$ is always larger than that of the seed $n(\lambda_s)$ and idler $n(\lambda_i)$.

In a collinear geometry, this results in the following inequation using equations **(2-2)** and **(2-1)**:

$$\frac{n(\lambda_p)}{\lambda_p} > \frac{n(\lambda_s)}{\lambda_s} + \frac{n(\lambda_i)}{\lambda_i}, \tag{2-3}$$

$$\text{equivalent to} \quad k_p > k_s + k_i. \tag{2-4}$$

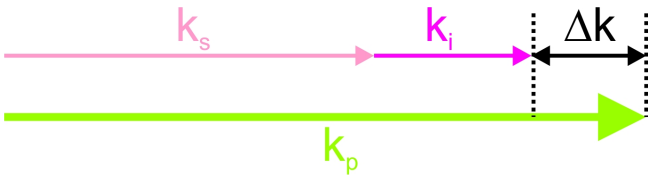

Figure 2-1 Wave-vector mismatch in a collinear geometry.

The wave-vectors are represented in figure 2-1 for a collinear geometry. The phase-matching condition does not need to be satisfied rigorously but the wave-vector mismatch $\Delta\mathbf{k}$, defined as

$$\Delta\mathbf{k} = \mathbf{k_p} - \mathbf{k_s} - \mathbf{k_i}, \tag{2-5}$$

leads to a drop in the conversion efficiency of this nonlinear process. In the presence of a non-zero wave-vector mismatch the interacting waves will progressively run out of phase as they propagate through the crystal, causing a decrease of the generated signal-idler pair. Destructive interferences will then gradually annihilate the original build up of the signals.

Collinear phase-matching can be achieved by exploiting the birefringence in nonlinear crystals. In a negative uniaxial birefringent crystal, the refractive index for the extraordinary wave n_e is smaller than for the ordinary wave n_o. For an extraordinary wave propagating along an angle θ with respect to the optical axis, the effective refractive index $n_e(\theta)$ experienced by this wave varies continuously between n_o and n_e according to the angle θ, with

$$n_e(\theta) = \frac{n_e n_o}{\sqrt{n_o^2 \sin^2\theta + n_e^2 \cos^2\theta}}. \tag{2-6}$$

Collinear phase-matching in a birefringent crystal consists in determining the angle θ that verifies $\Delta k = 0$, which can be written as

$$\text{either} \quad \frac{n_{pe}(\theta)}{\lambda_p} = \frac{n_{so}}{\lambda_s} + \frac{n_{io}}{\lambda_i}, \tag{2-7}$$

$$\text{or} \quad \frac{n_{pe}(\theta)}{\lambda_p} = \frac{n_{so}}{\lambda_s} + \frac{n_{ie}(\theta)}{\lambda_i}, \tag{2-8}$$

depending on the nature of the interacting waves.

Equations **(2-7)** and **(2-8)** lead to type-I ($e \rightarrow o + o$) and type-II phase-matching ($e \rightarrow o + e$), respectively. As an example, the dispersion of the nonlinear crystal beta barium borate (BBO) is plotted in figure 2-2.

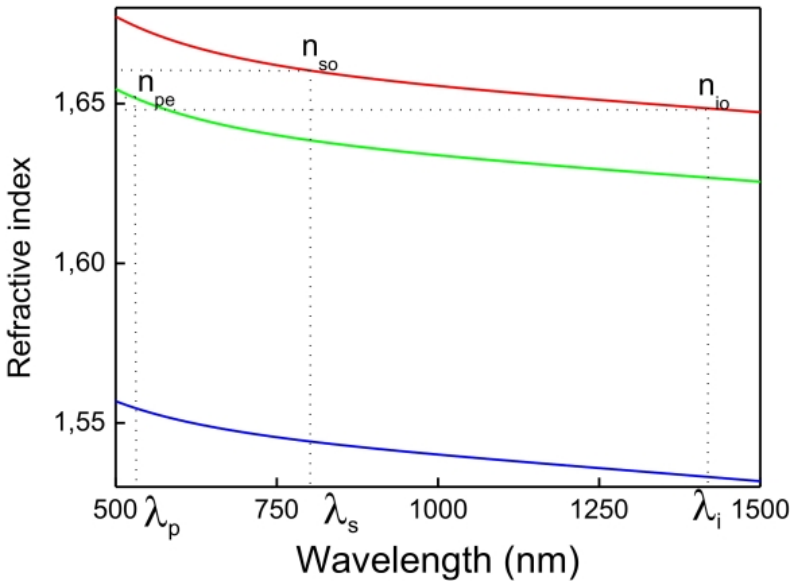

Figure 2-2 **Dispersive curve of BBO for an ordinary wave (red line) and an extraordinary wave for $\theta = 0°$ (blue line). For $\lambda_p = 515$ nm and $\lambda_s = 800$ nm, the idler wavelength is $\lambda_i = 1445$ nm. Type-I phase-matching is obtained in BBO for $\theta = 22.7°$ in a collinear geometry (green line).**

Other phase-matching techniques include temperature phase-matching, which uses the dependence of the birefringent crystal refractive indices on the temperature, and quasi-phase matching, where the phase mismatch is compensated periodically in a spatially modulated crystal.

In this thesis, only type-I phase-matching in negative uniaxial crystals will be implemented for the amplification of ultrashort pulses.

2.2 Amplification of ultrashort pulses

Neglecting pump depletion during amplification and assuming no idler wave at the beginning of the process, the intensity of the amplified signal I_s can be derived from the coupled-wave equations within the slowly-varying envelope approximation for flat-top spatial and temporal beam profiles [38]. For an initial signal intensity I_{s0}, the intensity after amplification inside a crystal of length L is given by

$$I_s(L) = I_{s0}\left[1+\left(\frac{\kappa \sinh(gL)}{g}\right)^2\right], \tag{2-9}$$

$$\text{with } g = \sqrt{\kappa^2-\left(\frac{\Delta k}{2}\right)^2}, \tag{2-10}$$

$$\text{and } \kappa = 2d_{eff}\sqrt{\frac{\omega_s\omega_i Z_0 I_p}{n_s n_i n_p 2c_0^2}}. \tag{2-11}$$

d_{eff} is the effective second-order nonlinear coefficient of the crystal, I_p is the pump intensity, n is the refractive index for the different interacting waves and Z_0 is the vacuum impedance, which is approximately equal to 377 Ω.

For exact phase-matching ($\Delta\mathbf{k} = 0$), $g = \kappa$ and equation **(2-9)** simplifies to

$$I_s(L) = I_{s0}\left[1+\sinh^2(\kappa L)\right] \approx \frac{I_{s0}}{4}\exp(2\kappa L) \quad \text{if} \quad \kappa L \gg 1. \tag{2-12}$$

In this perfect case, the amplified seed grows exponentially. From equation 2-12, higher gains are possible by either increasing the crystal length or by using higher pump intensities. Unfortunately, using longer crystals is not a solution for ultrashort pulses, as dispersion will make the pump and signals propagate at different speed in the crystal, limiting their actual interaction length.

According to equation **(2-7)**, perfect angular phase-matching can be achieved for monochromatic waves in a collinear geometry through an appropriate orientation of the birefringent crystal. However, in the presence of ultrashort pulses, $\Delta\mathbf{k}$ needs to be minimised over the whole spectral range of the signal in order to amplify all wavelengths efficiently.

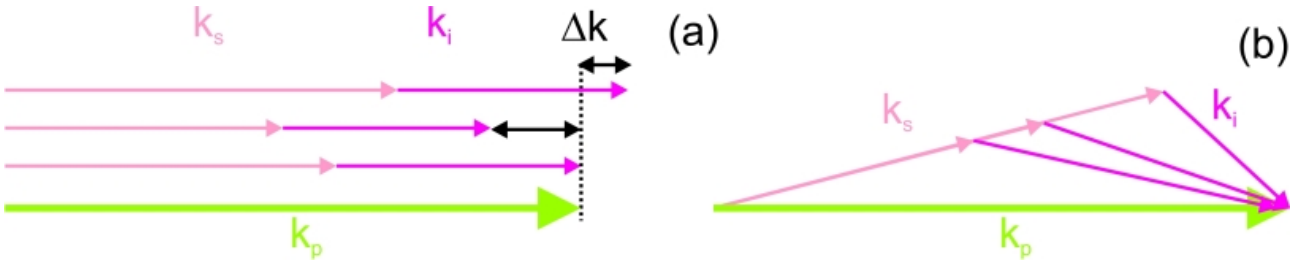

Figure 2-3 Comparison between collinear (a) and non-collinear geometries (b). In a collinear geometry, perfect phase-matching is achieved at a given signal wavelength. In a non-collinear geometry, the direction of the idler wave-vector is wavelength dependent, offering an additional degree of freedom to minimise Δk for broadband phase-matching.

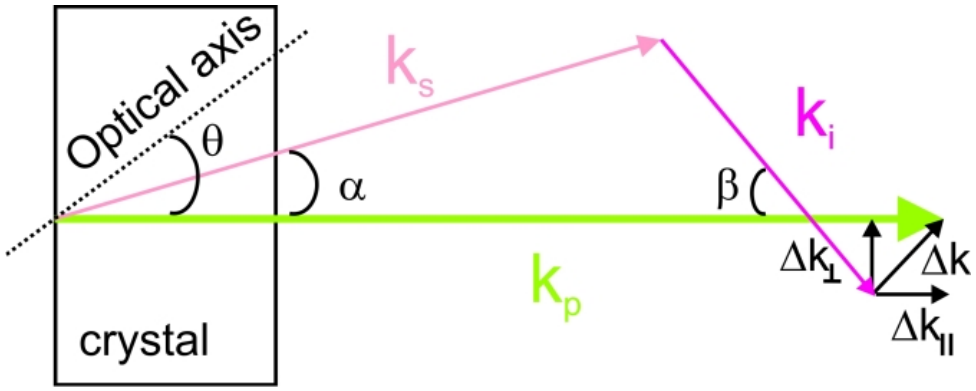

Figure 2-4 Wave-vectors in a non-collinear OPA for type-I phase-matching. The wave-vector mismatch can be decomposed in a horizontal component $\Delta k_{\parallel}$ along the pump and a vertical component $\Delta k_{\perp}$.

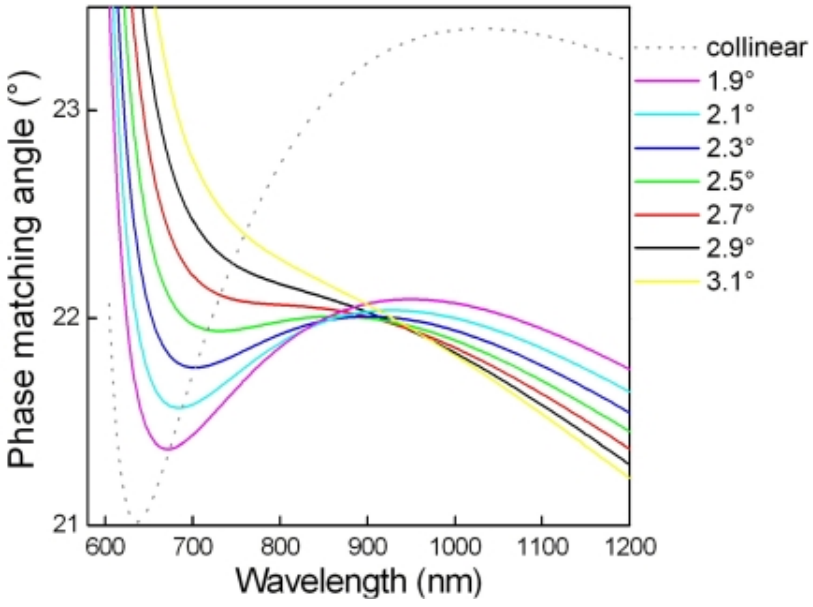

Figure 2-5 Phase-matching angle θ for different non-collinear angles α in a BBO type-I OPA with $\lambda_p = 515$ nm. In a collinear configuration, phase-matching can only be achieved in a very narrow spectrum range. For $\alpha \approx 2.5°$, the wavelength dependence of θ is almost vanished from 700 nm to 1000 nm, allowing amplification of ultrashort pulses centred around 850 nm.

Assuming perfect phase-matching for a signal frequency ω_s, an increase $\Delta\omega$ of the signal frequency is accompanied by an equal decrease of the idler frequency, since energy conservation is automatically satisfied in a parametric process where no energy transfer takes place from the pump to the crystal. Nonetheless, this does not ensure phase-matching and a non-vanishing wave-vector mismatch arises at the frequency $\omega_s + \Delta\omega$. In the case of a monochromatic pump, the wave-vector mismatch can be approximated to the first order by

$$\Delta k \cong -\frac{\partial k_s}{\partial \omega_s}\Delta\omega + \frac{\partial k_i}{\partial \omega_i}\Delta\omega = \left(\frac{1}{v_{gi}} - \frac{1}{v_{gs}}\right)\Delta\omega, \tag{2-13}$$

where $v_g = \dfrac{\partial\omega}{\partial k}$ is the group velocity of the pulse.

The full-width at half-maximum (FWHM) of the phase-matching bandwidth can be approximated from equations **(2-9)** and **(2-13)** to:

$$\Delta k_{FWHM} \cong 4\sqrt{\ln 2}\cdot\sqrt{\frac{\kappa}{L}} \quad \text{if} \quad \kappa L \gg 1 \quad \text{and} \quad \kappa \gg \frac{\Delta k_{FWHM}}{2} \tag{2-14}$$

$$\Delta\omega_{FWHM} \cong 4\sqrt{\ln 2}\cdot\sqrt{\frac{\kappa}{L}}\cdot\frac{1}{\left|\dfrac{1}{v_{gi}} - \dfrac{1}{v_{gs}}\right|}. \tag{2-15}$$

Equation **(2-15)** makes apparent that the difference of group velocities between the idler and the seed will restrict the phase-matching bandwidth and thus limit the use of longer crystals. A solution to this problem consists in employing a non-collinear geometry, as illustrated in figure 2-3. While in the collinear case the group velocities of the seed and idler are set, non-collinear optical parametric amplification (NOPA) allows to match the group velocities by adjusting the angle between the seed and the pump [68].

The orientation of the wave-vectors are represented in figure 2-4. The angles α and β are the angles of the signal and idler beams in respect to the pump. α is fixed by the geometry and is referred as the non-collinear angle, while β is wavelength-dependent. As before, θ is the phase-matching angle. For broadband phase-matching, the wave-vector mismatch should be affected as little as possible by a change of the seed frequency. According to figure 2-4, Δk can be decomposed into a parallel and a perpendicular component:

$$\Delta k = \begin{cases} \Delta k_{\parallel} &= k_p - k_s\cos\alpha - k_i\cos\beta \\ \Delta k_{\perp} &= k_s\sin\alpha - k_i\sin\beta \end{cases}, \tag{2-16}$$

Ideally, both components of Δk should equal zero. Assuming a monochromoatic pump and plane waves, the wave-vector mismatch can be derived to the first order and written as

$$\Delta k \cong \begin{cases} -\dfrac{\partial k_s}{\partial \omega_s}\cos\alpha\Delta\omega + k_i \sin\beta \dfrac{\partial\beta}{\partial\omega_i}\Delta\omega - \dfrac{\partial k_i}{\partial\omega_i}\cos\beta\Delta\omega = 0 \\ \dfrac{\partial k_s}{\partial \omega_s}\sin\alpha\Delta\omega - k_i \cos\beta \dfrac{\partial\beta}{\partial\omega_i}\Delta\omega - \dfrac{\partial k_i}{\partial\omega_i}\sin\beta\Delta\omega = 0 \end{cases}, \qquad \textbf{(2-17)}$$

Through multiplication of $\Delta k_{\parallel}$ by $\cos(\beta)$ and $\Delta k_{\perp}$ by $\sin(\beta)$ with subsequent addition, the expression simplifies to

$$\frac{\partial k_s}{\partial \omega_s}\cos\Omega + \frac{\partial k_i}{\partial \omega_i} = 0 \;\text{ with }\; \Omega = \alpha + \beta, \qquad \textbf{(2-18)}$$

which is equivalent to

$$v_{gs} = v_{gi}\cos\Omega. \qquad \textbf{(2-19)}$$

Equation **(2-19)** shows that Δk can be cancelled around the seed frequency ω_s when the projection of the idler group velocity on the signal direction is equal to that of the seed. To illustrate this, the phase matching angle θ is plotted for different values of α for a parametric amplifier based on BBO in figure 2-5. One can see that the phase-matching bandwidth strongly depends on this non-collinear angle. A residual mismatch will nevertheless arise from higher-order terms of the Taylor expansion of Δk.

Assuming perfect phase-matching for the signals ω_{s0} and idler ω_{i0}, the wave-vector mismatch can be written as:

$$\Delta k \approx n_{i0}\omega_{i0} - n_i\omega_i, \quad \text{with} \quad n_{i0}\omega_{i0} = \sqrt{n_p^2\omega_p - n_s^2\omega_{s0} - 2n_{s0}\omega_{s0}n_p\omega_p\cos\alpha}. \qquad \textbf{(2-20)}$$

The amplified spectra calculated from equations **(2-9)** and **(2-20)** are compared in figure 2-6 for a collinear and non-collinear OPA based on BBO.

In summary, the non-collinear phase-matching technique can provide larger amplification bandwidths by an effective matching of the signal and idler group velocities. High gains over large spectral range are possible provided the crystal and focusing parameters are chosen adequately. Thin crystals are essential for amplification of ultrashort pulses, because the accumulated phase-mismatch ΔkL lowers the intensity of the amplified signal as shown in equation **(2-9)**. The lower gain in thinner crystals can be compensated by higher pumping intensities, typically in the order of tens of GW/cm^2. These intensities can be easily obtained from millijoule-amplifiers operating at lower repetition rates with quasi-collimated beams. Such an OPA is described in chapter 3. Mode-locked oscillators have been recently scaled to the multi-microjoule level, making them suited for pumping parametric amplifiers at MHz repetition rate with focused beams. Chapter 6 will present the realisation of a MHz OPA driven by a thin-disk oscillator and address in more details the design issues for parametric amplification of ultrashort pulses.

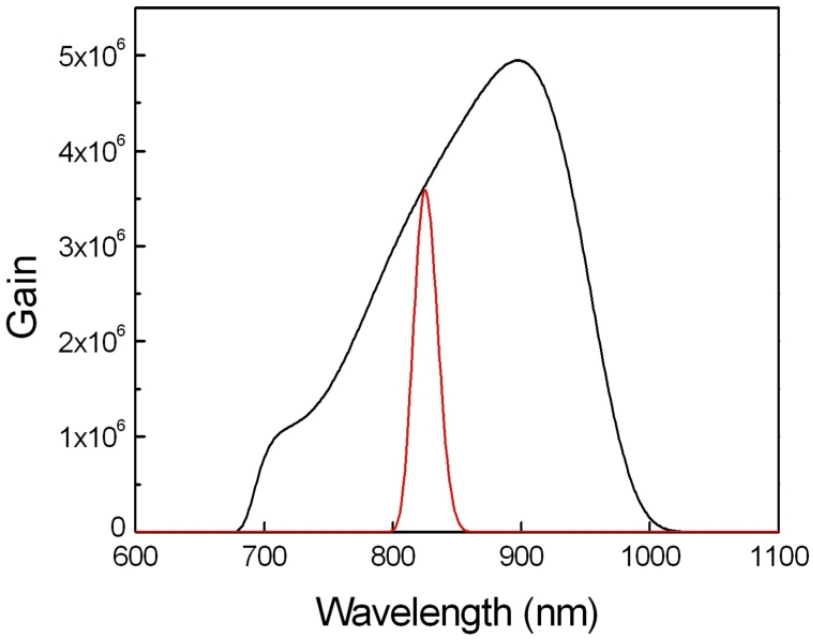

Figure 2-6 **Parametric gain for type-I amplification in a collinear (red line) and in a non-collinear geometry (black line). The parameters for the calculation are $\lambda_p = 515$ nm, $I_p = 18\,\mathbf{GW/cm^2}$, L= 4 mm, $\theta = 22.9°$ in the collinear case, $\theta = 22.02°$ and $\alpha = 2.6°$ in the non-collinear case.**

2.3 Stretching and compression of femtosecond pulses

2.3.1 Efficiency and seed pulse duration

Efficient energy extraction requires temporal overlap between the seed and pump pulses. In high-power OPCPA systems, the pump source is typically narrow-band with pulse durations ranging from a few tens of nanoseconds to approximately a picosecond depending on the technology used like a Q-switched laser [39], a master oscillator power amplifier [28] or a high-energy oscillator [34]).

Since the pump pulses are substantially longer than the seed pulses, the seed pulses are temporally stretched before amplification by a dispersive delay line. Ideally, the pump pulse should be flat-top-shaped and the seed pulse should be of comparable duration to obtain homogeneous amplification across the seed spectrum. Indeed, as schematically shown in figure 2-7, a Gaussian pump pulse leads to a non-uniform gain profile across the chirped seed pulse. The edges of the pulses and hence the edges of the spectrum will experience a lower gain resulting in a reduction of the amplified pulse bandwidth. In addition, timing jitter will be translated into instabilities of the amplified spectrum. Pulse shaping techniques based on multi-stage Michelson interferometers and fibre gratings have already been applied to the generation of picosecond flat-top pulses from a superposition of Gaussian pulses [41, 42]. However temporal pulse shaping is not a trivial issue and will not be addressed in this work.

The amplification bandwidth is thus not only determined by the phase-matching bandwidth of

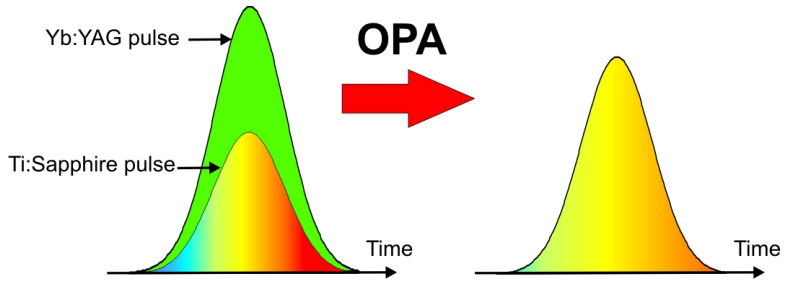

Figure 2-7 **Spectral gain narrowing with chirped seed pulses and Gaussian pump pulses. Due to the limited gain bandwidth the edges of the chirped seed pulse (left) are less amplified than the central part. The amplified seed (right) has a narrower spectrum, as shown by the narrower colour gradient on the right.**

the nonlinear crystal but also by the pump pulse profile. In OPCPA systems, there is a trade-off between efficiency and bandwidth which is determined by the seed-to-pump pulse duration ratio. Small ratios permit homogeneous amplification by maintaining the pump intensity almost constant during amplification. On the other hand, the efficiency is lowered because a large fraction of the pump energy is discarded. From previous works [43], a good compromise can be obtained for a seed-to-pump ratio of about 50%.

2.3.2 Dispersion management techniques

There are several ways to create chromatic dispersion in order to lengthen or recompress a pulse. The pertinence of one approach upon another depends on the amount of group delay dispersion (GDD) necessary, the damage threshold and dimensions of the optical device, the pulse bandwidth and the tolerated losses. The mathematical definitions of the parameters related to the dispersion of ultrashort pulses (group velocity, group delay...) are listed in the annex C.

Diffraction gratings and prisms allow for the generation of large optical delays between the different spectral components of a pulse by exploiting the wavelength dependence of the refraction and diffraction angles, respectively [40]. In these schemes, the input beam is spatially dispersed through diffraction (gratings) or refraction (prisms) and subsequently reshaped, resulting in a wavelength-dependent optical delay. Depending on the chosen geometry, the optical system can produce a positive or a negative GDD. The major drawbacks of these systems are their extreme alignment sensitivity, relatively high losses and large footprints. Further advances in grating technology have recently permitted the realisation of highly efficient transmission and reflection gratings with diffraction efficiencies above 97% [44].

Chirped mirrors

The concept of chirped mirrors for introducing group delay goes back to 1994 and was originally intended for intracavity dispersion compensation in mode-locked oscillators [45]. Their robustness was a crucial point for the commercialisation of the first sub-10 fs lasers [46]. Indeed these dispersive elements create an alignment-insensitive group delay based on their wavelength-

dependent penetration depth structure. The principle of operation of such mirrors is presented in figure 2-8.

Chirped mirrors consist of a dielectric quarter-layer stack exhibiting a monotonic variation of the multilayer period. This approach enables the realisation of tailored dispersion profiles including higher-order dispersion terms by ajustments of the mirror design. In chirped amplifier systems, their implementation would permit to significantly reduce the overall-size of the set-up, where large areas are commonly occupied by the stretcher and the compressor. So far, they have been essentially used in CPA systems for final adjustment of the necessary dispersion because of their originally low average dispersive values.

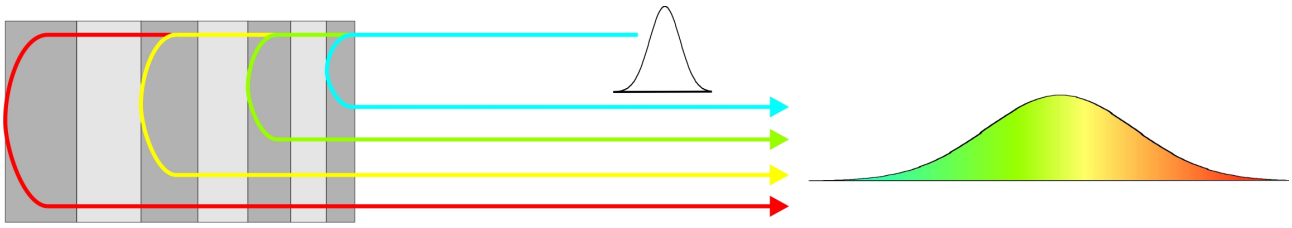

Figure 2-8 Pulse stretching in a negatively chirped mirror.

The conception of mirrors with extreme parameters in terms of average GDD and bandwidth is not trivial and requires optimisation of the reflection and dispersion properties based on complex algorithms. In addition, precise fabrication necessitates controlled manufacturing techniques due to the narrow tolerance on the layer thickness. Only recently, these multilayer structures have proven to be an alternative to conventional dispersion techniques by an increase in the accuracy of the layer deposition process and the introduction of novel designs [97]. A low-loss all-dispersive-mirror compressor was successfully implemented in our laboratory for the compression from ~5 ps to 20 fs after chirped pulse amplification [47]. Despite the high number of reflections on these mirrors (>50), the overall throughput reached approximately 90%. Such dispersive mirrors open up the way towards robust high-throughput and compact compressor systems.

2.3.3 Pulse characterisation techniques

Following parametric amplification, the pulse are recompressed by another delay line of opposite GDD from the stretcher. This is typically done by measuring the recompressed pulse characteristics and correcting the dispersion accordingly. For pulses below a few tens of femtoseconds, third-order dispersion (TOD) compensation becomes imperative and therefore necessitates accurate pulse diagnostic techniques. Detailed information about these techniques can be found in reference [48].

The most straightforward way to measure a pulse is to probe it with a much shorter reference signal. The intensity cross-correlation is based on this principle. In this scheme, the measured pulse and the reference pulse are spatially overlapped in some nonlinear medium in order

to generate a sum-frequency or difference-frequency signal, which intensity is function of the relative delay introduced between the two pulses. This signal is then recorded by a photodiode as shown on figure 2-9. Obviously, this method becomes problematic as the duration of the pulse of interest decreases. In addition, in order to retrieve the pulse duration from the cross-correlation measurement, the duration and the shape of the pulse should be known.

The autocorrelation was the first approach used to determine the duration of an ultrashort pulse by convoluting the pulse with itself. One of the most widely used autocorrelation technique is the second-order intensity autocorrelation owing to the simplicity of its set-up. In a very similar way to the intensity cross-correlation, the pulse is split in two parts and crossed inside a nonlinear crystal for second-harmonic generation. In an intensity-based measurement, the information about the temporal phase of the pulse electrical field is lost. This may not be an issue for picosecond pulses, however the possibility to identify and measure a chirp is essential for femtosecond pulses. This shortcoming can be partially overcome in a closely related measurement technique, known as interferometric autocorrelation. In this set-up, the pulses are superimposed in a collinear geometry in order to produce an interference pattern, which contains some phase information of the pulse. As opposed to the intensity autocorrelation, this signal is not background-free since it is superposed to the two additionally emitted second-harmonic signals, but the peak-to-background ratio is 8:1. This method is usually preferred for pulses below $\sim$100 fs but it still presents some limitations. First, the deconvolution of the autocorrelation function requires here also a first assumption on the pulse shape in order to extract the actual pulse duration. Second, the autocorrelation being by definition symmetric, different pulse shapes can lead to identical autocorrelation traces. Therefore, additional measurements are required to fully characterise the pulse.

In the last decade, two techniques have emerged as powerful diagnostic tools of ultrashort pulses by collecting information in the spectral domain. Combined with a programmable acousto-optic filter, they allow for precise pulse recompression provided the measurement of the pulse and its retrieval are done accurately [49].

Spectral phase interferometry for direct electric field reconstruction (SPIDER) uses spectral interferometry between two spectrally-shifted pulse replica to retrieve the spectral phase [50]. This involves splitting the pulse into three parts: two replica offset by a small delay and one pulse stretched in a dispersive line. The pulses are crossed inside a nonlinear crystal for sum-frequency (or different-frequency) generation. Due to this small delay, the pulse replicas are recombined with different spectral parts of the chirped pulse, leading to two sum-frequency signals with shifted central wavelength (spectral shear). By measuring their spectral interferences for a calibrated delay, the spectral phase can be extracted using an inversion algorithm and the pulse can be reconstructed accordingly. The main advantage of this approach is its direct non-iterative measurement of the electric field, but it suffers from calibration issues.

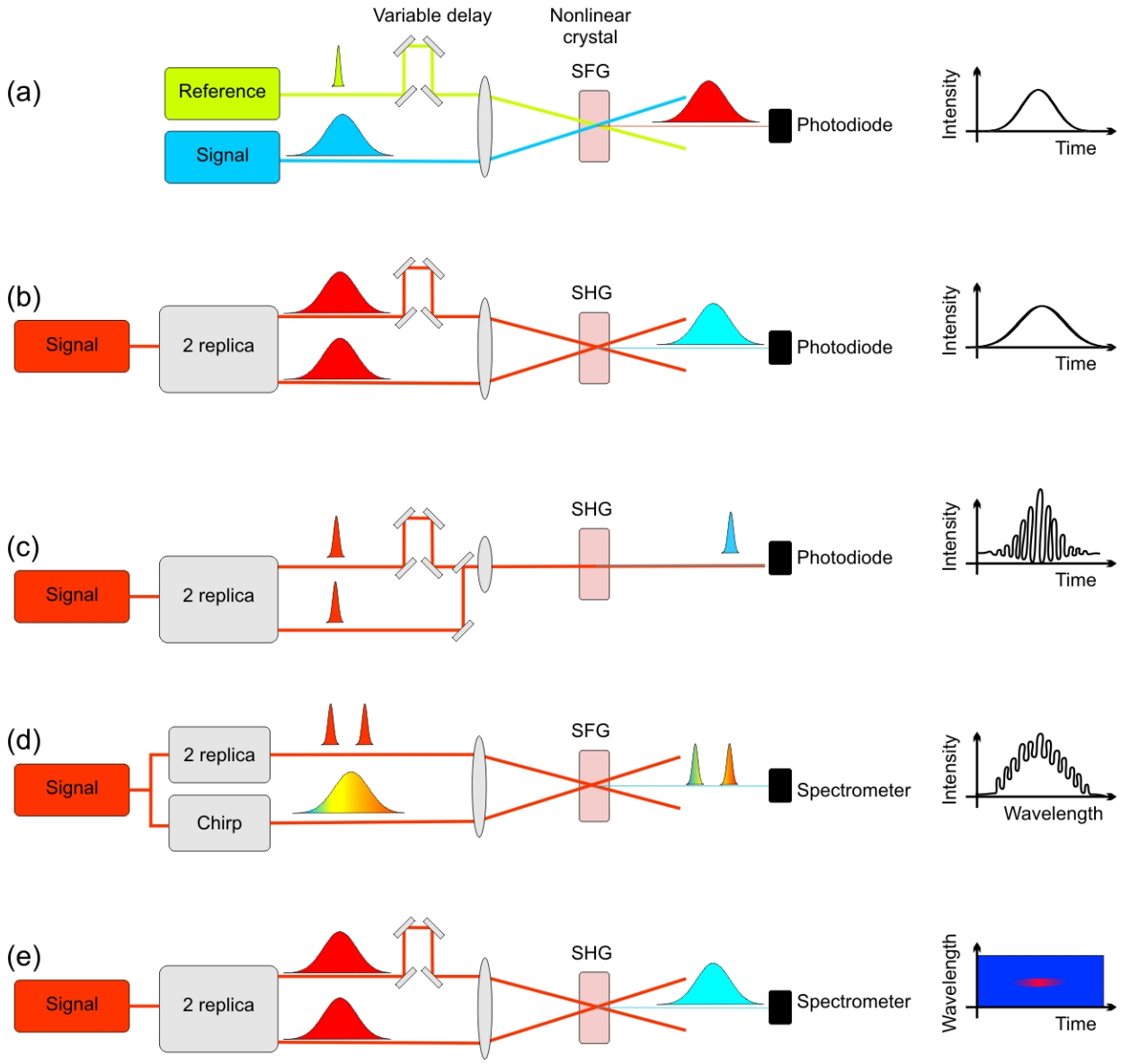

Figure 2-9 **Examples of pulse measurement techniques. (a): Intensity cross-correlation, (b): intensity autocorrelation, (c): interferometric autocorrelation, (d): SPIDER and (e): FROG set-ups. SHG: second-harmonic generation. SFG: sum-frequency generation.**

Another technique known as frequency-resolved optical gating (FROG) operates simultaneously in the time and spectral domain [51]. In its simplest form, FROG consists of an intensity autocorrelator set-up where a spectrometer is inserted to record the generated second-harmonic spectra as a function of the timing delay between the two pulses. An iterative phase retrieval algorithm is then implemented to reconstruct the temporal and spectral features of the pulse. Some minor ambiguities remain such as the absolute phase, the translation in time (both present in SPIDER) and the direction of time. As opposed to the intensity autocorrelation, this FROG measurement leads to a quasi-unique pulse solution. FROG devices have been derived into various geometries for increasing its accuracy, sensitivity, versatility or practicability. As a example of these recent developments, grating-eliminated no-nonsense observation of ultrafast incident laser light E-fields, in short GRENOUILLE, allows for single-shot FROG measurement in a very compact set-up [52].

Unfortunately, all these phase-sensitive devices are still not on the market for pulse duration below 10 fs. For the characterisation of shorter pulses, one has to rely on home-made systems or use commercial interferometric autocorrelators down to to 5 fs.

2.4 Pump sources for parametric amplifiers

The realisation of an OPA sets high demands on the pump laser in terms of energy, mode and pulse profiles, as well as stability. First, high-intensity pump pulses are crucial for parametric amplification of broadband pulses since they enable the use of thinner crystals. Second, the pulses should exhibit excellent beam quality to ensure homogeneous amplification of the signal beam profile. Third, the pump temporal profile should be free from any pedestals or wings to permit efficient pump-to-signal conversion. Fourth, the pulse energy fluctuations should be low to obtain stable parametric amplification. Finally, due to the absence of energy storage in the nonlinear crystal, strict temporal overlap between the pump and the seed pulses is necessary in a parametric process. As a consequence, synchronisation of the two laser sources is required.

Provided the synchronisation is not an issue, short pump pulses are favourable for parametric chirped pulse amplification. Since the pump pulses are substantially longer than the seed pulses, efficient energy extraction from the pump implies the use of highly chirped seed pulses. Extensive stretching introduces additional losses for the seed and tends to lead to distorted pulse profiles, which necessitate complex adaptive dispersion management techniques to achieve optimal recompression. With shorter pump pulses, in the range of a picosecond, the seed pulses can be easily lengthened through chromatic dispersion in a transparent bulk material. For 6-fs seed pulses, 3 cm of fused silica are sufficient to stretch the pulses to 500 fs. Recompression would be simultaneously simplified and could consists of multiple bounces on highly efficient dispersive multilayer mirrors.

As compared to nanosecond pulses, higher pumping intensities are possible due to the increased optical damage threshold for picosecond pulses [53]. For pulse durations τ_p below 20 ps, the

threshold increases even faster than the $1/\sqrt{\tau_p}$ scaling law. By driving parametric amplifiers with a picosecond pump pulse, higher peak intensities are achievable and larger amplification bandwidths can be expected from thinner crystals.

Since the spatial length of a picosecond pump pulse is much shorter than the typical thickness of the nonlinear crystal (∼5 mm), reflections of the amplified seed from the crystal surfaces are not amplified by the pump. Hence, better pulse contrast ratios of the amplified seed are expected due to the absence of parasitic oscillation and amplification of post-pulses at these pump pulse durations [54].

High-energy pump sources are conventionally derived from amplification of low-energy oscillator pulses, typically in the nanojoule level, after reducing the repetition rate (sub-Hz to few kHz) to decrease the thermal load on the amplifier elements. Recent developments on high average power mode-locked oscillators led to the direct generation of pulse energies beyond 25 μJ [32], opening the way toward MHZ OPAs. Following, the principles and constraints of pump lasers will be introduced for amplifier-based systems and high-energy mode-locked oscillators.

2.4.1 Regenerative amplifiers

Regenerative amplifiers are a powerful scheme for amplifying selected pulses inside an active resonator by allowing multiple passes through a gain medium. A selected low-energy pulse is "trapped" into a resonator by an optical switch. While this pulse experiences amplification at each round trip, the other pulses are kept out of the resonator. Once the gain is saturated, the optical switch couples the amplified pulse out and let a new pulse in for amplification. The general scheme of such amplifiers is depicted in figure 2-10.

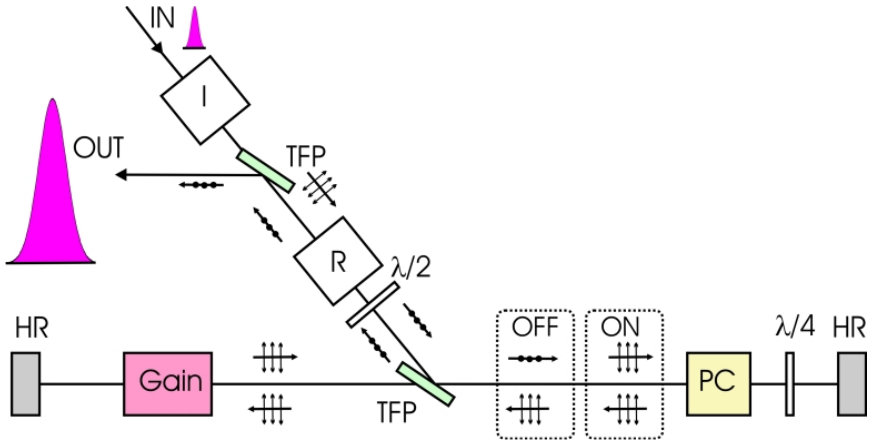

Figure 2-10 **Layout of a regenerative amplifier. HR: high reflector, PC: Pockel's cell, TFP: thin-film polariser, I: isolator, R: rotator, λ/4: quarter-wave plate and λ/2: half-wave plate.**

The optical switch usually consists of a polariser, a Pockel's cell and a quarter-wave plate. A Pockel's cell is an electro-optic device, in which an externally applied DC voltage is coupled into a modification of the refractive index of a nonlinear crystal. Typically the voltage is chosen so that the phase-shift introduced between the two orthogonal components of the electric field

with respect to the crystal optical axis, originates a rotation of the initial polarisation by 90° in a double-pass.

The principle of coupling in and out is simple. An initial s-polarised seed pulse is reflected from the polariser and directed to the Pockel's cell. At that stage no voltage is applied, so that the polarisation is rotated by 90° after the double-pass through the quarter-wave plate. As a result, the p-polarised pulse is transmitted through the polariser and propagates towards the gain medium. In the mean time, a quarter-wave voltage is applied to the Pockel's cell. Thus, in combination to the quarter-wave plate, a rotation of the polarisation by 180° is introduced. The p-polarised pulse is consequently "trapped" inside the resonator and amplified at each round trip through the gain medium, as long as the voltage is maintained on the Pockel's cell. Once the voltage is switched off, the pulse is coupled out by the cavity polariser.

To separate the incoming pulse train from the amplified one, a rotator in combination to a half-wave plate are usually used. These two optical elements cause a rotation of the incoming pulse polarisation by 90° (p $\rightarrow$ s), while the outcoupled pulse polarisation stays unchanged (p $\rightarrow$ p). The outcoupled pulses are consequently reflected by the outside polariser. In addition, an isolator is commonly inserted between the seed oscillator and the amplifier to protect the oscillator from a leakage through the polariser.

Regenerative amplifiers present many advantages over multipass amplifiers. Increasing the energy of the pulses is easily done by increasing the duty cycle of the Pockel's cell, thereby increasing the number of passes through the gain. If the regenerative amplifier is designed to support only the fundamental mode TEM_{00}, the output pulse will exhibit diffraction-limited beam quality, regardless of the initial spatial abnormalities. By operating the amplifier in a saturated regime, the stability of the amplified pulse can be below 1% [31].

These amplifiers are very attractive when very high gains are required to scale up the pulse energy. Yet, with increasing number of round-trips, nonlinear effects become more pronounced. Eventually the accumulated phase-shift, essentially originated from Kerr-nonlinearity inside the Pockel's cell, may create pulse and beam distortions setting eventually an upper limit to the pulse amplification. To overcome this, chirped pulse amplification may be necessary at the cost of additional complexities in the system. Another issue is the increased timing jitter usually observed after amplification. Indeed, after a large round-trip number, small changes of the cavity length due to thermal effects or mechanical perturbations can be translated into a large timing drift from pulse to pulse. In an OPCPA system, this might result in unstable amplification both from shot to shot and on a longer time scale. To some extend, improvement of the timing jitter is possible by reducing the time span between the pulse injection into the regenerative amplifier and its outcoupling. This implies either designing shorter resonators or using higher pumping intensities for increased single-pass gain. In addition, pulse instabilities tend to appear at repetition rates close to the gain medium inverse upper state lifetime, which can even take the extreme form of chaotic pulsing behaviour [55]. In some cases, stable operation

can be found inside an intermittent single-energy regime. Using this regime, pulse energies exceeding 20 mJ were recntly demonstrated in our laboratory [31].

In conclusion, regenerative amplifiers are mostly suited for the generation of energetic pump pulses at repetition rates between 1 to 100 kHz but necessitate a careful design with possibly CPA to maintain stable operation at increasing pulse energies.

2.4.2 Mode-locked oscillators

In a resonator, a multitude of different longitudinal laser modes verifies the oscillation condition, $L = q\frac{\lambda}{2}$, where L the resonator length, q an integer number and λ the wavelength of the longitudinal mode. The number of possible oscillating modes is determined by the gain bandwidth of the laser medium and filtering effects from the cavity optical elements. When no phase relationship exists among these modes, the resulting interferences between the existing longitudinal modes would lead to a noise-like output. However, due to the high number of modes, this noise actually levels out to a stable continuous signal. On the contrary, if the modes oscillate in phase (or with a fixed phase relationship), the laser will emit a periodically enhanced signal from the constructive interferences of the longitudinal modes. The laser is then said to be mode-locked. Through coupling of the different longitudinal modes, the laser can produce pulses which duration is directly related to the number of coupled modes [56]. Besides the longitudinal modes, the transverse modes can also interfere in the mode-locking process causing instabilities in the pulse formation mechanism due to the gain competition between them. Fundamental transverse mode of the laser resonator is hence a prerequisite for stable mode-locking operation.

Two different approaches can be used to mode-lock an oscillator. One relies on the implementation of a modulator inside the resonator, which introduces time-varying cavity losses, usually via an acousto-optic or an electro-optic modulator, synchronised to the cavity round-trip. Such techniques are referred as active mode-locking. The achievable pulse duration lies in the picosecond domain and is ultimately limited by the external modulation signal [56]. Shorter pulse duration can be however obtained by passive mode-locking, in which the pulse induces its own modulation through the nonlinear response of an intracavity element.

Passive mode-locking can be achieved through the insertion of a saturable absorber [57]. The latter introduces lower absorption losses for higher incident optical intensities, thus favouring the pulsed regime over the continuous wave operation in a resonator. Another scheme relies on the direct use of an active medium subject to Kerr-nonlinearity [58]. In the presence of Gaussian beams, the Kerr-nonlinearity induces self-focusing effects from the space-(and time)-dependent refractive index n(r,t) given by

$$n(r,t) = n_0 + n_2 I(r,t), \qquad \textbf{(2-21)}$$

where n_0 and n_2 are the linear and nonlinear refractive index, respectively, and I(r,t) is the

spatio-temporal intensity profile. With an appropriate cavity design, one can use the consecutive focusing of the laser mode in the gain medium to generate a nonlinear effective gain from the spatial overlap between the pump and the laser mode. Owing to the quasi-instantaneous response of Kerr-nonlinearity, the laser behaves as in presence of an ultrafast saturable absorber, making the generation of ∼6 fs pulses based on Ti:Sapphire medium possible [59].

For high-power oscillators, mode-locking is preferably done with a saturable absorber because it eliminates the risk of optical damage in the gain medium through tight focusing and simplifies the resonator design and alignment. Indeed, Kerr-lens mode-locked oscillators need to be operated close to the stability limit where substantial changes of the laser mode occur. On the other hand, passive mode-locking with saturable absorbers reduce the damping of relaxation oscillations and may lead to Q-switching instabilities in the pulse train. Figure 2-11 compares the CW- and Q-switched mode-locked regimes. CW mode-locked operation is possible provided that the laser and resonator parameters fulfil the stability criterion [60] given by

$$E_p^2 > E_{L,sat} E_{L,sat} \Delta R, \tag{2-22}$$

where $E_{L,sat}$ and $E_{A,sat}$ are the saturation energies of the gain medium and the absorber, respectively. E_p is the intracavity pulse energy and ΔR the absorber modulation depth. Equation **(2-22)** shows that saturable absorbers with low saturation fluence and low modulation depth are preferable because it lowers the pulse engery threshold for stable operation. Yet, with too low values of ΔR, pulse perturbations will not be as efficiently suppressed by the absorber.

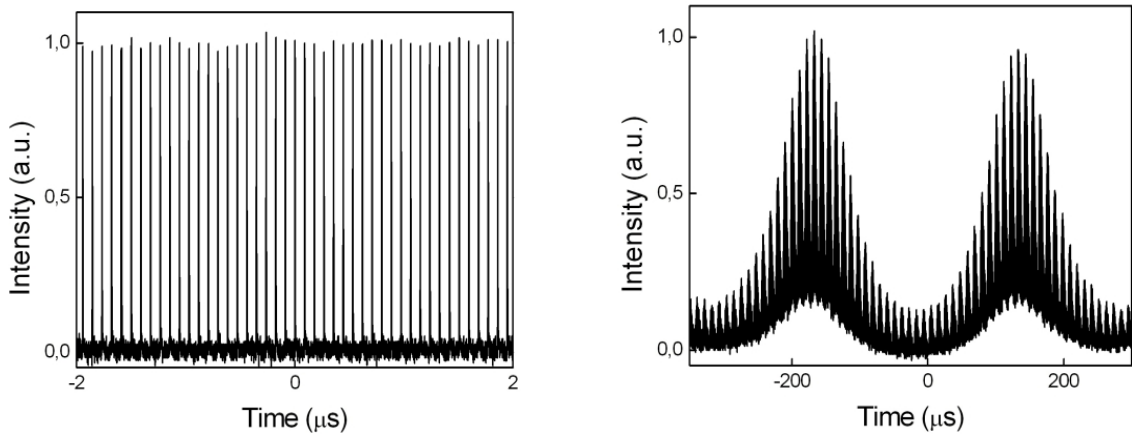

Figure 2-11 CW mode-locking (left) and Q-switched mode-locking (right).

Semiconductor Bragg reflectors

Semiconductor Bragg reflectors (SBRs) are well established for mode-locking ultrafast lasers [61]. They consist of a saturable absorber layer integrated into a Bragg mirror. In these devices, high intensity radiations are mostly reflected, while the lower intensities are partially absorbed. Their saturable absorption originates from the accumulation of electrons in the conduction band and the depletion of the valence band upon incidence of intense light, preventing further photon absorption. They are sometimes also referred as semiconductor saturable absorber mirror.

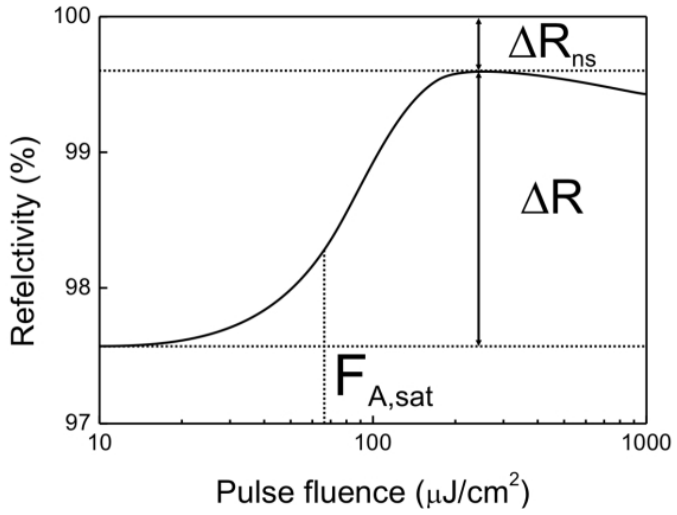

Figure 2-12 SBR nonlinear reflectivity.

Besides the above-mentioned saturation fluence and modulation depth, the most relevant parameters of a SBR are: its centre wavelength of operation and its recovery time τ_A. For high-energy oscillators, the damage threshold is an additional critical feature. For a SBR, the saturation fluence defines the necessary fluence to increase the nonlinear reflectivity by $1/e \cdot \Delta R$ with respect to the linear reflectivity, where ΔR is the maximum nonlinear change of the mirror reflectivity. A typical reflectivity curve of a SBR is shown in figure 2-12. According to their recovery times, SBRs are classified between slow absorbers ($\tau_A > \tau_p$) and fast absorbers ($\tau_A < \tau_p$). Another critical parameter is the non-saturable losses, which are the residual absorption losses for pulse energy densities far above the saturation fluence. These may originate from the imperfect reflectivity of the Bragg reflector, scattering losses due to surface defects or the onset of two-photon absorption at higher fluence. Such losses lead to a heat deposition in the SBR, which can impede high-power lasing operation. Characterisation techniques of SBR dynamics and nonlinear losses can be found in reference [62].

The main advantage of these devices is the possibility to tune their characteristics over several orders of magnitude through modifications of their designs and growth parameters, allowing wide ranges of lasing operation and independent optimisation from the cavity design.

Soliton mode-locking

Mode-locking requires that the different longitudinal modes retain their phase relationship. However, due to dispersion, the different spectral components will travel at different speeds, thereby lengthening the pulses as they circulate through the cavity. Simultaneously, Kerr-nonlinearity induces a time-dependent phase-shift according to the time-dependent pulse intensity (equation **(2-21)** in the time domain), leading to a variation of the instantaneous frequency along the pulse. The leading edge of the pulse is shifted to lower frequencies, while the trailing edge is shifted to higher frequencies. This effect, known as self-phase modulation (SPM), causes a positive chirp and spectral broadening. Control over the group velocity dispersion and the nonlinearity inside the resonator becomes hence essential for ultrashort pulses.

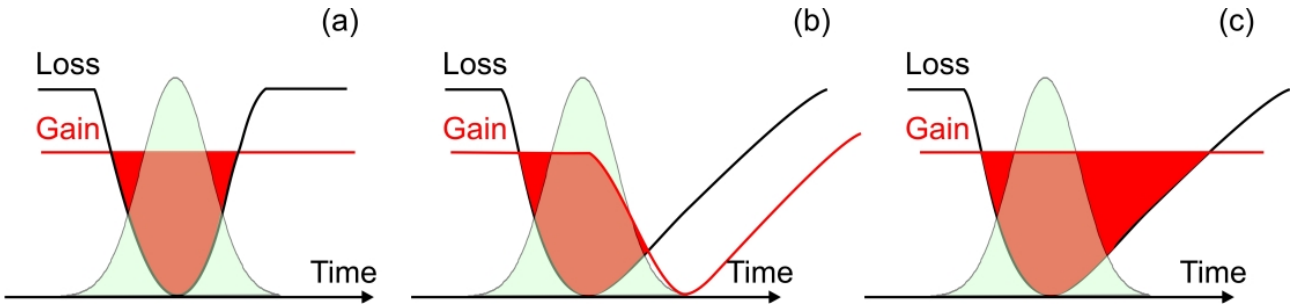

Figure 2-13 **Mode-locking with a fast absorber (a), a slow absorber and gain saturation (b) and a slow absorber with soliton formation. In soliton mode-locking, there is a window of positive net gain behind the pulse, therefore the pulse shaping mechanism cannot be only explained by the absorber.**

Optical solitons are pulses propagating with an invariant shape; they occur when dispersive effects are compensated by self-phase modulation. In a resonator, soliton-like pulses can be generated in the presence of anomalous dispersion balancing the Kerr-nonlinearity. Since the two effects are typically tight to different intracavity components (prisms, mirrors, gain medium...), the pulse profile is not constant inside the cavity but depends on the local predominance of dispersion or nonlinearity. For this reason, such pulses are in general referred as quasi-solitons. While the pulse shaping mechanism is essentially achieved in the soliton regime through an interplay between negative dispersion and self-phase modulation [63], mode-locking necessitates some additional initiating and stabilisation effects, usually from a saturable absorber.

The pulse shaping mechanisms with different combinations of saturable absorber and gain saturation are compared in figure 2-13. Because of the remaining net gain following the pulse, noise may grow outside the pulse and eventually destabilise the mode-locking process in the case of a slow absorber. However, the intensity of this noise is not sufficient to induce nonlinear effects. Consequently, the background noise experiences predominantly dispersive effects and is gradually shifted out of the gain window, as schematically shown in figure 2-14. Thus, instabilities can be cleaned up through the action of the saturable absorber.

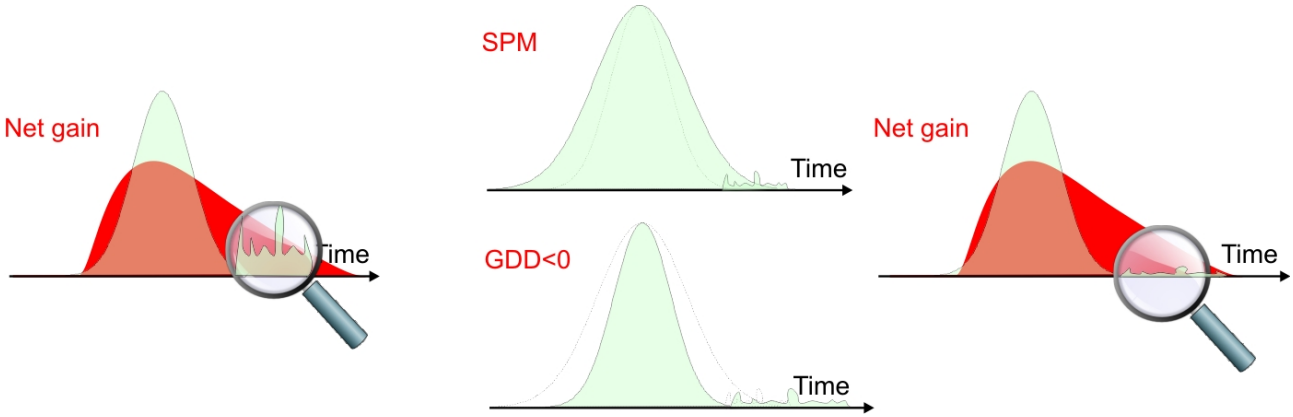

Figure 2-14 **Pulse shaping mechanism in the soliton regime. The low-intensity noise behind the pulse experiences essentially dispersion, while the pulse is lengthened by SPM and recompressed by the negative GDD. The dispersed noise is pushed out of the gain window and consequently suppressed.**

The propagation of soliton pulses through a dispersive nonlinear transparent medium is described by the nonlinear Schrödinger equation [38]. In the soliton mode-locking regime, the pulse duration can be approximated from the fundamental solution of this wave equation, assuming a continuous distribution of SPM and GVD in the resonator and neglecting the effects of the saturable absorber and the finite gain bandwidth in the pulse shaping process. Soliton mode-locking leads to transformed-limited pulses with hyperbolic secant pulse shape, which pulse width is determined by the interplay between negative dispersion and nonlinearity. The condition for stable soliton operation is given by:

$$\tau_p \approx 1.76 \frac{2|\mathrm{GDD}|}{|\gamma_{\mathrm{SPM}}|\mathrm{E_p}} \quad \text{with} \quad \gamma_{\mathrm{SPM}} = \frac{4\mathrm{n_2 L}}{\lambda \mathrm{w}}, \tag{2-23}$$

where τ_p defines the pulse duration, GDD the dispersion and E_p the intracavity pulse energy. γ_{SPM} is the nonlinear phase-shift in a material with nonlinear refractive index n_2 accumulated over a length L for a Gaussian beam of radius w and central wavelength λ. According to equation **(2-23)**, shorter pulse durations can be obtained by decreasing the dispersion. However, the soliton may break into longer pulses if the dispersion becomes too low. These longer pulses, hence with narrower bandwidth, will be indeed selectively amplified over a single shorter soliton, which will suffer predominantly from the limited gain bandwidth. This onset of multiple pulsing ultimately sets a limit for the shortest pulse achievable through soliton mode-locking

In a passively mode-locked oscillator, Q-switching instabilities are of major concerns, since the peak intensity of the Q-switched pulses may be above the optical damage threshold of the cavity elements. For soliton mode-locked oscillators, this tendency towards Q-switching is mostly counterbalanced by soliton effects and gain filtering [60]. Should the energy of the pulse increase consecutively to relaxation oscillations, self-phase modulation will lead to a broadening of the pulse spectrum. Yet, this pulse will experience a lower gain because of the limited gain bandwidth resulting in an additional stabilising effect against pulse perturbations.

The development of a mode-locked oscillators is certainly not a trivial issue as it requires a careful optimisation of the cavity design, its dispersion and the saturable absorber parameters. Now reaching the multi-microjoule level, mode-locked oscillators offers an attractive solution for pumping optical parametric amplification at MHz repetition rates.

2.5 Pump-seed synchronisation techniques

Unlike gain media with inversion storage, the parametric amplifier poses a severe challenge of ensuring strict synchronisation between the pump and seed pulses. Indeed, a timing precision within a fraction of the pump pulse duration is required for stable and efficient amplification inside the nonlinear crystal.

Two general approaches to synchronised few-cycle OPCPA schemes can be distinguished. One relies on a colour-shifted seed, derived from an intense pump source, ensuring automatically op-

tical synchronisation between the two laser sources. Such systems are based on superfluorescene-seeded [65] or white-light-continuum-seeded parametric amplifiers [27, 66, 67, 68]. Consequently, the duration of the amplified pulse is relatively near to the pump duration, while the phase of the pulse may experience shot-to-shot variations.

By contrast, amplifiers seeded with coherent white light are capable of reducing the duration of the amplified pulse down to several optical cycles, i.e. by orders of magnitude below the pump pulse duration [27, 67]. Nevertheless, these devices require short, typically sub-200-fs intense pulses for reliable white light generation. Therefore, white-light-seeded few-cycle amplifiers are driven exclusively by chirped-pulse amplifiers predominantly based on Ti:Sapphire [27, 66, 67, 68] and, more recently, on Yb-doped laser crystals [69]. Superfluorescent devices are unsuitable for carrier-envelope phase-controlled amplification, whereas white-light-seeded amplifiers may exhibit CEP self-stabilisation under special conditions [11, 70].

A straightforward solution to CEP-controlled parametric amplification, similarly to the case of its laser-amplifier counterpart [13], is to use a pre-stabilized seed source [71, 72]. This idea was recently implemented by Hauri *et al* [18], who demonstrated CEP stability preservation in an OPCPA seeded from a CEP-locked Ti:Sapphire oscillator and pumped by the second harmonic of a Ti:Sapphire amplifier that was also seeded by the same oscillator. While offering a very elegant solution to the problems of CEP control and optical synchronisation, this system, nonetheless, has the power upscale constraints mentioned above. Scaling up the output of the CPA Ti:Sapphire pump laser becomes particularly unattractive because this laser in turn requires an upgrade of its own pump source - a green Q-switched ns laser.

The dependence on ultrashort pump lasers is a severe constraint for the development of both superfluorescence- and white-light-seeded amplifiers. Indeed the pump necessitates a gain material supporting a large amplification bandwidth and allowing energy scaling. Unfortunately, most laser materials do not perfectly combine these two conditions, thus limiting their implementation in high-power OPCPA systems.

In the other approach, one laser source is optimised for the generation of narrow-band high-energy pump pulses, while the seed laser consists of a broadband oscillator delivering low-energy pulses. The generation of ultrashort pulses is in this case decoupled from that of high-energy pump pulses by selecting two different gain media with optimal characteristics for one or the other purpose. In this scheme, the scaling of the parametric amplifier output is directly related to the scaling of the narrow-band pump source. Most commonly, the pump is an amplifier-based source, operating in the few Hz to few kHz repetition rate, depending on its energy output.

In the presence of two independent sources, active synchronisation can be achieved by controlling the laser cavity length, hence the laser repetition rate, by means of electronic phase-locked loops (see section 5.2.1). Obviously, the difficulties with active synchronisation directly depend on the pump pulse duration. While active synchronisation of nanosecond Q-switched pulses does not involve a major effort, sub-picosecond locking necessitates the implementation of faster

electronics and complex control loops.

Passive synchronisation, on the other hand, relies on a self-stabilisation of the repetition rate via a nonlinear coupling of the pulses [26, 64]. Though timing jitters of a few femtosecond were demonstrated with these methods, the tolerance to cavity length-mismatch in the order of 10 µm limits their practical use. Indeed, locking can only be maintained over a few minutes as thermalisation cause drifts in the optical path lengths.

In this thesis, high-repetition rate OPCPAs are developed based on a two-colour approach with a broadband seed oscillator and an external pump laser. This work includes the realisation of high-power pump sources and the implementation of reliable synchronisation schemes. In chapter 3, a simple synchronisation technique is demonstrated using a single master oscillator for all-optical synchronisation between picosecond pump and seed pulses in a few-cycle kHz-OPCPA system. In chapter 5, an active synchronisation using a combined electronic-optical control loop is developed for the locking of two mode-locked oscillators. This enables parametric amplification of ultrashort pulses at MHz repetition rates from high-energy pump oscillators.

3 KHz optical parametric chirped pulse amplifier

In high-power optical parametric chirped pulse amplifiers, due to the heat disposal and pumping efficiency reasons, it is more economical to employ a stand-alone (multi-)kHz picosecond pump laser that is optimised for production of high-energy narrow-band pulses. This approach was used in references [24, 25, 77], where a broadband Ti:Sapphire oscillator, employed as OPCPA seed, was synchronised with the master oscillator of a picosecond pump laser based on Nd: YAG using a complex electronic servo loop [78]. State-of-the art active synchronisation loops [77], based on pricey GHz electronics, make it possible to keep the RMS timing jitter between the seed and pump pulses on a sub-picosecond level. Whereas this locking precision satisfies well the demands of OPCPA pumped by Nd-based picosecond lasers (pulse duration range 20-100 ps), it is insufficient for use with sub-picosecond Yb-based pump lasers.

As prospective OPCPA pump sources, Ytterbium (Yb) lasers [79] promise to be vastly superior to their Neodymium (Nd) counterparts because of the shorter pulse duration, reduced parasitic heat, higher output power, and suitability for CPA operation. Using pump pulses in a 1-ps range, one can realize ultrabroadband saturated parametric gain in nonlinear crystals as thin as 1 mm [80] without running into problems with the accumulated phase-shift in the parametric amplifier. Shaped pulses with a bandwidth of several nanometres from Yb-based lasers are also advantageous in terms of maximising OPCPA conversion efficiency, reducing superfluorescence background and avoiding gain narrowing. The desired near-rectangular pump pulse profile can be attained by temporal stretching and pulse wing shaping of the broadband pump pulse. The use of such chirped multi-ps pump pulses, however, will not lower the demand for femtosecond timing precision, because the latter is dictated by the steepness of the pump pulse edges.

3.1 Injection seeding of the pump laser

Different opportunities for passive optical seed-pump pulse synchronisation in OPCPA are surveyed in this section to explain our chosen strategy. An interesting OPCPA approach consists in employing two-colour passively synchronised sources. The motivation behind this concept is the need to provide strong seed signals that are sufficiently above the amplified spontaneous emission (ASE) level in both the OPCPA and the injection-type pump laser. One possibility of realising a two-colour scheme is to employ self-stabilisation of two mode-locked oscillators lasing at the seed and pump wavelengths, respectively, via a nonlinear optical (Kerr-lens) mechanism [26]. In terms of complexity, however, this method is not easier to implement than active synchronisation of two independent mode-locked oscillators.

Another option to consider is a parametric or Raman-type frequency-converter that creates a narrowband spectral component at the wavelength of the picosecond amplifier. A suitably intense wavelength-shifted pulse can be generated in a synchronously pumped optical parametric oscillator (OPO) driven by the broadband seed laser oscillator. Unfortunately, the OPO itself

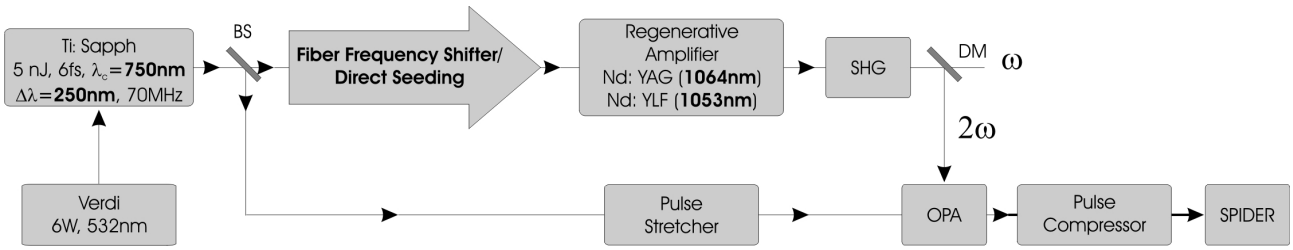

Figure 3-1 **Injection seeding with and without PCF for all-optically synchronised OPCPA; BS, 50 % beamsplitter; DM, dichroic mirror, SHG, second harmonic generation**

requires active cavity stabilisation. In a cavity-less alternative, a very weak frequency-shifted pulse was produced in a travelling wave superfluorescent parametric generator [81]. A separate two-stage cw-pumped parametric amplifier was used to boost this signal to the level suitable for seeding a laser amplifier.

In this work, two straightforward solutions to the synchronisation problems of two-colour OPCPA schemes are presented for a pump laser based on an amplifier. They combine the simplicity of passively synchronised OPCPA schemes using a single seed oscillator, with the flexibility and scalability of the actively synchronised two-source approach for optimising independently pump and seed lasers. Both solutions are illustrated in figure 3-1.

3.1.1 Frequency-shifted seeding

The first approach relies on a broadband Ti:Sapphire oscillator for seeding an OPCPA stage and a frequency shifter for seeding a pulsed pump laser. In our set-up, schematically presented in figure 3-1, the output of a 6-fs 5-nJ 70-MHz chirped-mirror Ti:Sapphire oscillator [59] is divided into two equal parts. One part is directed into an OPCPA stage and the other is frequency-converted to obtain the seed for a picosecond Nd:YAG regenerative amplifier.

In the case of our unamplified oscillator pulses, parametric frequency-shifters [81] become extremely inefficient because of the low pump field intensity and group-velocity matching issues. Under these circumstances, soliton phenomena in optical fibres suggest an interesting alternative to standard strategies of frequency conversion. Optical solitons propagating in media with a nonlinear response experience reshaping and continuous frequency down-shifting due to the Raman effect [82]. This phenomenon, called soliton self-frequency shift (SSFS) [83, 84], provides a convenient way of generating ultrashort pulses with a tunable carrier frequency. Photonic crystal fibres (PCFs) [85] substantially enhance this nonlinear-optical process [86] due to a strong field confinement in a small-size fibre core and the possibility to tailor dispersion of guided modes by varying the fibre structure [87].

The key advantages of the SSFS-based strategy of frequency shifting originate from the intrinsic properties of Raman-shifted solitons [88]. In particular, the central frequency of the red-shifted soliton can be tuned by varying the fibre length and the input pulse energy. Radiation energy carried by this signal is localised in the time domain within a short spike, dominating the

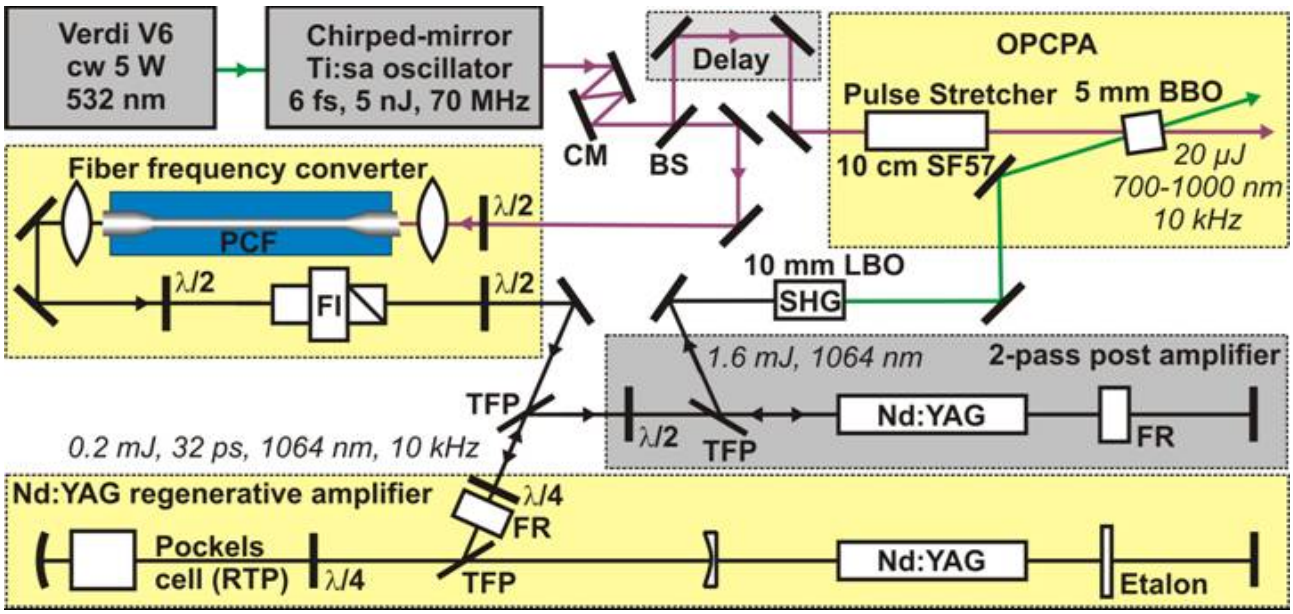

Figure 3-2 **Layout of soliton-based synchronised OPCPA. PCF: photonic crystal fibre, TPF: thin-film polarizer, CM, chirped mirrors, BS: 50 % beamsplitter, $\lambda/2$: half-wave plate, $\lambda/4$: quarter-wave plate, Nd:YAG: side-CW-pumped gain modules, FI: Faraday isolator, FR: Faraday rotator, DM: dichroic mirror, SHG: second harmonic generation.**

temporal envelope of radiation intensity in the fibre. Because of the anomalous group-velocity dispersion of the PCF, the red-shifted soliton becomes delayed and eventually isolated, both spectrally and temporally, with respect to the rest of the pump field. This isolation of the frequency-shifted soliton suppresses the interference between the solitonic part and the rest of the spectrum of radiation field.

For a PCF with a characteristic length of tens of centimetres, the amplitude of the soliton spike in the temporal envelope of radiation intensity is typically an order of magnitude higher than the intensity of the remainder of the SPM-broadened pump field and Cherenkov-type emission, both of which are spread out in time. As a result, the frequency-shifted solitonic component is observed in experiments as the most stable part of the output spectrum [88], which is free of interference fringes, typical of the nonsolitonic part of the radiation field, including Cherenkov emission.

In the context of laser amplifier seeding, the combined spectro-temporal localisation of the SSFS pulse makes it ideally suited for suppressing the ASE inside the laser cavity. In addition, the high amplitude stability of the SSFS pulse is very important for maintaining stability of the amplifier output at repetition rates that are well above the inverse population relaxation time of the laser gain medium. At such repetition rates, although the average output power can be saturated, the energy of each amplified pulse cannot be saturated individually. Therefore, stable and intense seed pulses are required.

3.1.2 Direct seeding

The second approach to all-optical synchronisation relies on an octave-spanning Ti:Sapphire [89, 90] oscillator, which is used for both seeding the OPCPA and its pump laser. In a similar way to our first solution, the output of the broadband oscillator is split into two equal parts, one to be parametrically amplified and the other to be injected into a regenerative amplifier and serve as a pump. This solution permits a radical simplification of our previous OPCPA scheme, as it suppresses the frequency-shifting set-up described above. However these oscillators require the introduction of highly advanced broadband chirped mirrors, that are still capable of maintaining a picojoule energy level within the bandwidth of a typical picosecond regenerative amplifier. Such level of the injected seed is required to compete efficiently with the ASE in the picosecond amplifier.

To achieve direct optical seeding of the OPCPA pump source, some design modifications need to be introduced in the femtosecond seed oscillator and the pump amplifier. First, by inserting a pair of frequency-shifted set of chirped mirrors and tuning the intracavity dispersion with a pair of wedges, the near-infrared (NIR) spectral components of the Ti:Sapphire oscillator can be enhanced without reducing the overall bandwidth nor the output power. Second, the regenerative amplifier is based on Nd:YLF, since it has a slightly blue-shifted gain material compared to Nd:YAG (Nd:YLF, λ=1053 nm, Nd:YAG, λ=1064 nm). Through these corrections of the OPCPA system, the spectral overlap between the pump and the seed lasers can be increased sufficiently to provide the necessary picojoule seed for the regenerative amplifier.

3.2 Optically synchronised OPCPA

In these experiments, several commercial and research types of PCFs capable of supporting the SSFS regime were investigated. Finally the commercial fibre NL-PM-750 (Crystal Fibre A/S) was selected since it exhibited a particularly clear solitonic feature in the NIR. The output spectrum of a 20-cm-long PCF injected with 2-nJ oscillator pulses is presented in figure 3-3.

The oscillator light was injected with a f=7.5 mm aspheric lens. The central wavelength of the spectral soliton was fine-tuned by adjusting the wave plate in front of the PCF and optimising the focusing. Figure 3-4 shows the optical coupling for frequency-shifting.

To improve mechanical stability of the PCF and avoid problems with optical damage, a monolithic fibre assembly was prepared by Menlo Systems GmbH. Larger-core-diameter end caps were spliced to the PCF. In addition, the end cap on the incoupling side was wedge polished to avoid retro-reflection into the Ti:Sapphire oscillator, which could destabilise the mode-locking process. The fibre assembly was fixed directly on the oscillator breadboard whereas the focusing and collimating lenses were mounded on xyz-translators. Mounting the fibre assembly in this way permits alignment-free operation for several weeks. A small adjustment of the incoupling objective is only necessary upon the realignment of the oscillator.

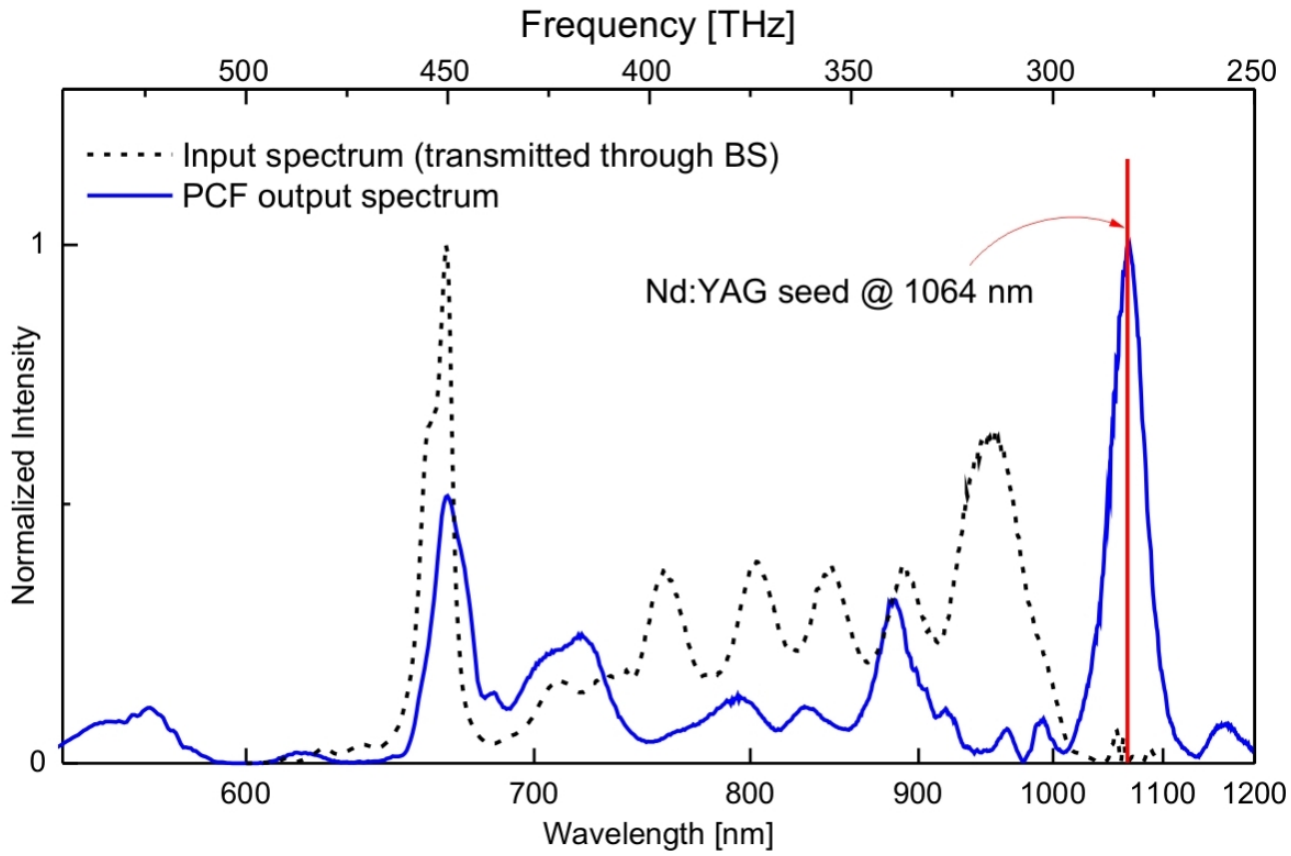

Figure 3-3 Wavelength-shift in the photonic crystal fibre. The solid curve shows an output spectrum optimised for injection seeding at 1064 nm. The input spectrum from the Ti:Sapphire oscillator is shown as dashed curved. BS: Beam splitter

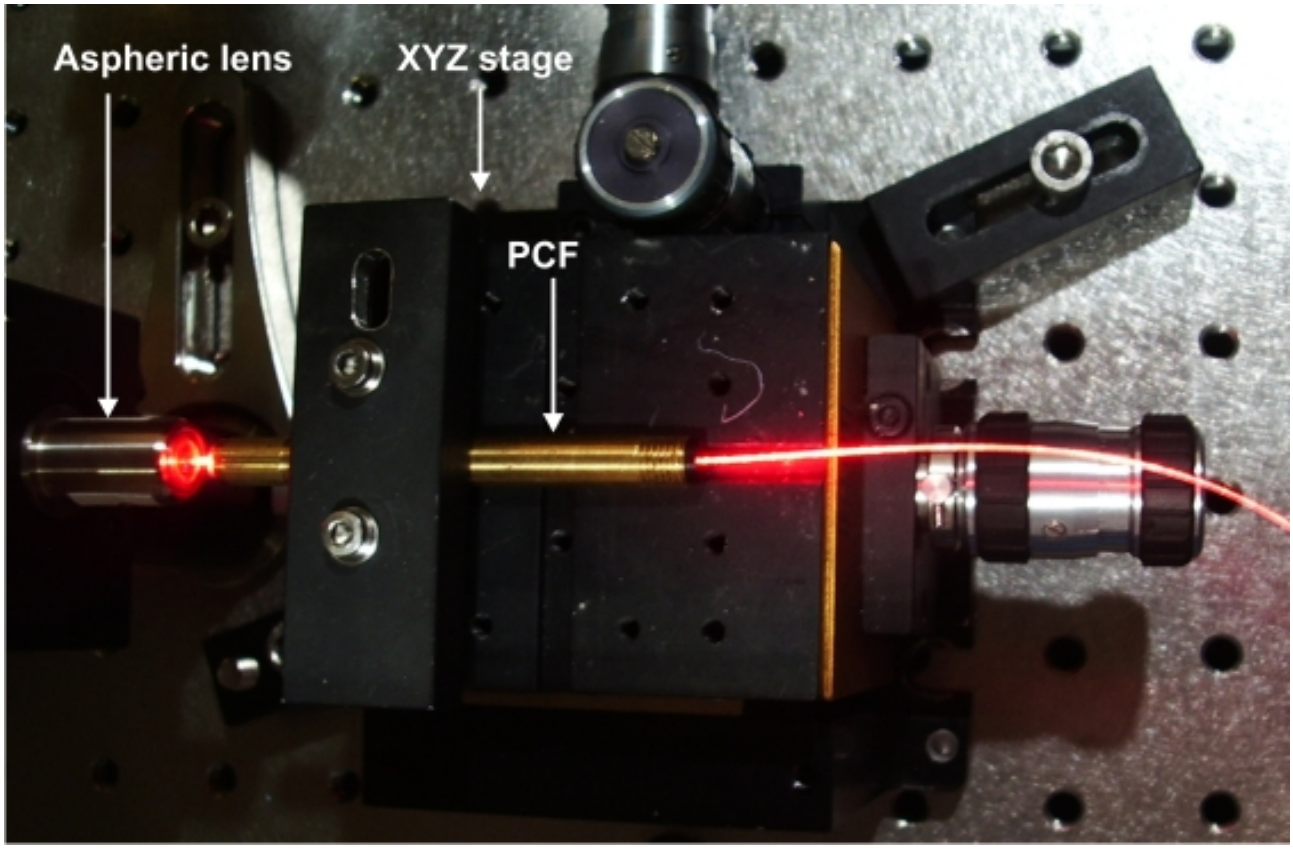

Figure 3-4 Fibre and coupling unit.

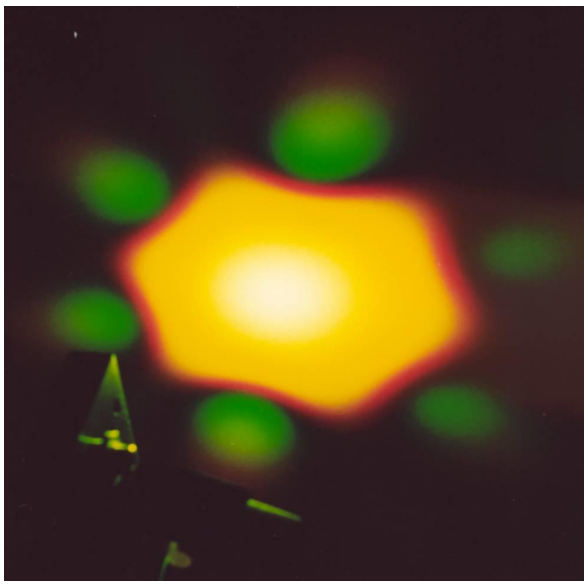

Figure 3-5 Beam profile at the output of the fibre. The beam pattern reveals the waveguide structure of the PCF.

The output of the PCF, shown in figure 3-1, is directed into a home-made Nd:YAG regenerative amplifier. The coupling efficiency into the amplifier can be optimised by tuning the position of the recollimating lens after the PCF, allowing for fine adjustment of the input seed beam divergence. The fibre delivers a Gaussian-like beam profile, as shown in figure 3-5 determined by its fundamental propagation mode. To protect the fibre from a back reflection or leakage through the out-coupling polariser of the regenerative amplifier, a Faraday isolator was introduced after the PCF. The estimated seed pulse energy contained within the gain bandwidth of Nd:YAG is ~2 pJ, which proved to be sufficient to obtain clean pulse amplification and suppress the nanosecond Q-switched-pulse background.

This is evidenced by figure 3-6a, which shows the intracavity pulse train corresponding to the build-up of the amplified pulse in each cavity round-trip. The regenerative amplifier operates in the regime of average power saturation and delivers 240-μJ pulses at a 10-kHz repetition rate (2.4 W average power). If the seed pulse from the PCF is blocked, the output power of the regenerative amplifier drops to 50 mW, which corresponds to the onset of an unsuppressed nanosecond Q-switched pulse. In order to generate a nanosecond pulse of the same energy as in the regime of seeded picosecond amplification, the opening time of the Pockel's cell need to be extended by 5-10 additional cavity round-trips. Therefore, for the given round-trip gain of the amplifier, the seed pulse energy is clearly sufficient to overcome ASE issues. An intracavity etalon was used to control the duration of the amplified picosecond pulse and prevent optical damage and self-phase modulation inside the regenerative amplifier. With a 0.8-mm-thick etalon, the regenerative amplifier delivers clean near-Gaussian 33-ps pulses. The background-free autocorrelation traces obtained with different intracavity etalons are shown in figure 3-6b.

The regenerative amplifier is based on a ∅4 mm Nd:YAG rod in a laser-diode cw-pumping cavity (model RD40, Northrop Grumman Cutting Edge Optronics). The length of the pumped

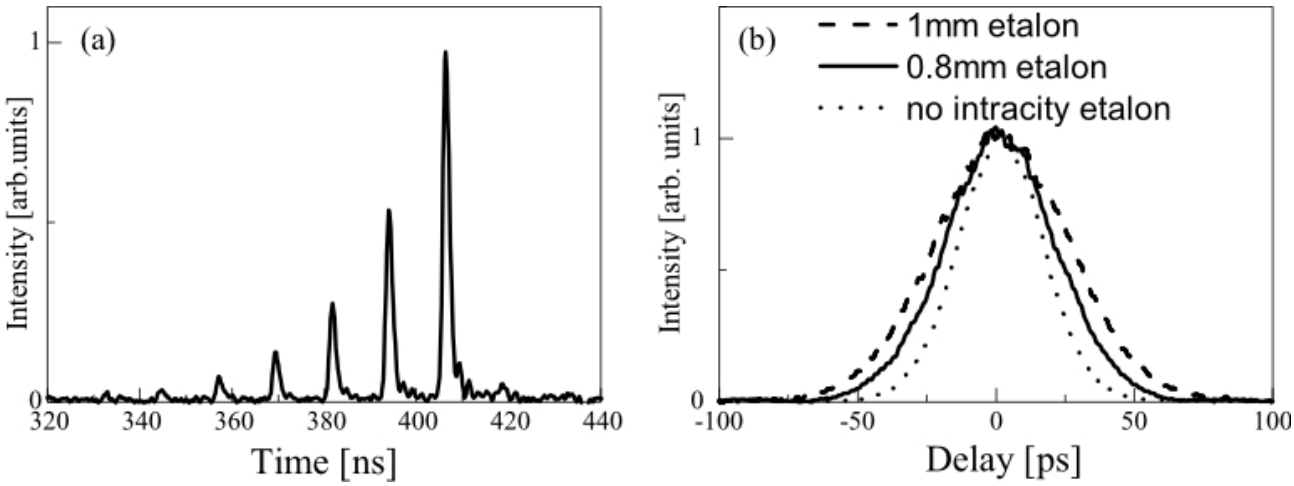

Figure 3-6 **Performance of the regenerative amplifier seeded with an optical solitonic pulse from a PCF: (a) intracavity pulse train of pulses amplified to the energy of 0.2 mJ; (b) background-free autocorrelation with and without intracavity etalon for a fixed number of intracavity roundtrips**

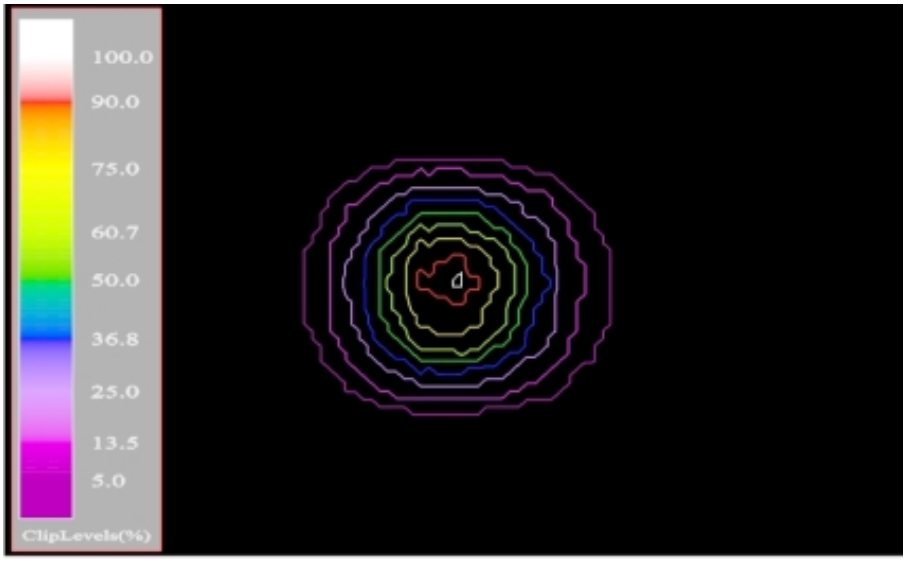

Figure 3-7 **Amplified beam profile.**

region is about 63 mm. The 5×5-mm-aperture RTP Pockel's cell was purchased from Bergmann Messgeraete Entwicklung KG. After a double-pass home-made cw-pumped 4×100-mm Nd:YAG booster, we obtained 1.6-mJ pulses at 1064 nm in a TEM_{00} mode. The amplified beam profile is depicted in figure 3-7. A Faraday rotator was installed between the passes to compensate thermally-induced birefringence of the YAG crystal and enable polarisation out-coupling. 0.8-mJ pulses at 532 nm were obtained in a 10-mm-long critically phase-matched type-I LBO crystal. The achieved 50% frequency doubling efficiency is an additional proof of the clean seeding and amplification process in our picosecond amplifier chain.

In the case of the directly-seeded Nd:YLF amplifier, the energy of the oscillator pulses confined within the gain bandwidth at 1053 nm was limited to approximately 1 pJ. However, this seed energy was still sufficient to overcome the level of spontaneous emission in this lasing medium that has a lower gain cross-section than Nd:YAG. The regenerative amplifier, based on the same

amplifier head as that of Nd:YAG, delivers up to 4 mJ at 1 kHz from a 3×63 mm Nd:YLF rod without any post-amplification. A KD*P Pockel's Cell with 1"-aperture is used to couple the pulses in and out because of its higher damage threshold. By introducing a 0.8-mm-thick intracavity etalon, clean Gaussian 27-ps pulses can be obtained after about 40 cavity round-trips. The measured beam pointing stability is better than 3 μrad. The SHG conversion efficiency in a 10-mm LBO crystal is up to 57% and the energy stability of the SHG pulse is better than 1.3%.

To investigate the usability of the frequency-shifted synchronisation technique, a single-stage parametric amplifier was built up based on a 5-mm-long noncollinearly phase-matched BBO. Due to the noncollinear geometry and tight beam focusing, the real interaction length in BBO was below 3 mm. The seed pulses were stretched in a dispersive glass block to attain efficient pump-to-signal energy conversion. The spectrum of the resultant 20-μJ signal pulses is depicted in figure 3-8 and corresponds to a nearly maximum theoretical bandwidth for the given crystal and pumping configuration.

In addition, the reliability of direct seeding was tested in one- and two-stage parametric amplifiers pumped by the directly seeded Nd:YLF regenerative amplifier as introduced in figure 3-1. The seed pulses were down-chirped to approximately 40 ps in a negative dispersion stretcher, based on holographic transmission diffraction gratings. The stretcher overchirped the seed pulses to compensate for the positive dispersion in the programmable acousto-optic filter (DAZZLER, Fastlite) and obtain an adequate temporal overlap between the pump (27 ps) and seed pulses (25 ps) at the OPA crystal. With the available SHG power of the Nd:YLF amplifier, the broadband pulses are amplified with energies up to 50 μJ for a single-stage OPA and 150 μJ in two stages in 4-5-mm-thick non-collinearly pumped BBO crystals. The two BBO crystals in the two-stage configuration were first pumped by 300 mW and then by 1.2 W to minimise the bandwidth narrowing through amplification. The spectrum and the group delay of a compressed 11.3-fs pulse, obtained in a saturated single-stage OPA, and the corresponding pulse parameters are given in reference [135].

Remarkably, the performance of the broadband OPA shown in figure 3-8 is reliably reproduced each working day without any need to adjust the pump-seed delay, which has been previously impossible in the actively stabilised OPCPA setup [25].

3.3 Timing jitter

The evaluated residual timing jitter between the seed and the pump pulses lies in the sub-30-fs domain and could not be measured by optical cross-correlation techniques available to us. The above-shown results of parametric amplification, a type of cross-correlation measurement, reveal no traceable jitter. In this following section, the possible sources of residual timing jitter are discussed.

The most important contribution to the residual jitter in our system results from the cavity

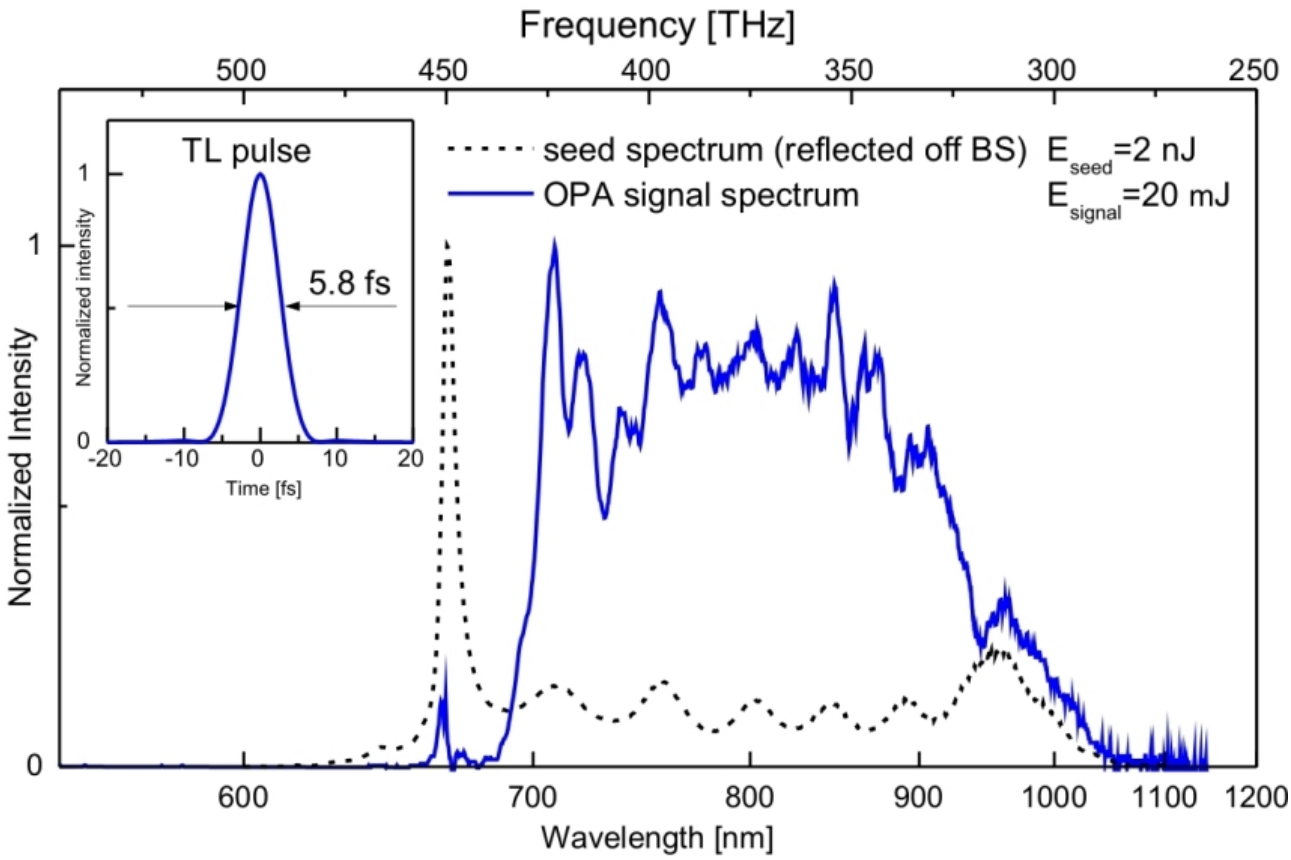

Figure 3-8 **Results of single-pass parametric amplification with PCF-seeded regenerative amplifier. Solid curve, amplified seed spectrum that supports sub-6-fs pulse duration assuming perfect recompression (inset); dashed curve, seed spectrum.**

length drifts of the Ti:Sapphire oscillator and of the regenerative amplifier. The short-term drift caused by mechanical instability can be disregarded, because the time span between the pulse injection into the regenerative amplifier and the Ti:Sapphire pulse injection into the OPCPA stage is merely 300-400 ns, well below the period of conceivable vibrations in a laboratory. The long-term drift is related to the thermal expansion of the cavities of the regenerative amplifier and the seed oscillator and depends on the ratio of the cavity lengths and the number of cavity round-trips from the moment of seeding of the regenerative amplifier. With simple thermal stabilisation of the laser base plate, it should be possible to control the cavity length to within a fraction of 1 μm. In addition, thermal drift can be compensated by choosing approximately equal lengths of the oscillator and regenerative amplifier cavities, provided the rate of cavity expansion is similar.

In the case of PCF-based frequency-shifted seeding, another source of timing jitter is related to the intensity noise at the input of the solitonic fibre. Because of the nonlinear nature of SSFS, intensity fluctuations of the Ti:Sapphire oscillator give rise to a variance of the soliton wavelength-shift, which is translated, through the group delay, into a timing jitter of the soliton part of the field at the output of the fibre, used as a seed in our experiments. The sensitivity of the soliton to the variations of the input intensity was evaluated using a numerical model of SSFS in PCF [88] which uses the generalised nonlinear Schrödinger equation, including high-order dispersion effects and the Raman response of fused silica. According to these simulations, a 1% variation in the input pulse energy gives rise to additional spectral, $\delta\lambda$, and temporal, δt, shifts of the soliton estimated as:

$$\frac{\delta t}{\Delta t} \simeq \frac{\delta\lambda}{\Delta\lambda} \simeq 0.7\%, \qquad \textbf{(3-1)}$$

where Δt and $\Delta\lambda$ are the time and wavelength Raman-induced shifts of the soliton in the absence of input energy variations. For the PCF length used in these experiments, Δt is $\sim$5 ps, which corresponds to $\delta t \simeq 30$ fs. Potentially, this timing jitter can be reduced through the optimisation of the PCF dispersion profile. In addition, it must be pointed out that this jitter estimation is rather conservative because the pulse-energy noise of a Ti:Sapphire oscillator can be below 0.2% RMS [91].

3.4 Conclusion

In conclusion, a significant improvement in OPCPA synchronisation was demonstrated as well as a substantial reduction of the complexity and cost of the entire system. Our frequency-shifting method opens the way to combine ubiquitous Nd-based picosecond amplifiers and emerging 1-ps-range Yb-based amplifiers with widely available several-nJ broadband Ti:Sapphire seed oscillators, when no spectral overlap with the pump is achievable. Recently this technique was successfully implemented to a 640 fs fibre-based chirped amplifier pump source in a 2 MHz-OPCPA system producing 500 nJ pulses with 20 fs pulse duration [34]. The pump pulses were derived from a Ti:Sapphire seed laser after soliton generation in a photonic crystal fibre and

amplification to 15.5 μJ in a three-stage fibre-amplifier.

Direct seeding permits a radical simplification of an OPCPA scheme based on a stand-alone pump source and a broadband seed, as it suppresses the frequency-shifting set-up. However these oscillators require the introduction of highly advanced broadband chirped mirrors, that are still capable of maintaining a picojoule energy level within the bandwidth of a typical picosecond regenerative amplifier. Intermediate fibre amplifiers can be used to increase the seed energy level [31] before the regenerative amplifiers. In addition, they allow for improved spectral features and beam profile, leading to improved seed incoupling ratios.

Our simple all-optical seed-pump pulse synchronisations permit hassle-free parametric amplification of ultrashort light pulses and can be straightforwardly scaled according to the energy of the amplified pump pulse.

4 Mode-locked thin-disk oscillator

4.1 Thin-disk concept

One of the major challenges in the development of high average power solid-state lasers is the thermal management of the laser cavity components, and in particular of the laser medium. Since a substantial amount of the pump radiation is converted into heat, thermal effects such as thermal lensing or thermal birefringence are particularly pronounced in the laser medium. Ultimately they can lead to a thermal fracture of the material. In addition, nonlinear effects inside the laser material can lead to severe degradations of the laser characteristics via self-focusing or self-phase modulation. These phenomena originate respectively from the spatial and temporal dependence of the intensity, which are coupled into a modification of the material refractive index by the generation of a nonlinear polarisation.

The thin-disk concept, as shown in figure 4-1, relies on a very thin laser material mounted on a large heat sink [92]. Through this geometry, a large ratio of the cooled surface to the heated volume can be realised. Consequently, highly efficient heat removal is obtained, giving rise to only a small temperature increase as compared to the dissipated power. Since the diameter of the pump beam is much larger than the laser material thickness, the configuration leads to a quasi-longitudinal heat flow along the optical axis of the laser. The associated temperature profile is nearly homogeneous within the pumped region and causes only weak thermal lensing and depolarisation losses. Thermal aberrations, confined to the border region of the pump volume, can be neglected by designing the cavity in which the laser mode is slightly smaller than the pumped area. Thanks to its unique cooling capacity, the thin-disk geometry allows the generation of laser radiation with high beam quality even at extreme pumping intensities.

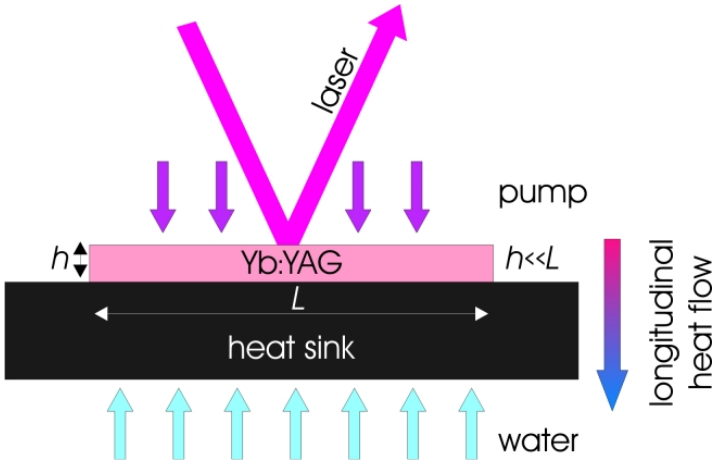

Figure 4-1 Thin-disk principle.

In the thin-disk approach the active medium is pumped from the top, typically from fibre-coupled laser diodes, resulting in a very short absorption length. The typical thickness of a disk lies between 100 and 300 µm, while its diameter is usually of a few mm. To ensure

efficient absorption of the pump, a multi-pass optical scheme is implemented by means of a parabolic mirror, which re-collimates the pump in combination with a roof prism to redirect the unabsorbed light onto the disk as depicted in figure 4-2. Subsequently, the thin-disk requires distinctive coatings for its front and back surface. The front side necessitates an anti-reflection coating at the pump wavelength and at the lasing wavelength, while a high-reflection coating at both wavelengths is deposited on the back side. The thin-disk can be then used in the cavity as a folding mirror allowing for a double pass per round-trip through the gain.

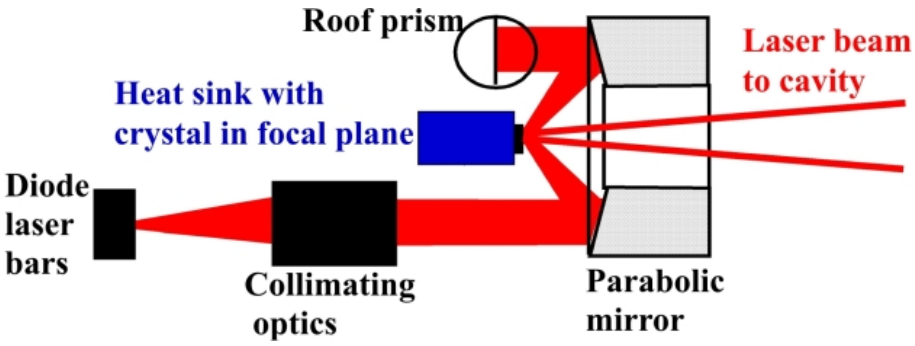

Figure 4-2 Set-up of a thin-disk laser head.

The limited thermal lensing attached to the thin-disk makes the technology particularly attractive for designing high-average-power mode-locked lasers. Indeed, one of the prerequisites for mode-locking is a diffraction-limited beam quality because the pulse formation process would undergo perturbations from the competition between higher-order transverse modes. Another major advantage is the limited amount of nonlinear phase-shift introduced by the thin-disk, relaxing the problem of the dispersion management at higher energy level (see section 2.4.2).

4.2 A scalable system

One of the most interesting features of the thin-disk concept is its direct power scalability arisen from its quasi-longitudinal heat flow. By using larger disk diameters while keeping the pump density constant, the temperature profile of the disk is almost unchanged [93] and the ouput power is increased accordingly. Based on this technology, commercial systems were developed using multiple thin-disk heads reaching more than 10 kW of CW output power, and 8 kW after coupling into a high-power fibre delivery system [94]. In the ns-pulsed regime, energies in the hundreds of millijoule level were demonstrated in a cavity dumped system [95].

In section 2.4.2, the basic structure and mode of operation of semiconductor Bragg mirrors (SBRs) were introduced. In a similar manner to the thin-disk, the SBR geometry leads to a longitudinal heat dissipation since the absorber layer is much smaller than the beam diameter. By doubling the mode area on the SBR, a doubling of the pulse energy is possible without affecting the pulse formation. Thermal and mode-locking issues can be successfully tackled even at high-power levels, as long as the laser parameters are chosen properly (intracavity dispersion, mode size in the gain and on the SBR, SBR design and gain medium properties).

Combining both technologies offers a power-scalable solution for passively mode-locked lasers. Providing a suitable gain medium and a SBR design, it allows for the generation of ultrashort pulses at high-average power directly from an oscillator. Mode-locked powers up to 80 W were generated from an Yb:YAG thin-disk laser [96]. Recently Neuhaus *et al.* demonstrated energies up to 25 µJ directly from an Yb:YAG oscillator by implementing a multi-pass design through the thin-disk [32]. In the next section, the critical points for designing femtosecond lasers at high-average power will be reviewed.

4.3 Design consideration

4.3.1 Gain material

The conception of a femtosecond oscillator operating at high-average power calls for a meticulous attention in the choice of a laser material. Besides the spectroscopic properties, the optical, thermal and mechanical properties of the material are important parameters. While the dopant essentially defines the spectroscopic behaviour, the thermo-mechanical and thermo-optical properties are typically given by the host material. The combination of laser ions and host material determines the relevance of a laser material for the generation of femtosecond pulses at high-average power.

Over the past decades, Yb:YAG has emerged as a prominent material for systems with high-CW average power and high-pulse energy [79]. Some of the most interesting properties of the material are listed below:

1. very low quantum defect (efficiency $> 91\%$ at 940 nm)
2. large absorption band (10 nm @ 940 nm [79])
3. high thermal conductivity of YAG (6.5 W/mK @ 5% Yb doping [98])
4. broad emission band (~ 6 nm; 100 fs with Kerr-lens mode-locking [99])
5. high doping levels possible without quenching ($> 20\%$)
6. no excited-state absorption or up conversion
7. high tensile strength of the host material
8. long lifetime of upper laser level (~ 1 ms)
9. cubic structure
10. availability of high-quality crystals with large dimension.

Because of the low heat deposition resulting from a low quantum defect, the Yb^{3+} ion is particularly well suited for high-power applications. Despite a high lasing threshold inherent to its quasi-three-level lasing scheme, Yb:YAG is very attractive for diode-pumped systems. Indeed, its absorption band is located in the near-infrared, a region for which reliable high-power, high-

brightness InGaAs diodes are available. Furthermore, its large absorption band loosens the requirement on the temperature stabilisation, hence the stabilisation of the emission wavelength, of the laser diodes. Its high thermal conductivity permits high pumping intensities for increased gain. In addition, its cubic structure leads to isotropic properties resulting in a homogeneous distribution of thermo-mechanical stress inside the material, which is particular beneficial for achieving a uniform cooling. Finally, its very simple lasing scheme without higher-lying levels excludes excited-state absorption and up-conversion losses. With high-density pumping capacity and high cooling efficiency, the lasing threshold is easily overcome and high optical efficiency achieved. Yb:YAG is available with high doping concentrations without major degradation of the material spectral properties. Thus, thinner crystals with higher doping concentrations can be produced, conducting to a shorter pump absorption length, a reduction of material dispersion and nonlinear phase-shift. Yb:YAG has been inserted into various laser geometries with impressive results for slabs [33] or rods [100]. However, the diode-pumped thin-disk approach showed the most versatile laser developments for both oscillator and amplifier systems [94].

During the last decade, the interest for ceramic laser media has dramatically increased with the availability of improved quality samples. Compared to the melt growth technique, ceramic materials offer numerous advantages: reduced costs, short production time and large aperture. In addition, their fabrication allows designs of composite structure (doped/undoped, different doping ions) with complex shapes. Using the proper fabrication technique, Yb:YAG ceramic material can be produced with similar optical quality to the crystalline form [101]. In the future, high-power thin-disk lasers and amplifiers could benefit from the development of ceramic media with smooth gradient dopant distributions. Such doping profile is associated with a smoother temperature profile, hence reduced thermal effects are expected at higher pumping intensities [102]. Despite all these interesting features, the new ceramic technology requires further developments in the production of high-quality material before large-scale commercialisation.

More recently developed, the Yb^{3+} doped sesquioxide materials have become particularly attractive for the development of new high-power femtosecond sources based on thin-disk technology [103, 104]. They exhibit good thermo-mechanical properties, while supporting a larger amplification bandwidth than Yb:YAG [105]. Some of these new materials will be reviewed later in section 4.6.2

4.3.2 Resonator design

The cavity design is at the centre of the conception of any lasers, as it will essentially determine the laser performances in terms of output power, beam profile and operation stability. The laser resonator can be precisely modelled through ABCD-matrix calculations [107] when the characteristic behaviour of each cavity elements is well-defined. Additional conditions on the laser mode arise for mode-locked oscillators to ensure stable pulse operation (see equation 2-22). In this section, the most crucial points for the design of a high-energy resonator are discussed.

As mentioned earlier, the presence of higher-order modes corrupts the pulse formation process. Therefore, the cavity should support only the fundamental transverse mode. This condition can be easily fulfilled by choosing a laser mode slightly smaller than the pump mode, typically 80%, while keeping a good power extraction from the pump. Placing an aperture in the cavity can enforce fundamental-mode lasing but it will result in additional cavity losses.

In the case of a resonator subject to thermal lensing, the laser can operate in the fundamental transverse mode only within two stability zones, each of them exhibiting distinct stability characteristics [106]. Magni *et al.* demonstrated that the misalignment sensitivity is larger in zone II, where the axis displacement rapidly diverges towards one end. This becomes an issue for systems with relatively small stability range, which is more often the case in high-power lasers due to their increased thermal lensing. Even though thermal lensing is moderate in a thin-disk geometry, it is still beneficial to design a cavity lasing in zone I, ideally operating in the centre of the stability range. In this case, the dependence of the laser mode radii is the weakest on the change of the dioptric power of the thermal lens.

Kerr-nonlinearity may yield to a degradation of the spatio-temporal properties of the soliton pulses. Therefore a resonator with large beam diameters is preferable to reduce the intracavity intensity. On the other hand, larger laser modes lead to a higher sensitivity of the cavity to small perturbations and cause a decrease of the cavity stability range, inversely proportional to the beam radius squared [106].

In section 2.4.2, the problems of Q-switching instabilities in passively mode-locked oscillators with saturable absorbers were briefly introduced. Stable CW mode-locked operation requires a threshold intracavity pulse energy. Below this value, the oscillator output consists of a mode-locked pulse train which amplitude is typically modulated in the kHz range. Some of these pulses will then have a drastically increased peak intensity, in some cases incompatible with the operation of some cavity elements (SBR, chirped mirrors). As shown in equation **(2-22)**, strong saturation of the SBR relaxes the condition on the intracavity pulse energy. A cavity design with smaller mode on the SBR can therefore reduce the tendency towards Q-switched mode-locking. On the other hand, this can also lead to SBR damage or pulse break up [108].

In the end, there is a trade-off between minimising the thermal effects by designing a cavity with larger modes and increasing the mechanical and pulse stability by operating the laser with smaller mode diameters.

4.3.3 Dispersion

As mentioned earlier in section 2.4.2, soliton mode-locking requires a balance between the group delay dispersion and the self-phase modulation. Scaling up the pulse energy leads to an enhancement of the Kerr-nonlinearity inside the cavity, which requires a readjustment of the cavity dispersion to stabilise the pulse formation process, as shown in equation **(2-23)**. Dispersion management develops into a problematic at higher energy levels, as it becomes

difficult to combine high dispersion values with low losses and large bandwidths.

In high-power soliton mode-locked oscillators, the dispersion is usually introduced by a series of chirped-mirrors rather than by a prism pair to reduce the nonlinear effects inside the cavity. Commercially available chirped mirrors typically range between -50 fs^2 and -1000 fs^2 of negative group delay dispersion (GDD).

In comparison to other laser designs, the nonlinear phase-shift introduced by the thin-disk itself is very small, owing to the ∼100 µm thickness of the gain medium. The thin-disk approach is hence particularly well suited for designing mode-locked oscillators with high intracavity intensity. However, at low repetition rates (< 10 MHz), thus for long cavities, the nonlinearity of air may become predominant among all source of nonlinearities and difficult to compensate by commercial dispersive mirrors with typical group delay values below -1000 fs^2. Table 4-1 shows a comparison of nonlinear contributions between different elements in a 10 MHz cavity.

Material	n_2 (cm^2/W)	L (mm)	γ_{SPM} (rad/W)
Air	$4 \cdot 10^{-19}$	30000	$4.7 \cdot 10^{-9}$
Yb:YAG	$6 \cdot 10^{-16}$	0.8	$1.8 \cdot 10^{-10}$
Fused silica	$3 \cdot 10^{-16}$	1	$1.2 \cdot 10^{-10}$

Table 4-1 Comparison of nonlinear contributions in a 10-MHz thin-disk oscillator assuming an average 1-mm beam radius.

Three different laser approaches have successfully overcome the problems of dispersion compensation with increasing output pulse energies. The first concept relies on the decrease of the total self-phase modulation by operating the laser in helium [109]. Indeed, helium exhibits a nonlinear refractive index about 100 times lower than air [110]. Using this approach, pulse energies up to 11.3 µJ were obtained from an extended cavity thin-disk oscillator [111]. Though relatively easy to implement, purging continuously the cavity with helium is a pricey solution and is therefore not suited for a prolonged operation of the laser system.

An alternative technique makes use of a high out-coupling ratio to reduce the intracavity intensity and thus the total nonlinearity [32]. Multiple passes through the gain medium allowed for a out-coupling value of 78% by an increase of the cavity round-trip gain. While offering a very elegant solution to the nonlinearity management, a muli-pass arrangement requires a complex resonator design, which is inevitably bond to a smaller stability range. In such systems, the thermal behaviour of each optical elements needs to be precisely known for an appropriate modelling of the resonator. This becomes particularly challenging for lasers with various optical elements exhibiting different thermal properties, as it is the case in reference [32].

The third approach, which is the one followed in this thesis, relies on the design of highly dispersive mirrors to compensate for the self-phase modulation in air. Here, the main advantage is the generation of high-energy pulses directly in air from a simple resonator design. Using this concept, we were able to demonstrate stable single-pulse operation in air up to 5 µJ using only three high dispersive multilayer mirrors for a total negative GDD of -15000 fs^2 [97].

Despite their large dispersion level, the mirrors still supported a bandwidth over 20 nm and had excellent reflectivity($> 99.9\%$).

4.4 1-ps 6−μJ thin-disk oscillator

4.4.1 Amplifier head

The laser module used in our Yb:YAG thin-disk oscillator was developed at the Institut für Strahlwerkzeuge in Stuttgart and is now commercially available from the company Dausinger-Giesen GmbH. It consists of an amplifier head pumped via fibre-coupled laser diodes emitting up to 500 W of average CW power at 940 nm.

At the front, a parabolic mirror images the disk on itself to make use of the unabsorbed light in each pass. At the back, a turning prism allows for a doubling of the passes. In total, the pump light is directed 16 times into the thin-disk and almost complete absorption is achieved. To minimise thermal effects on the parabolic mirror which could affect the pump spot, the front panel is water-cooled.

By slightly decreasing the distance between the fibre output and its re-collimating lens from its optimal position, the pump image on the disk can be shaped into a more diffuse spot. This configuration allows for a smoother temperature gradient at the edge of the pump spot and therefore a reduction of thermal aberration in this vicinity, which is essential for maintaining a fundamental transverse mode. The pump diameter was set to 2.8 mm to allow for a reasonably large stability range and moderate nonlinear effects.

The thin-disk used throughout this thesis had an Yb^{3+}-doping concentration of 7% and was polished down to 200 μm with a small wedge (0.1°) to eliminate interferences between satellite pulses in the gain material originating from imperfect anti-reflection coatings. A parallel thin-disk would indeed act as a Fabry-Perot interferometer, hence limiting the pulse bandwidth through etalon effect and disturbing the pulse formation process. The edges of the front surface of the disk were additionally smoothened, so that lateral parasitic lasing becomes impossible despite the high amplification gain.

The crystal features a concave curvature without pumping, which is caused by the soldering procedure on the heat sink. Interferometric measurements were carried out to check the surface quality of the disk and determine its initial curvature. The changes in the disk dioptric power were investigated under pumping condition by analysing the beam parameters of an incident beam reflected from the disk. This measurement was undertaken with another disk with identical crystal thickness and doping concentration. The lasing behaviour of our laser confirmed that both disks had similar curvatures.

Figure 4-3 shows that for higher pump power, the thin-disk flattens. This behaviour can be easily explained by the higher heat deposition at the centre of the disk, which creates an

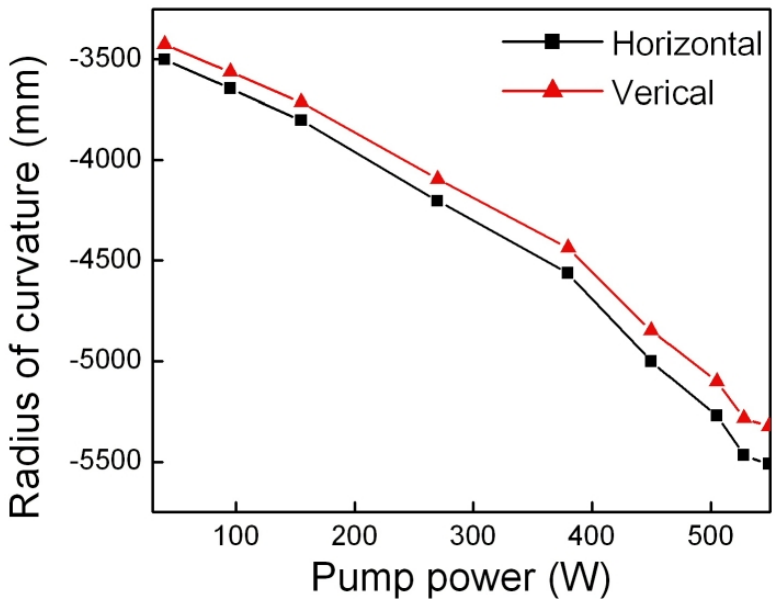

Figure 4-3 Thermal-induced lens of an Yb:YAG thin-disk under pumping condition.

additional defocusing effect. The ellipticity of the disk is negligible, which permits a resonator design without any particular astigmatism compensation scheme.

4.4.2 Resonator

For modelling the laser, thermal effects on the cavity mirrors and in the SBR are neglected. The target parameters for the cavity are reported below:

- total cavity length: ∼15 m for ∼10-MHz repetition rate,
- beam diameter on the disk: ∼2.4 mm for single mode operation (∼2.8 mm pump spot),
- disk curvature under pumping: ∼ROC−4500 mm,
- beam diameter on the SBR: <2 mm to avoid Q-switch instabilities,
- beam diameter on the output coupler: >2 mm to avoid excess nonlinearity in the material,
- small angle of incidence on the mirror : to avoid astigmatism.

Simulations through ABCD matrix calculations and experimental optimisations led to a very simple resonator with a double-pass through the thin-disk as shown in figure 4-4. Three curved mirrors control the critical mode sizes on the disk, output coupler and SBR. The beam radius inside the resonator is plotted in figure 4-5. Additional high-reflectors are inserted as folding mirrors to keep the set-up relatively compact. With this arrangement, the footprint of the laser is less than 1.5 m x 0.5 m. The different optical elements are listed in table 4-2.

To check the thermal stability of the laser, the stability range of its equivalent optical system is first determined as described in reference [106]. The resonator can be modelled by two plane mirrors that enclose a lens with variable focal length f between two generic optical systems

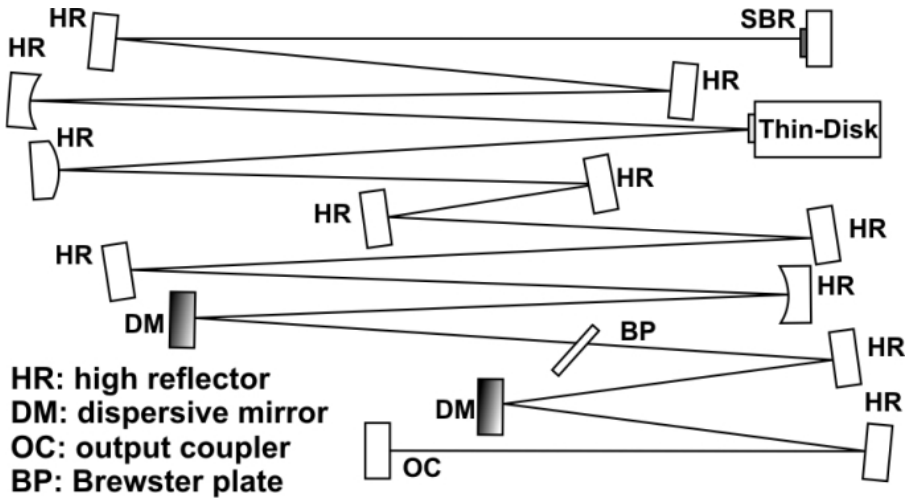

Figure 4-4 **Schematic of the laser set-up.**

Element	ROC (mm)	Distance
OC	∞	
M1	-5000	OC-M1: 5480 mm
M2	$+3000$	M1-M2: 3140 mm
TD	-4600	M2-TD: 1030 mm
M3	-4000	TD-M3: 1000 mm
SBR	∞	M3-SA: 2420 mm

Table 4-2 **Cavity design. OC: output coupler, M_i: mirror, TD: thin-disk.**

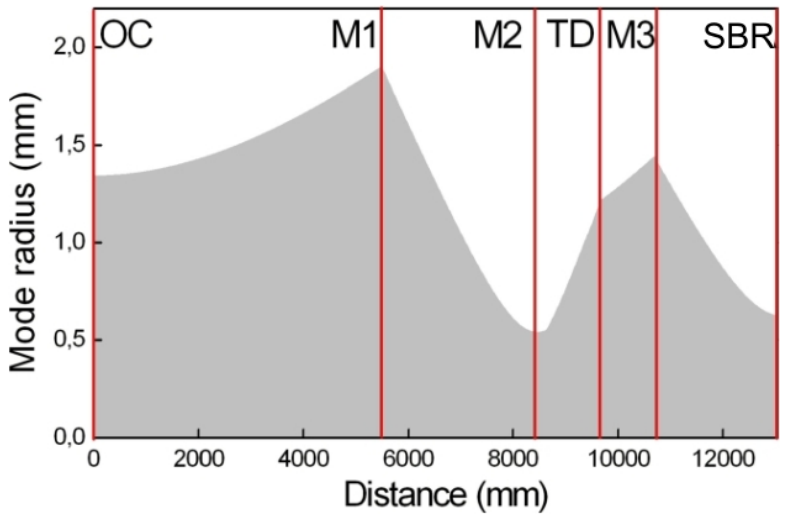

Figure 4-5 **Calculated $1/e^2$ beam radius inside the cavity.**

with transfer matrix $\mathbf{T_1}$ and $\mathbf{T_2}$. Using the formalism of [106], the transfer matrix $\mathbf{T}$ of the equivalent optical system, from the output-coupler to the SBR is given by:

$$\begin{aligned}
\mathbf{T} &= \mathbf{T_1} \cdot \begin{bmatrix} 1 & 0 \\ -\frac{1}{f} & 1 \end{bmatrix} \cdot \mathbf{T_2} \\
\text{with } \mathbf{T_1} &= \begin{bmatrix} 1 & 5480 \\ 0 & 1 \end{bmatrix} \cdot \begin{bmatrix} 1 & 0 \\ \frac{1}{-2500} & 1 \end{bmatrix} \cdot \begin{bmatrix} 1 & 3140 \\ 0 & 1 \end{bmatrix} \cdot \begin{bmatrix} 1 & 0 \\ \frac{1}{1500} & 1 \end{bmatrix} \cdot \begin{bmatrix} 1 & 1030 \\ 0 & 1 \end{bmatrix} \\
\text{and } \mathbf{T_2} &= \begin{bmatrix} 1 & 2420 \\ 0 & 1 \end{bmatrix} \cdot \begin{bmatrix} 1 & 0 \\ \frac{1}{-2000} & 1 \end{bmatrix} \cdot \begin{bmatrix} 1 & 1000 \\ 0 & 1 \end{bmatrix}
\end{aligned}$$

The simulation shows that the cavity features two stability ranges: one for positive focal lengths of the disk and one for negative values, which correspond respectively to zone I and zone II . The laser is stable for $f \in [-3900 \text{ mm}, -980 \text{ mm}] \cap [1700 \text{ mm}, +\infty[$.

At our pump intensities, the disk does not experience a change from concave to convex curvature. As a result, the laser can only operate in zone I. The focal length F of the resonator equivalent optical system is calculated in order to estimate the misalignment sensitivity due to thermal lensing. From figure 4-6, it can be seen that the change of the disk focal length causes only a moderate change of the resonator characteristics.

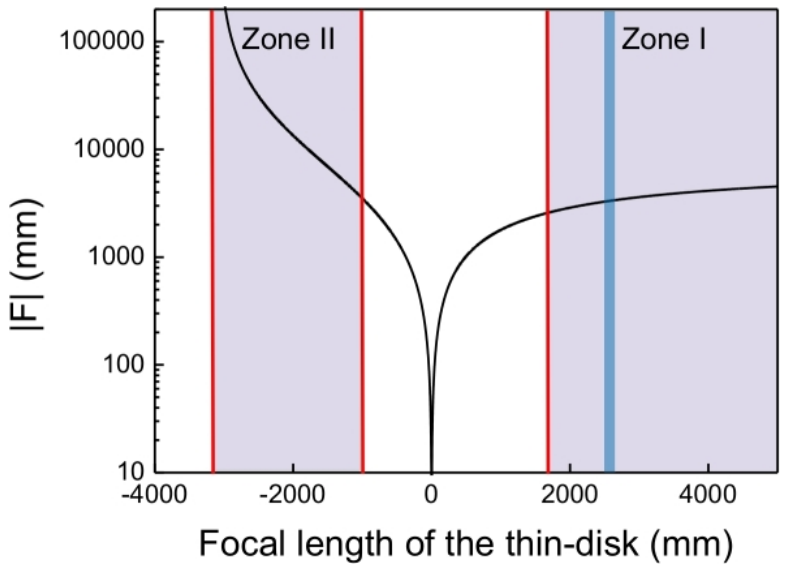

Figure 4-6 Absolute value of the focal length of the equivalent optical system as a function of the disk focal thermal lens. The blue vertical line represents the operating point of the laser.

4.4.3 Experimental realisation

Because of its cubic lattice, the Yb:YAG material does not induce linear polarised laser light. Mode-locking operation necessitates nevertheless a stable direction of polarisation. In order to

restrict the lasing polarisation, a 2-mm glass plate is inserted under Brewster angle to introduce higher losses for the vertical polarisation. This plate is installed between the output coupler and the next curved mirror, where the mode-sizes are relatively large to avoid additional nonlinear effects. The thin-disk leads to four residual reflections due to a relatively high value of its anti-reflection coating (0.5%). These beams had to be blocked by two water-cooled apertures, placed in front of the thin-disk.

Mode-locking is achieved by applying an external perturbation to the laser when it operates in the CW regime. For this purpose, the output coupler is mounted on a translation stage. The pulse formation process is then initiated, when the user releases the preloaded spring. The maximum power can be extracted with a 12% output coupler. At the other end of the cavity, a SBR is introduced to passively mode-lock the oscillator. The selected SBR is commercially available (BATOP SAM-1040-1-500fs) with a saturation fluence of 90 $\mu J/cm^2$ and an modulation depth of 0.5%. The non-saturable losses are quite high, with about 1%. The relaxation time constant is 500 fs. Experiments were also undertaken with SBRs from the same supplier with 0.4% and 0.8% modulation depth but lead to poorer results. In the first case, the pulse duration was not as short and in the second case, the laser experienced some instabilities leading to some damage of the SBR.

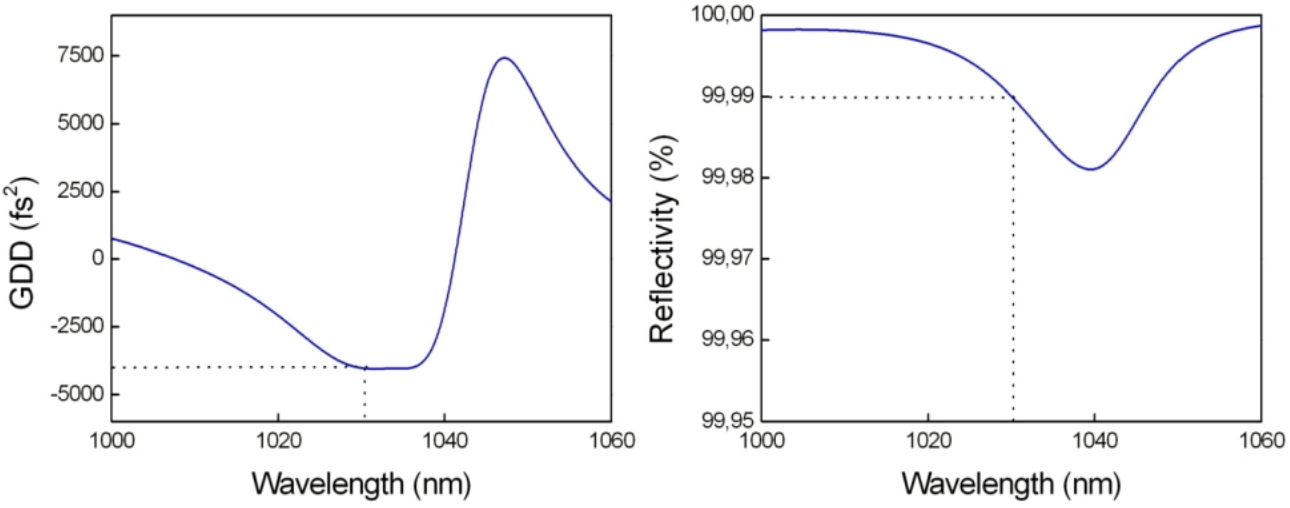

Figure 4-7 Dispersion (left) and reflectivity of the highly dispersive mirror HD51.

These parameters are surely not ideal for an oscillator delivering pulses in the microjoule level. Indeed, ideally the SBR should exhibit a low saturation fluence to allow for a lower threshold against Q-swichted mode-locking, see equation **(2-22)**. In addition, the non-saturable losses should be small to limit the heat deposition. In the oscillator, the intracavity power reaches approximately 500 W, the SBR absorbs then approximately 5 W of average power. In order to minimise thermal effects, the SBR is fixed to a water-cooled mount.

For this thin-disk oscillator, new dispersive mirrors were produced with a negative group delay dispersion of -4500 fs^2 and a reflectivity $> 99.95\%$. The characteristics of these mirrors are plotted in figure 4-7. Using such mirrors, only few bounces are necessary to compensate for the

intracavity nonlinearity.

The cooling of the laser is managed by three independent circuits to isolate the most critical elements. Fluctuations of the flow rate should be as low as possible on the thin-disk, as they could generate mode-locking instabilities due to mechanical vibrations. The thin-disk is cooled down to 17°C by a water-to-air chiller with a temperature precision of 0.1° and a flow rate of 0.7 l/min. The parabolic mirror, SBR and beam blockers are also cooled using a water-to-water chiller. Though this water undergoes some seasonal temperature variations, it did not affect the laser performances. The laser diodes are temperature-stabilised by an automatic adjustment of the input water flow passing through the heat exchanger of their cooling unit.

4.4.4 Pulse characterisation

With an incident power of 310 W, the laser delivers 70 W of mode-locked average power resulting in an optical-to-optical efficiency of 22.6%. Switching from CW to mode-locked operation, an increase of the average output power in the range of $10-20\%$ is observed. The slope efficiencies for the two regimes are plotted in figure 4-8. With the selected SBR and the cavity parameters, self-starting pulsed operation was not possible. Mode-locking was nevertheless easily initiated through the moving-mirror technique, described in the previous section.

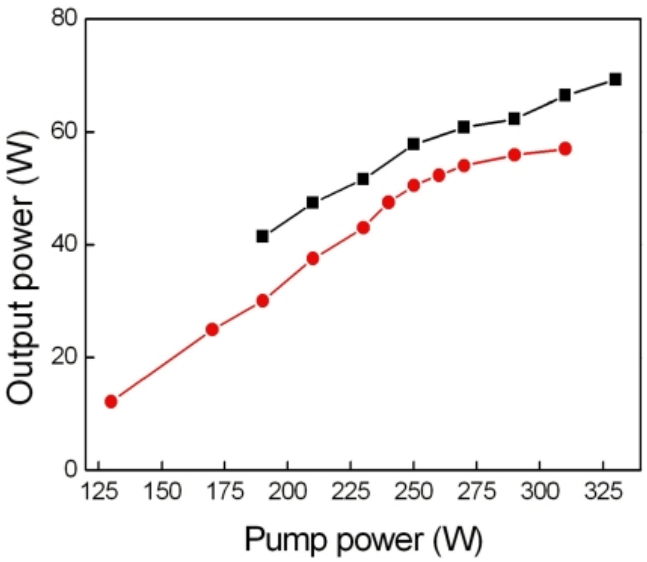

Figure 4-8 Efficiency of the thin-disk oscillator in CW (circles) and in ML regimes (squares).

At 11.5-MHz repetition rate, this corresponds to a pulse energy of 6 µJ. Single-pulse operation in air was confirmed by the high second-harmonic conversion efficiency reported in section 4.5. In previous works [112], the formation of multiple pulses simultaneously oscillating in the cavity has been the bottle-neck for scaling up the energy.

Beyond 310 W of pump power, the output power saturates at 70 W. A degradation of the mode quality is also visible, while pulsed operation becomes unstable. The cavity simulations did not suggest any dramatic modification of the laser mode at this pumping level. However,

these simulations only included a thermally-induced lens inside the gain medium. Additional thermal effects may arise in other cavity optical components, which eventually restrict the laser operation to lower pump powers. These effects are most likely to occur inside the saturable absorber, where there is a substantial heating due to the non-saturable losses.

Increasing the mode size on the SBR would help reducing those thermal effects. Unfortunately, inspection of these commercial SBR under a microscope reveals some surface defects (scratches, impurities, voids), which limit the usability of large spot diameters. Furthermore an increase of the mode size would be accompanied by a shortening of the resonator stability range. Ideally, an investigation using interferometric measurements under lasing operation should be undertaken to characterise precisely the thermal behaviour of the SBR. This would help designing resonators with larger invariance against thermal lensing. To allow further scaling of the pulse energy, implementation of new SBRs with lower non-saturable losses seems nevertheless unavoidable.

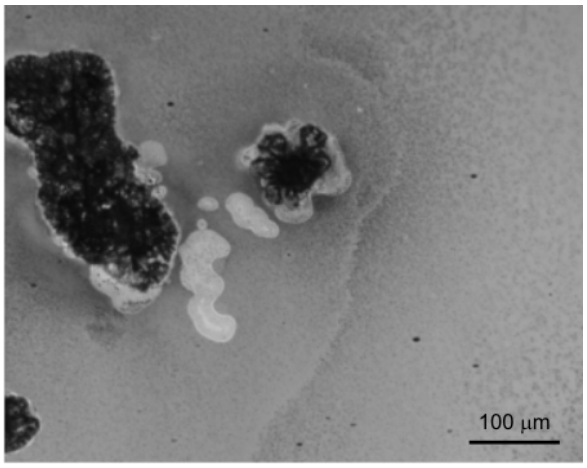

Figure 4-9 SBR damage.

Typically, the laser is operated with 62W of average output power for a total pump power of 260 W. If not mentioned otherwise, the following results were obtained at this power level. Under this condition, the laser performances were maintained for more than six months, at an average of 8 hours of continuous operation per day, without any noticeable degradation. Despite the large intracavity pulse energy, with over 50 µJ, the different components of the laser did not damage under regular use. Damages only occurred when the laser was submitted to extremely high mechanical perturbations, typically after accidentally knocking the optical table with heavy components. The consecutive vibrations cause brief but dramatical Q-switching instabilities. Figure 4-9 shows such damage spots. For a calculated beam radius of 640 µm on the SBR, the peak intensity reaches almost 9 GW/cm^2 assuming a Gaussian beam profile. The saturation parameter, defined as the ratio between the pulse fluence and the absorber fluence, is equal to 45 and thus relatively high. Under such strong saturation of the absorber, the pulse may break into closely spaced multiple pulses due to the reduced loss penalty for the following pulses [108]. However, this effect was never observed at this saturation level. Other works with similar parameters have also confirmed single pulse operation in this regime [109].

The spatial quality of the laser beam is characterised by measuring its M^2 parameter [56]. A fraction of the beam was focused using a 500-mm lens onto a CCD camera (WincamD) which recorded the beam waist across the focus. The laser beam profile and the M^2 measurement are presented in figure 4-10. By a proper optimisation of the pump and laser mode overlap inside the disk, the oscillator cavity supports only the TEM_{00} fundamental laser mode. This results in a near diffraction-limited beam with a measured M^2 below 1.1.

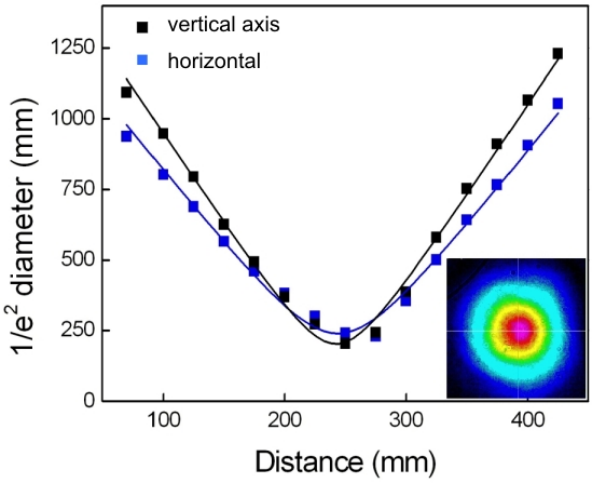

Figure 4-10 M^2 measurement and beam profile (inset) at 62 W.

Stable single-pulse operation is obtained with approximately -18000 fs^2 of negative group delay dispersion per cavity round-trip, using only two dispersive mirrors. In contrast to reference [109], the laser can simply be operated in air. The pulse duration was estimated from the measurement of their intensity autocorrelation using the autocorrelator Pulsecheck from APE GmbH. The pulses are nearly transform-limited with a FWHM pulse duration of 1.1 ps assuming a Gaussian shape, and a spectral bandwidth of 1.4 nm centred at 1030 nm. The pulse duration did not depend on the position of the Brewster plate inside the cavity. This confirms that the most important source of self-phase modulation originates from the ambient air. The thin-disk causes indeed only moderate nonlinearities, as calculated earlier in table 4-1.

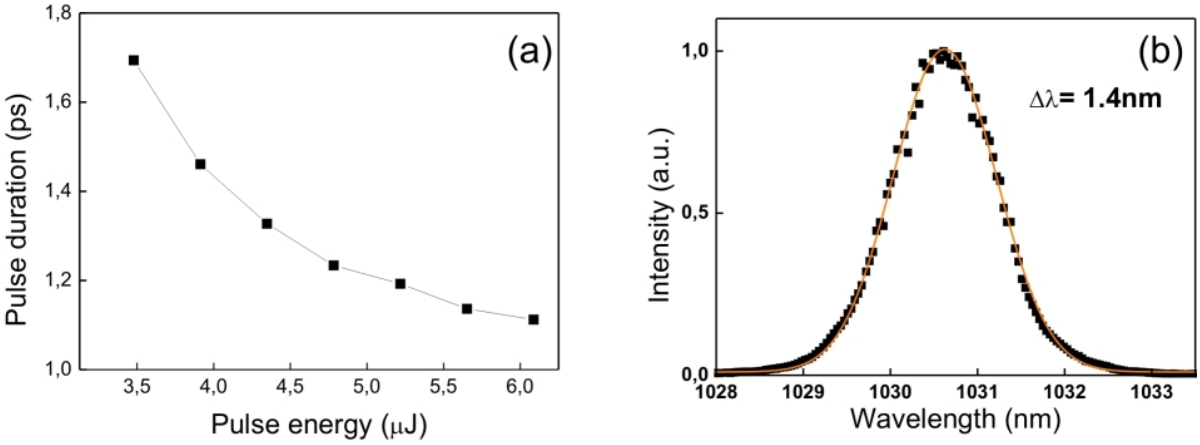

Figure 4-11 (a) Pulse durations at different output energies. (b) Optical spectrum at 62 W.

The evolution of the pulse duration at higher energy is depicted in figure 6-6a for a fixed

amount of intracavity dispersion. From this figure, it is apparent that the pulse duration is inversely proportional to the pulse energy, which is typical of soliton mode-locked oscillators. Shorter pulse duration at the highest pulse energy should be possible by decreasing slightly the intracavity dispersion. In this laser, the pulse energy from the oscillator is not limited by the onset of double-pulsing but by the degradation of the mode quality at higher pump power. This suggests that the dispersion is not yet optimised at an output pulse energy of 6 μJ.

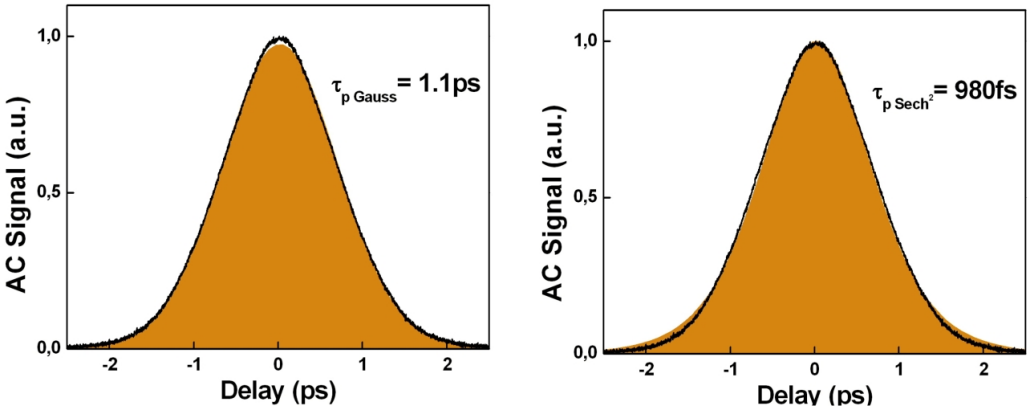

Figure 4-12 Gauss (left) and Sech^2 (right) fits of the oscillator pulses.

The fundamental soliton solution to the nonlinear Schrödinger equation is a pulse with a squared hyperbolic secant (Sech^2) temporal shape [38]. Figure 4-12 compares the Sech^2 and Gaussian fits of the pulse autocorrelation trace. From these pictures, it is difficult to determine the closest fit and thus the actual shape of the pulse. The ambiguity of the pulse definition is translated into an uncertainty of the pulse duration. This divergence from the theoretical shape is due to the simplification of the model, which does not take into account higher-order dispersion terms nor include pulses shaping effects from the SBR.

Multiple pulsing was observed when the introduced negative dispersion was reduced and/or when the intracavity pulse energy was increased by lowering the outcoupling ratio. A decrease of the conversion efficiency in the second-harmonic generation can reveal the presence of secondary pulses (figure 4-13), as it indicates a drop of the peak intensity on the doubling crystal. A high dynamic range autocorrelator can also be used to detect secondary pulses.

The measurement of the power spectrum of the light intensity can be used to characterise pulse fluctuations [113]. Such power spectra are obtained from the processing of a photodiode signal by a radio-frequency (RF) spectrum analyser. The determination of the actual laser noise from the power spectrum is a complicated matter, therefore this measurement was only a qualitative indication of the laser noise levels. The output pulses are recorded using a relatively slow photodiode (10 ns rise time, Thorlabs DET10C) and a 50-GHz analyser (Agilent E4447A). This combination is not very fortunate as it is limited by the bandwidth of the photodiode.

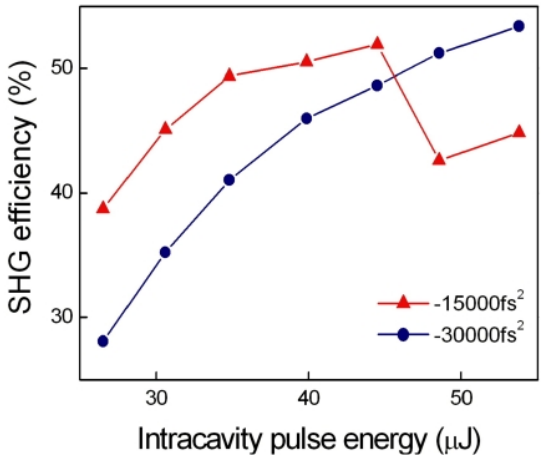

Figure 4-13 Conversion efficiency at different dispersion levels in a type-I, with $\theta = 22.8°$ and $\phi = \frac{\pi}{2}$. The outcoupling ratio was reduced to 6%. The focusing parameters were not optimised for highest conversion efficiency.

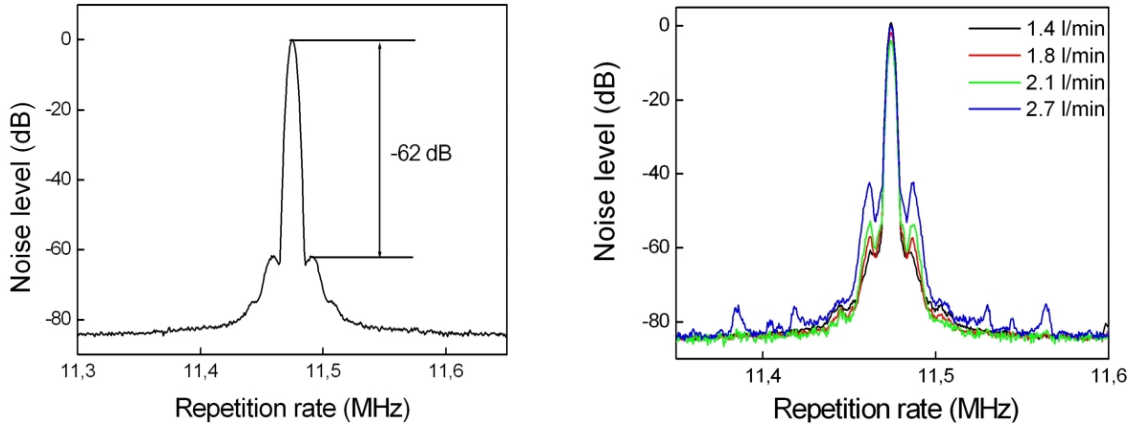

Figure 4-14 RF spectrum at 6 μJ (left) and RF-spectra for different flow rates (right).

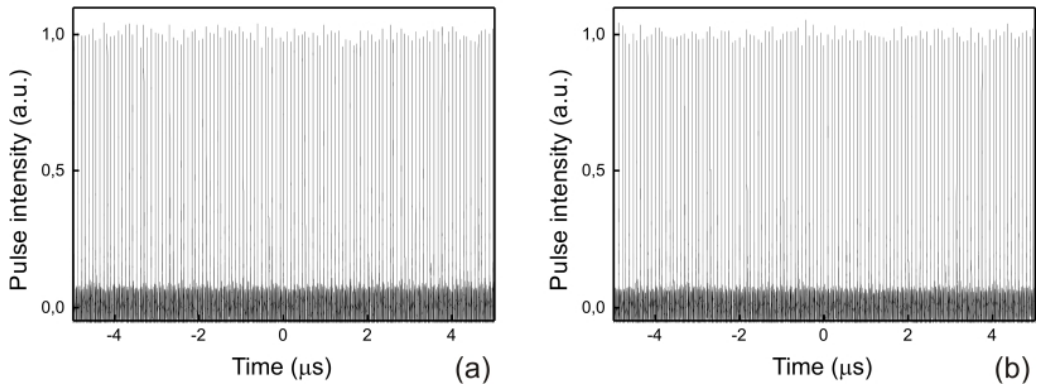

Figure 4-15 (a) Yb:YAG pulse train at 62 W. (b) Frequency-doubled pulse train at 25 W.

The RF-spectrum indicates a suppression of the side-bands above 60 dB around the fundamental harmonic of the laser repetition rate, as shown in figure 4-14. The spectrum was recorded with a resolution bandwidth of 2.7 kHz and a 300-kHz span. The level of these side-bands are correlated with the cooling flow rate behind the thin-disk. Because of its small thickness, mechanical vibrations from the turbulent water are easily transferred to the disk. These vibrations disturb the mode-locking process leading to an intensification of the noise, as seen from the deterioration of the laser RF-spectrum at higher flow rates. To increase the thermal stability of the laser system, the original water-cooled chiller was replaced by a smaller temperature-stabilised air-cooled chiller. This chiller delivers a maximum flow rate of 0.7 l/min. Despite the lower cooling capacity, the oscillator delivered exactly the same lasing performances.

The pulse to pulse stability is measured by recording the intensity fluctuations of the pulses with a photodiode. The pulse train, plotted in figure 4-15a, exhibits a RMS intensity fluctuation of 2.2%. This value is relatively high for a mode-locked oscillator since stability below 0.2% has been reported with Ti:Sapphire oscillators [114]. Yet, such results were only demonstrated with inherently stable low-energy Kerr-lens mode-locked oscillators delivering a maximum pulse energy of a few-nJ.

4.5 Second-harmonic generation

With 6 µJ, the pulse energy of the Yb:YAG thin-disk oscillator is sufficiently high to pump a parametric amplifier stage. Since the photon energy of the Ti:Sapphire pulses ($\propto \frac{1}{\lambda_{\mathrm{Tisa}}}$) lies above that of the Yb:YAG infrared pulses, the thin-disk output needs to be first frequency-doubled to amplify the near-infrared seed. The experimental set-up of the second-harmonic generation stage is shown in figure 4-16.

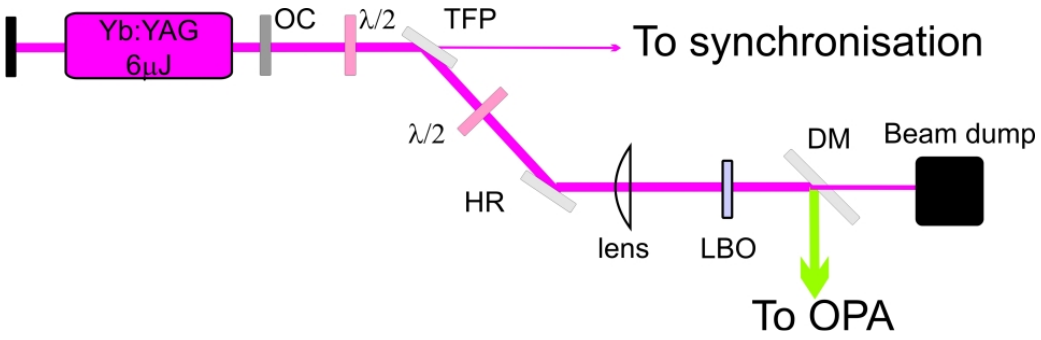

Figure 4-16 Experimental set-up for frequency doubling. OC: output coupler, TFP: thin-film-polariser, λ/2: half wave plate, HR: high reflector, DM: dichroic mirror.

Lithium Triborate LiB_3O_5 (LBO) is commonly used for high-power nonlinear applications. Indeed, it combined a very high damage threshold (> 10 GW/cm^2 for ns pulses) with good opto-mechanical properties. In addition, it can be produced in large dimensions with high optical quality. Finally, its large nonlinear coefficient (d_{32} = 1.17 pm/V) leads to a high effective nonlinear coefficient for type-I second-harmonic generation (SHG) driven at 1 micron in the XY-plane, making it particularly attractive for high-power SHG from Yb-based lasers.

Since the conversion efficiency scales with the intensity and the length of the nonlinear crystal, it is in general possible to compensate for the lower peak intensity by using longer crystals. However, this only holds for signal with limited optical bandwidth, as broader spectra rise phase-matching issues. Owing to the high beam quality of the infrared oscillator and its narrow bandwidth, one can take advantage of longer crystals to increase the conversion efficiency without the risk of optical damage at high intensity. The SHG stage consists of a 4-mm critically-phase-matched type-I LBO crystal. The Yb:YAG pulses are gently focused to an approximately 200-µm spot for limited divergence inside the crystal. With our focusing parameters, the Rayleigh range extends over 12 cm and is then much larger than the crystal length allowing good conversion efficiency and little beam distortions.

Due to beam delivery losses from imperfect coatings of steering mirrors, polarisers, half waveplate and lenses (not all represented in figure 4-16), only 54 W of power are left in front of the doubling crystal. Yet, the SHG stage generates up to 43.5 W of 515-nm radiation with only 10.1 W of remaining fundamental power. These powers were measured after a dichroic mirror, which reflects the green and transmits the infrared light. Since the two radiations have opposite polarisations (horizontal for the fundamental, and vertical for the second-harmonic), a Glan-Thompson polariser was placed after the dichroic mirror to select the horizontal polarisation with an extinction ratio better than $1/10^6$. The residual 1030-nm radiation is then transmitted through the polariser. The leakage corresponds to less that 0.2% of the second harmonic signal, which confirms that the power measured after the dichroic mirror is essentially free of the fundamental radiation.

With 81%, the efficiency is remarkably high, while the mode quality of the second-harmonic signal remains excellent (figure 4-17). To our knowledge, this is the highest conversion efficiency obtained in a LBO crystal. Numerical simulations have shown that conversion efficiencies of 84% were possible with M^2 value below 1.1 [115]. Due to the strong saturation in the frequency conversion process, the pulse-to-pulse energy fluctuations in the green are of 2.2% RMS (figure 4-15), similarly to that of the fundamental.

4.6 Further scaling

Nonlinear phenomena arise from the interaction of highly intense coherent light with matter. Since for a Gaussian beam, the peak intensity I_p of a pulse is approximately equal to:

$$I_p \approx \frac{2E_p}{\pi w_0^2 \cdot \tau_p}, \qquad \textbf{(4-1)}$$

increasing the peak intensity is usually realised by using a higher pulse energy, a shorter pulse duration or a tighter focus. Here, only the possibilities of decreasing the pulse duration and scaling up the pulse energy for high-average power thin-disk oscillators will be discussed.

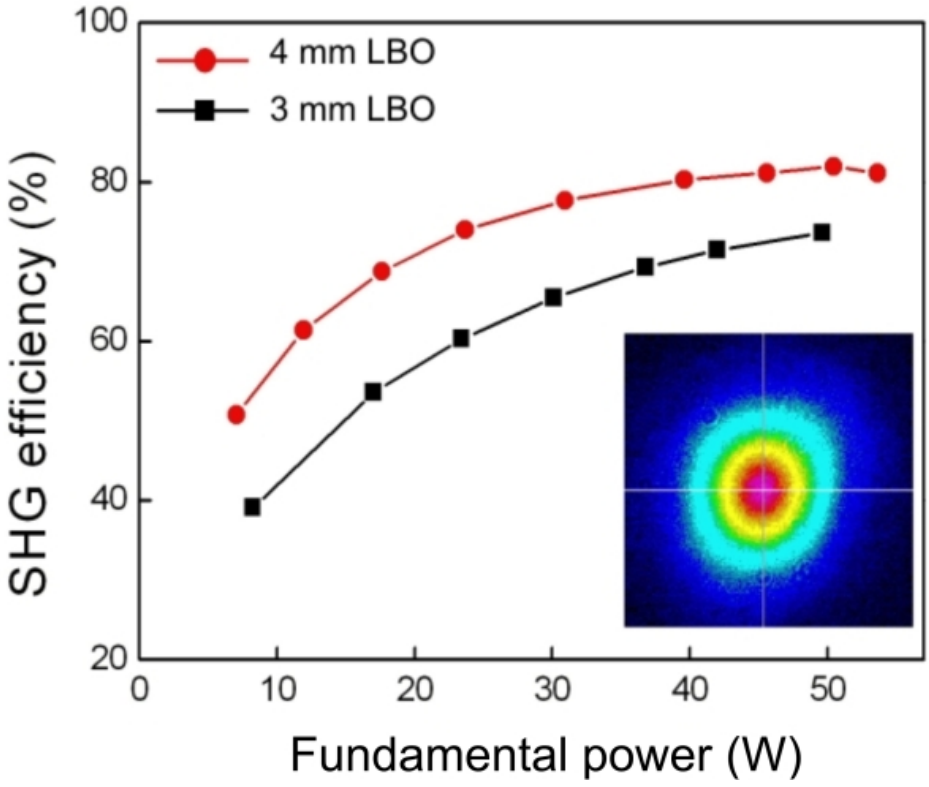

Figure 4-17 **Efficiency of the second harmonic generation. Inset: beam profile at the highest efficiency.**

4.6.1 Shorter pulse

Despite its large emission bandwidth of Yb:YAG ($\sim$ 6 nm), mode-locked operation at higher pulse energies leads to pulse durations closer to the picosecond than a few hundreds of femtoseconds due to the strong gain-filtering effects at higher saturated gain levels [116]. Selecting a host material with a broader bandwidth would allow for the generation of shorter pulses. Glasses exhibit a much broader emission spectrum than crystals owing to the broadening of the ion emission lines in an amorphous material. Nevertheless, they suffer from poor thermo-mechanical and thermo-optical properties, which limit their use in high-power systems.

As prospective material, the sesquioxides promise to be superior to the YAG counterpart because of the broader emission spectrum and excellent thermal properties. In particular lutetia (Lu_2O_3) stands out by its very high thermal conductivity of 11.0 W/m/K, which is almost not affected by the ytterbium doping [117]. This originates from the very similar masses and bonding forces between ytterbium and lutetium. The ytterbium-doping causes only a small disturbance to the crystal lattice and affects the phonon scattering only slightly. Consequently, the thermal conductivity of Yb-doped lutetia is nearly twice as high than that of Yb-doped YAG. One limitation to the development of lutetia-based lasers is its crystal growth, which requires high melting temperatures (>2400°C). Fabrication of Yb:Lu_2O_3 ceramics could perhaps elude this problem in the future [120]. Recently, pulse duration of 330 fs at $\sim$ 40 W power were obtained in a passively mode-locked Yb:Lu_2O_3 thin-disk oscillator [118]. Further scaling

should be possible, since the output power was only limited by the available pump power in this work.

Another approach is to design host materials consisting of mixed crystals. Through the inhomogeneous line broadening inherent to disordered lattice structure, the gain bandwidth is enlarged. Such structures are presented as hybrids between amorphous material and crystals. They indeed exhibit intermediate behaviours of the two: better thermal properties and larger emission spectrum. A recently developed material, Yb:$LuScO_3$ combines remarkably the spectral features of two sesquioxides, Yb:Lu_2O_3 and Yb:Sc_2O_3. The bandwidth, centred at 1039 nm, stretches over 20 nm. The thermal conductivity of 3.5 W/m/K remains sufficiently high for high-power operation. Used in a passively mode-locked thin-disk oscillator, this laser material produced pulses as short as 227 fs with 7.2 W of average power [119]. Yet, the difficulty to control the growth of these disordered crystals is still a severe limitation to their commercialisation.

In a similar concept, the generation of shorter pulses can be obtained from multi-gain-media oscillators rather than disordered crystals. In this case, the gain medium consists of two (or more) materials with slightly shifted peak emission. As compared to the disordered crystal approach, these lasers rely on single crystals with better opto-mechanical properties. Tokurakawa *et al.* built a mode-locked oscillator based on two ceramic pieces of Yb:Lu_2O_3 and Yb:Sc_2O_3 contacted to each other. The laser delivered 53 fs with 1W of output power without extra cooling [122]. Energy scaling would in that case require the development of improved contacting technique to permit higher pumping intensities. Another option consists in using two separate laser heads with different gain media in a cavity. This will however add enormous costs to the laser system. In addition, the management of two thermal lenses is expected to become rather challenging at higher pumping levels.

In 2003, Matsubara *et al.* studied the possibility of scaling the output power of a mode-locked Yb:YAG rod laser and predicted an average output power of 60 W with pulse duration of approximately 200 fs [123]. Since then, experimental work could only be demonstrated at much lower power level in the range of few hundreds of mW [99].

A major breakthrough in the development of high-energy oscillators was achieved in the net positive dispersion regime [124], where the pulse energy can be increased with even broader spectral bandwidth than in the solitary regime. While soliton mode-locking leads to transform-limited pulses, oscillators operating in the positive dispersion generate chirped pulses. As a result, the peak intensity is reduced, and thereby the nonlinearities, allowing for higher pulse energies. The positively chirped pulses are typically externally recompressed by means of a prism compressor and dispersive mirrors.

Simulations showed that for our oscillators, the absolute value of dispersion required for high-energy pulse stabilisation is substantially lower in the positive dispersion regime ($+900$ fs^2) than that in the negative regime (-18000 fs^2) [125]. In this regime, the bandwidth is estimated

to be approximately 3.5 nm, which would correspond to a pulse duration of 300 fs. Purging the cavity with helium or even vacuumisation could be then avoided. Nevertheless, for substantial energy growth, operation under vacuum of the oscillator would be highly beneficial.

4.6.2 Higher energy

The most straight-forward way to obtain higher pulse energy is to increase the average output power, while keeping the conditions for stable soliton pulse generation fulfilled (equation **(2-22)** and **(2-23)**). Resonators with multiple passes through the gain medium enable the use of higher outcoupling ratios, while reducing the intracavity power level. Stability issues may nevertheless arise from the complexity of the laser system. Without dramatically reducing the stability of our laser, an additional bounce or two on the disk should permit to reach pulse energies above 10 μJ with an appropriate cavity design.

An alternative approach to shift up the pulse energy frontier of mode-locked oscillators is based on a decrease of the repetition rate [126]. Extending the cavity length without affecting the transverse beam profile on the cavity critical elements can be accomplish by means of a Herriott-type multi-pass cavity [127, 128]. This design leads to a longer resonator with comparable average power to the original laser, while the pulse energy is increased by the ratio of the cavity lengths.

In low repetition rate thin-disk oscillators, the main source of nonlinearities originates from the air. Helium-flooded cavities can be used to overcome this problem but is accompanied with higher operation costs [109]. In addition, our experiments showed that the constant flow of helium in the cavity generates some lasing instabilities due to gas turbulence which were difficult to suppress. Equally-stable operation of the laser would require an optimised diffusion of the gas. Operation in low-vacuum seems thus more advantageous. Indeed, the oscillator cavity can be made very compact to fit in a simple vacuum chamber which would necessitate only a small-dimensioned pump.

Finally, better understanding of the thermal effects inside the SBR is essential for designing of stable resonators at higher intracavity powers. With this actual cavity design, the main limitation to higher output energy was the beam degradation above 310 W of pump power. Exploiting the full pump power of 500 W should allow to increase the pulse energy accordingly.

5 Pump-seed synchronisation for MHz parametric amplifier

5.1 Introduction

The use of sub-picosecond pulse duration in optical parametric amplifiers increases dramatically the constraints on the synchronisation, as accurate pump-seed timing is essential for efficient and stable amplification. Like any three-wave mixing process, the exchange of energy between the pump and the seed can only occur when the two pulses temporally - and spatially - overlap, since the energy is not stored inside the nonlinear crystal. Large timing jitter will severely degrade the performances of the amplifier by causing fluctuations of the amplified pulse energy and of the amplified spectrum. These instabilities could result in a partial incompressibility of the amplified pulses. In most systems, a timing jitter of approximately 10% of the pump pulse duration is desirable to maintain stable operation of the parametric amplification process. Besides its locking precision, the requirements for the synchronisation scheme are its long term stability and simplicity of use.

In chapter 3, an all-optical synchronisation scheme was demonstrated at kHz repetition rate using frequency-shifted Ti:Sapphire pulses to seed a Nd:YAG regenerative amplifier. This laser served then as a pump source for the amplification of the Ti:Sapphire seed. Recently this technique was successfully implemented to a 640-fs fibre-based amplifier pump source in a 2-MHz parametric amplifier producing 500-nJ pulses with 20-fs pulse duration [34]. The pump pulses were derived from a Ti:Sapphire seed laser after soliton generation in a photonic crystal fibre and amplification to 15.5 μJ in a three-stage fibre-amplifier.

This fibre approach is quite attractive for high-repetition-rate synchronised pump sources, however it requires the implementation of a stretcher-compressor in the amplifier chain to reduce the effects of self-phase-modulation accumulated along the fibre. Even with a large stretching ratio and a rigorous recompression, pulse distortions are not fully avoidable. At high-power level, the pump pulses commonly exhibit a pedestal and/or additional side pulses causing a degradation of the amplifier performances. For our MHz amplifier system, one possible synchronisation solution is to employ self-stabilisation of two mode-locked oscillators lasing at the seed and pump wavelengths via a nonlinear optical (Kerr-lens) mechanism [26]. While solving the problem of passive synchronisation of two-colour sources, this method necessitates a particularly complex and critical alignment of the two laser beams inside the Kerr medium. In addition, cavity-length fluctuations originated from environmental disturbances limit such locking scheme to shorter time scales, typically in the range of a few minutes.

Another option is to employ an active synchronisation scheme via servo-loops. There are two possibilities to determine the timing error between two pulses. One relies on an electronic phase measurement by comparing the repetition rates of the two laser sources, while the other

method uses the optical nonlinear interaction of the two pulses to measure directly their timing offset. In this chapter, a locking scheme combining an electronic and an optical control loop is demonstrated. This synchronisation unifies the performances of both locking methods and results in a timing jitter of ~ 100 fs.

5.2 Active synchronisation scheme

5.2.1 Electronic control loop: phase-locked loop

A phase-locked loop (PLL) is a regulator of the phase (thus of the frequency) of a signal by comparing its value to that of a reference signal. Figure 5-1 shows the function principle of a conventional PLL, which contains three basics elements: a phase detector, a loop filter and a voltage controlled oscillator (VCO). A VCO is an electronic oscillator, which oscillation frequency can be tuned by an applied voltage. The phase detector compares the frequency of the VCO with a reference source and generates an error signal. A low-pass loop filter is inserted to damp brusque changes at the input of the oscillator and to stabilise the loop. The VCO delivers then a signal with a corrected frequency of oscillation.

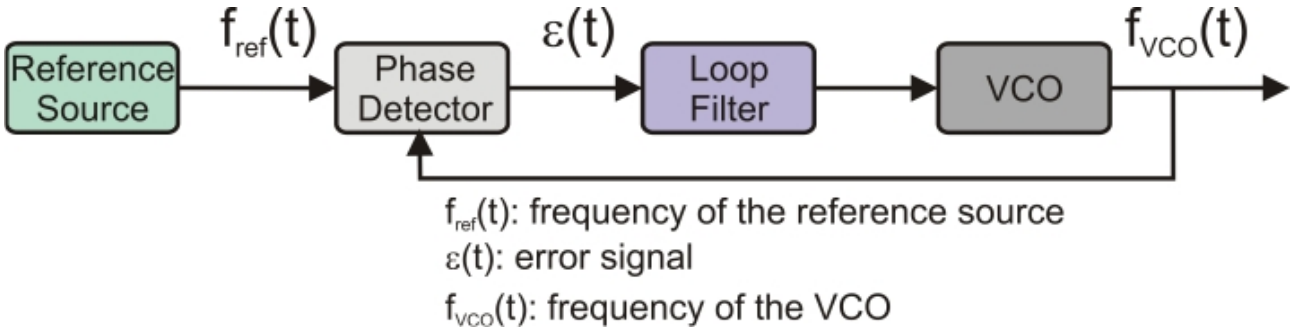

Figure 5-1 PLL block diagram.

In a similar way, PLL can be used to stabilise the repetition rate of a laser by controlling its cavity length. This can be easily done by placing a mirror of the laser cavity on a piezoelectric transducer (PZT). When the phase detector measures a mismatch with the repetition rate of the reference source, the PZT is activated to readjust the cavity length. The reference can be a microwave source or another laser pulse train. PLLs are relatively easy to implement and allow for a wide locking range which only depends on the design of the feedback loop. Although less than 1-ps timing jitter is achievable with electronic PLL [24], such active synchronisation employs pricey GHz electronics and presents a long-term phase drift, which originates from thermal drift and phase noise converted from amplitude noise [78].

5.2.2 Optical control loop: sum-frequency generation

Instead of mixing two electrical signals to produce an error signal, one can "mix" two optical signals in a nonlinear crystal. Indeed, the relative timing delay between two pulses can be

obtained by measuring the result of their nonlinear interaction as it is confined in time and space. Just like optical parametric amplification, sum-frequency generation is a three-wave-mixing process requiring energy conservation and phase-matching condition. The timing delay between the two pulses is translated into a change in the intensity of the SFG signal, as depicted in figure 5-2. The resulting SFG signal can then be used as a feedback signal in a control loop to stabilise the repetition rate of a slave laser to a reference laser via a PZT. This optical timing detection is often referred as cross-correlation.

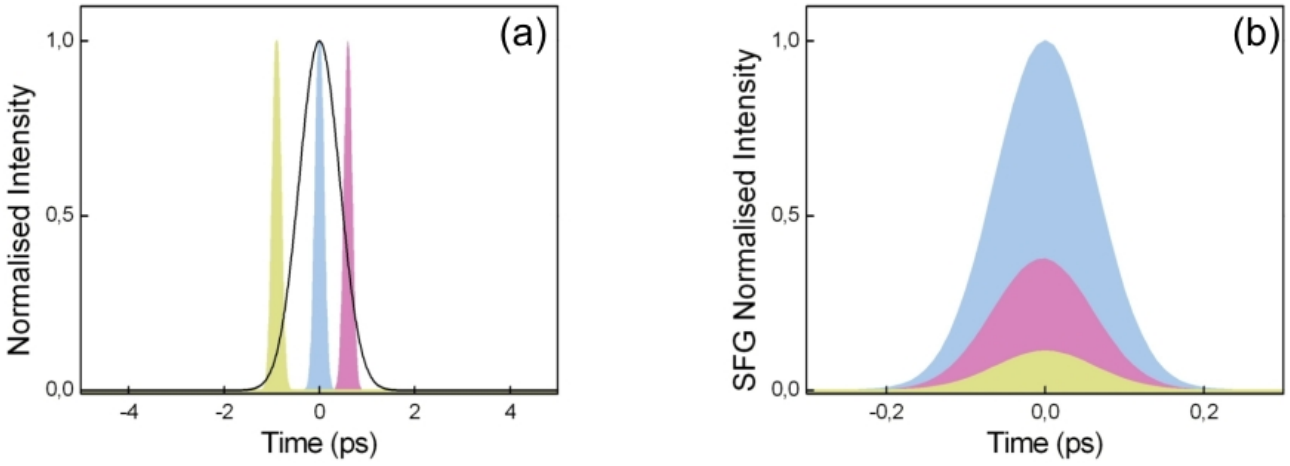

Figure 5-2 **(a) Reference laser pulse (solid line) and slave pulse with no timing error (blue shaded area), +600 fs delay (pink shaded area) and -900 fs delay (yellow shaded area). (b) Correlation signals for the corresponding timing offsets.**

Based only on the intensity of the SFG signal around its peak value, one cannot identify whether the slave pulse precedes or follows the reference pulse. Therefore, rather than setting the reference point for the feedback loop at the maximum of the SFG intensity, one can set it at half its peak value [129]. In this case, the intensity variations of the cross-correlation signal have a linear relation to the relative timing error between the two pulses. Another option is to use a balanced cross-correlator [130]. This optical scheme consists of two sum-frequency stages, one of which containing an additional optical delay as depicted in figure 5-3. The intensity of the signals generated in each stage depends on the relative timing delay between the two pulses on the nonlinear crystal. By subtracting these two SFG signals, one can generate an error signal for controlling the cavity length of the slave laser. The calculated error signals are plotted in figure 5-4 for different timing offsets.

The feedback loop requires a careful alignment of the balanced cross-correlator. The two sum-frequency stages should indeed deliver identical cross-correlation traces in order to obtain a symmetric error signal at the zero timing delay. The output of the balanced cross-correlator is shown on figure 5-5 for different optical delays. In addition, the introduced optical delay between the two stages should be optimised to allow for a compromise between sensitivity and locking range, as shown in figure 5-5. With a shorter delay, the sensitivity increases, but the locking range is clearly reduced. On the other hand, a too large delay can create a discontinuity in the slope of the error signal.

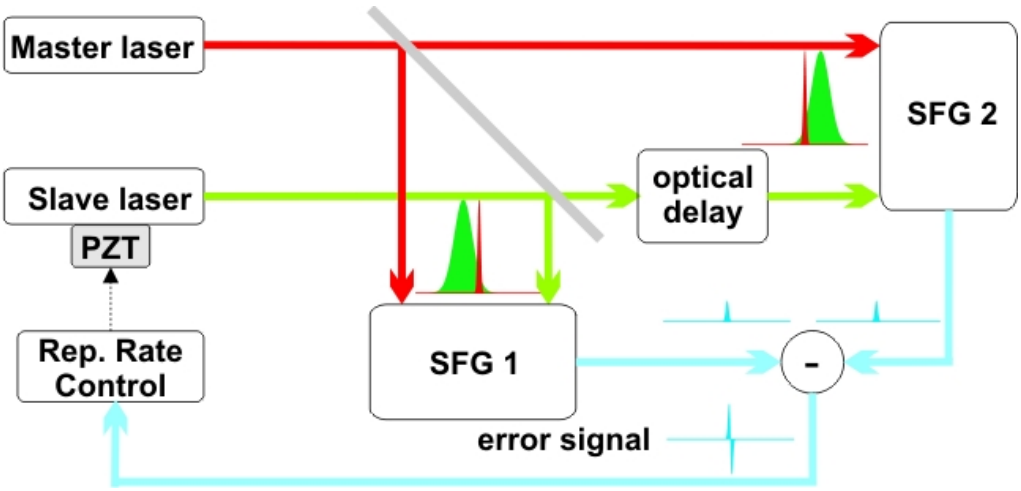

Figure 5-3 Balanced cross-correlator.

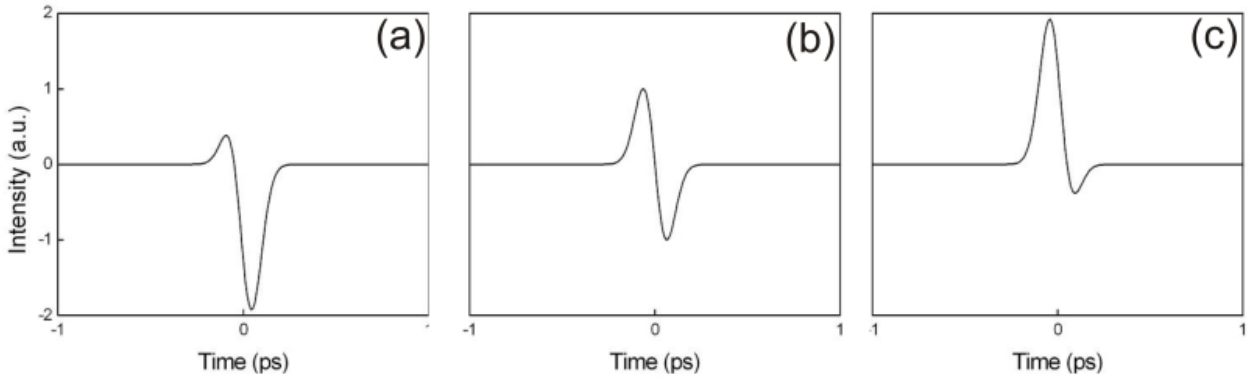

Figure 5-4 Calculated error signals with (a) -50 fs, (b) 0 fs and (c) +50 fs timing offset. The pulse durations are 150 fs for the slave and 1 ps for the master laser.

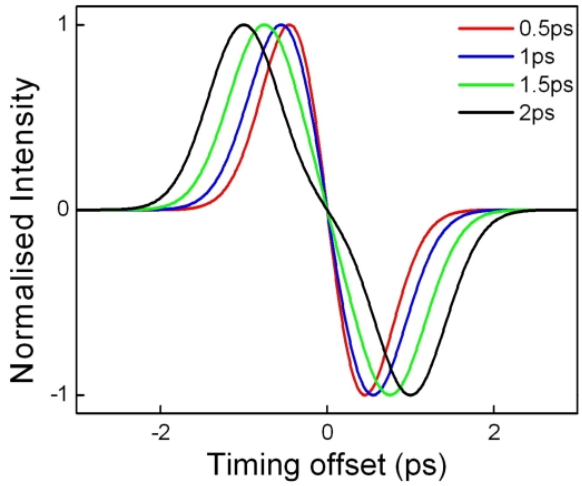

Figure 5-5 Calculated output of the balanced cross-correlator for different optical delays. The pulse durations are 150 fs for the slave and 1 ps for the master laser.

In comparison to a synchronisation scheme using only a phase comparator, the main advantage of an optical control loop is its accuracy with potentially timing jitter below a femtosecond [130]. Unfortunately, its locking range is limited by the laser pulse width making optical schemes only suitable for laser systems with moderate timing jitter. Miura *et al.* increased the dynamic range of their cross-correlator approach by stretching one pulse and detecting the bunch of SFG pulses when the timing error exceeded both pulse durations [129]. The repetition rate of this bunch was then related to the difference of repetition rates between the two lasers. In terms of complexity, this method is not easier to implement than an additional PLL.

5.2.3 Combined scheme

Designing a control loop based on electronic and an optical detection would allow to combine the large dynamic range of PLLs with the timing precision of the cross-correlation. Ma *et al.* proposed a synchronisation scheme relying on multiple PLLs with different timing resolutions and a SFG signal as an error signal in their last control loop [131]. With this combined approach, they achieved sub-10 fs timing jitter. However, the system was fairly complex, involving high-speed electronics, and its stability was only demonstrated over few minutes.

Obviously such timing precision would be superfluous for a parametric amplifier driven by 1-ps pump pulses. For our MHz system, a synchronisation scheme based on a PLL and a balanced cross-correlator was developed. The locking is done in two steps. First, the electronic loop approximately sets the repetition rate of the Ti:Sapphire oscillator. Second, the cross-correlator generates an optical error signal which adds a small correction to the main electronic loop. Thanks to the precision of the second feedback signal, this synchronisation scheme does not require high-speed photodiodes. The synchronisation overview is shown in figure 5-6.

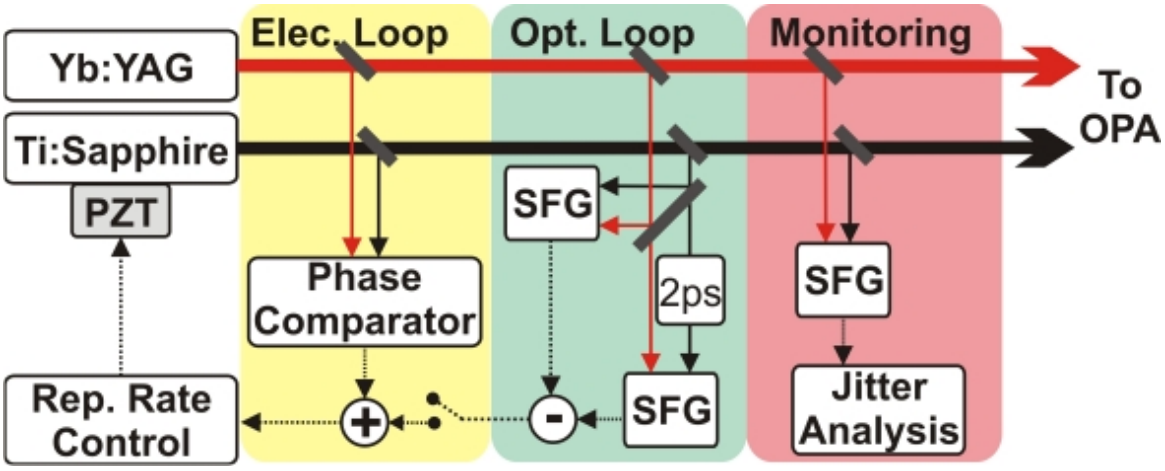

Figure 5-6 Block diagram of the synchronisation.

In this system, the Ti:Sapphire laser is assigned as the slave oscillator and operates at approximately 69 MHz, while the Yb:YAG laser was designed at 11.5 MHz. Thus only every 6^{th} pulse will be later amplified in the nonlinear crystal. In our first experiments, the Ti:Sapphire oscilla-

tor was set as the reference source and similar timing precision could be obtained. However, the Yb:YAG oscillator exhibited a stronger tendency towards Q-switching resulting in repetitive damages of the SBR.

5.3 Experimental realisation

5.3.1 Electronic synchronisation set-up

Two standard 1-ns photodiodes (Thorlabs FDS010) are used to detect the oscillator pulse trains and generate the signals at the input of the frequency mixer. The cavity length of the Ti:Sapphire oscillator is first roughly adjusted by tuning the position of one cavity mirror with a picomotor so that the beat frequency between the two lasers is minimised. This error signal is filtered and amplified before being processed by a proportional integrative regulator, which controls the movement the PZT inside the Ti:Sapphire resonator. The chosen PZT (PiezoJena P25/10) is able to compensate for drifts up to 50 µm with a ms-response time.

The electronic loop is operating at 414 MHz corresponding to the 6^{th} harmonic of the Ti:Sapphire laser repetition rate. The motivation to using higher harmonics of the repetition rate in PLLs is to obtain an enhanced signal-to-noise ratio. Nevertheless, the possibility of locking onto a "spurious" pulse increases as higher harmonics are being used, obliging the user to check for the pulse temporal overlap at each new locking. The relative phase between the two oscillator signals, hence the relative timing delay between the pulses on the sum-frequency stages, can be tuned by adjusting the position of one of two photodiodes which is placed on a translation stage.

When the gain factor of the proportional integrative regulator is set properly, the Ti:Sapphire oscillator is locked to the Yb:YAG laser. At that point, optical sum-frequency generation between the two lasers can already be observed but the timing jitter is too large for stable operation. Both SFG signals flicker in a few-second time scale making the optimisation of the balanced cross-correlator troublesome. To overcome this problem, a ramp is added to the electronic error signal which scans periodically the relative phase of the Ti:Sapphire signal. By doing this, a periodic temporal overlap of the two pulses is created on the nonlinear crystal leading to a time-averaged sum-frequency signal. These sum-frequency signals are less intense, however they are more stable and still significantly higher than the background noise. The ramp signal is maintained during the whole alignment process of the balanced cross-correlator and switched off prior to optical locking.

5.3.2 Optical synchronisation set-up

The balanced cross-correlator provides the feedback signal for the second optical loop. As shown on figure 5-7, a fraction of the two laser beams is directed onto two identical sum-frequency

set-ups. Typically, less than 10 nJ pulses from the Yb:YAG laser and 100 fJ pulses from the Ti:Sapphire oscillator are necessary for locking the two lasers. Each stage is composed of a 2-mm-thick BBO crystal critically phase-matched ($\theta = 25.9°$) for sum-frequency generation between the 1030-nm and the 800-nm radiations. The sum-frequency signal is generated at 450 nm and thus lies in the blue. In one stage, an optical delay of 2 ps is introduced by 0.6 mm of glass (Type B260). The beams are focused down on the nonlinear crystal to an 80-µm-diameter spot by a 150-mm lens. For careful adjustment of the spatial overlap, two cameras are positioned at the front of the crystal. The optical set-up is depicted in figure 5-7.

Another fraction of the beams is split just before sum-frequency generation in order to control the pulse arrival time on the crystal and allow for correction of the variable delay of the electronic loop. When both pulses temporally and spatially overlap in the BBO crystals, two sum-frequency pulses are generated. These signals are recorded by two slow photodiodes (Thorlabs FDS100) and subtracted to produce the second feedback signal. An aperture was inserted in front of each detector to block the unconverted 800-nm and 1030-nm radiations. In addition a blue filter is used to further improve the signal-to-noise ratio.

By switching on the ramp signal in the electronic loop, the sum-frequency signals can be observed on an oscilloscope and used to optimise the balanced cross-correlator. The intensities of the SFG signals are then tuned to the same level by adjusting the optical set-up and varying the gain level of each photodiode. Once activated, the optical loop adds a small correction to the basic electronic loop leading to stable and intense sum-frequency generation.

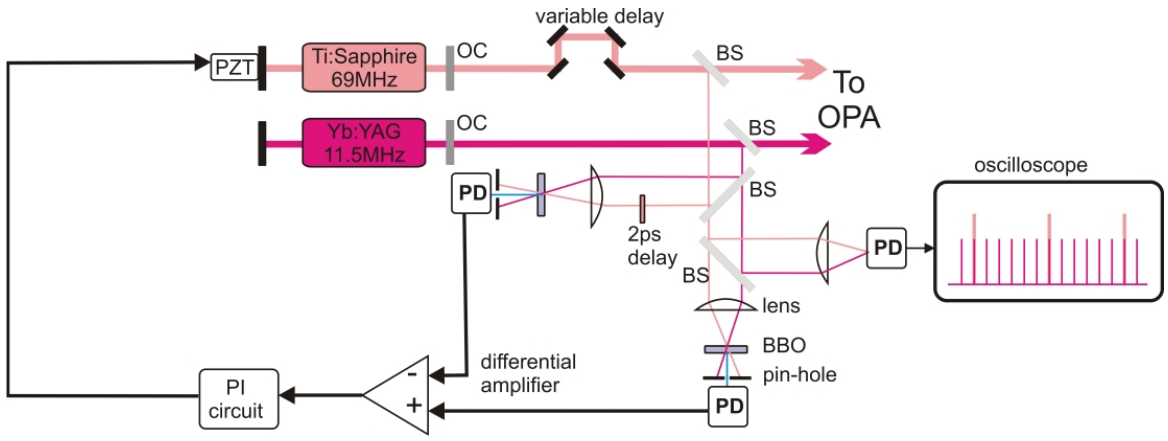

Figure 5-7 Optical control loop. OC: output-coupler, BS: beam-splitter, PD: photodiode, PI circuit: proportional integrative circuit.

5.4 Locking results

5.4.1 Cross-correlation measurement

The locking performances of this synchronisation scheme were first investigated by recording the cross-correlation trace between the Ti:Sapphire and the Yb:YAG pulses, as described in section 2.3.3. Indeed, the timing jitter between the two lasers can be estimated from the width

of the cross-correlation trace and the pulse durations of the two lasers. For this purpose, a third sum-frequency stage consisting of a 1-mm-thick BBO crystal was additionally set up as shown in figure 5-6. A motorised translation stage was installed in the optical path of the Ti:Sapphire beam to scan the relative delay between the two pulses.

Assuming that the temporal shape of both laser pulses and the probability distribution of the timing jitter have a Gaussian distribution, the cross-correlation function is given by:

$$I_c(t) = \exp\left\{-(4\ln 2)\frac{t^2}{\tau_c^2}\right\}, \tag{5-1}$$

$$\text{with } \tau_c = \sqrt{\tau_{tisa}^2 + \tau_{YAG}^2 + \tau_j^2}, \tag{5-2}$$

where τ_j is the full width half maximum (FWHM) of the timing jitter and τ_c is the FWHM of the cross-correlation function $I_c(t)$. τ_{tisa} and τ_{YAG} are the durations of the Ti:Sapphire and Yb:YAG pulses, respectively. The RMS timing jitter σ_j is then equal to

$$\sigma_j = \frac{1}{2\sqrt{2\ln 2}}\tau_j, \tag{5-3}$$

Figure 5-8 shows the improvement of the locking performance once the optical loop is activated. With only the electronic loop, no stable sum-frequency generation is possible.

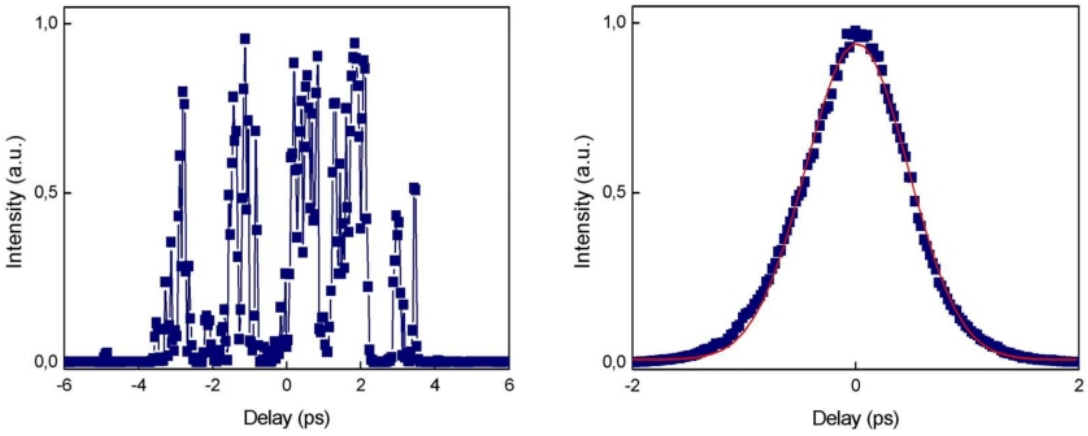

Figure 5-8 Cross-correlation trace with only the electronic loop (left) and after activating the optical loop (right).

The duration of the Ti:Sapphire pulses on the sum-frequency stage is estimated by calculating the total dispersion introduced by the different optical elements (cf annex A). For a 6-fs pulse propagating through 5 mm of fused silica, 2 mm of BK7 and 3 m of air, the pulse are lengthened to 150 fs on the nonlinear crystal. From the autocorrelation trace of the Yb:YAG laser in figure 5-9, the pulse duration is calculated to be 1.08 ps assuming a Gaussian shape. This result shows good agreement with the cross-correlation measurement with a FWHM of 1.11 ps suggesting a low timing jitter. From equation **(5-1)** and **(5-3)**, the FWHM timing jitter between the two mode-locked oscillators can be estimated to be 210 fs, corresponding to a RMS value of 90 fs.

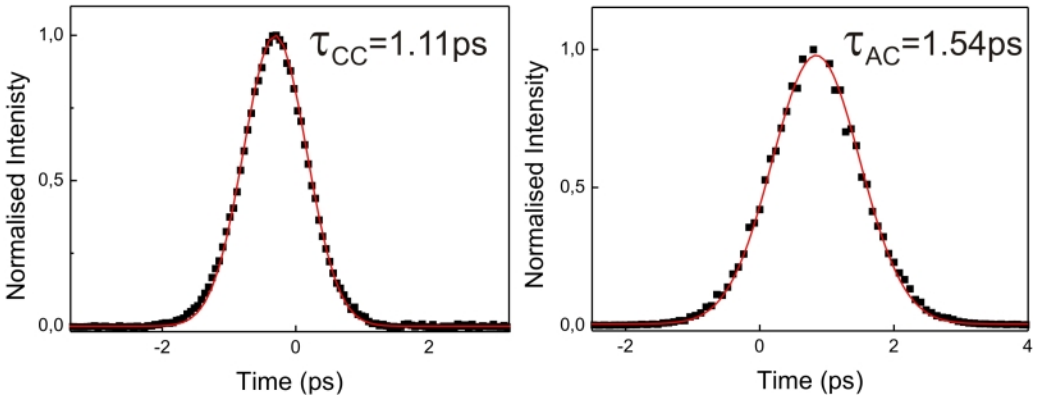

Figure 5-9 **Cross-correlation (left) and intensity autocorrelation (right) trace of the Yb:YAG pulse.**

5.4.2 Frequency analysis of the timing jitter

For further characterisation, one can analyse the pulse-to-pulse fluctuations of the sum-frequency signal when the two interacting pulses are offset by approximately half the pump pulse width. In this configuration, the timing jitter Δt is directly proportional to the measured intensity fluctuations ΔI as illustrated in figure 5-10. The RMS timing jitter σ_j can then be simply retrieved from the RMS intensity fluctuations and the calibrated slope of the correlation peak. In order to improve the locking performance, it can be useful to identify on which time scale the timing jitter mostly occurs. This can be done by calculating the Allan variance [133] which is defined by:

$$\sigma_j(\tau) = \sqrt{\frac{1}{2(m-1)} \sum_{i=1}^{m-1} (y_{k+1} - y_k)^2}, \qquad \textbf{(5-4)}$$

where τ is the sample time, y_k are the discrete averaged values of a signal over the sample time τ and m the total number of recorded data points of the signal. By estimating the Allan variance at different sample times, one can explore the characteristic time scales of the jitter. $\sigma_j(\tau)$ can be easily determined at different time scales from one sample of data by repeating the following procedure:

1. Calculate $\sigma_j(\tau)$,
2. Redefine the variables: y_k as $\frac{y_k + y_{k+1}}{2}$ and m as $\frac{m}{2}$,
3. Calculate $\sigma_j(2\tau)$.

To suppress the discrete nature of the pulse train at 11.5MHz, the sum-frequency signal is measured using a photomultiplier (Hamamatsu H7712-15) with a bandwidth below 500 kHz. Figure 5-11 shows the recorded signal over 2 s. For a maximum intensity of the sum-frequency signal at 2 units, and the FWHM of the cross-correlation peak at 1.11 ps, the conversion scale of the slope can be evaluated at 0.55 ps/unit. From these record of data, the timing jitter is quantified between 2 µs and 1 s; the results are shown in figure 5-12.

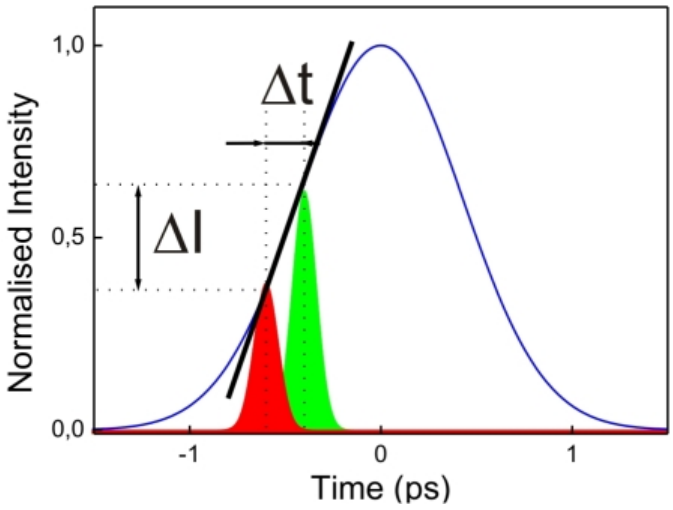

Figure 5-10 Schematic diagram of the timing jitter. Solid line, Yb:YAG pulse. Red and green filled area: SFG signal between the Yb:YAG pulse and the Ti:Sapphire pulse.

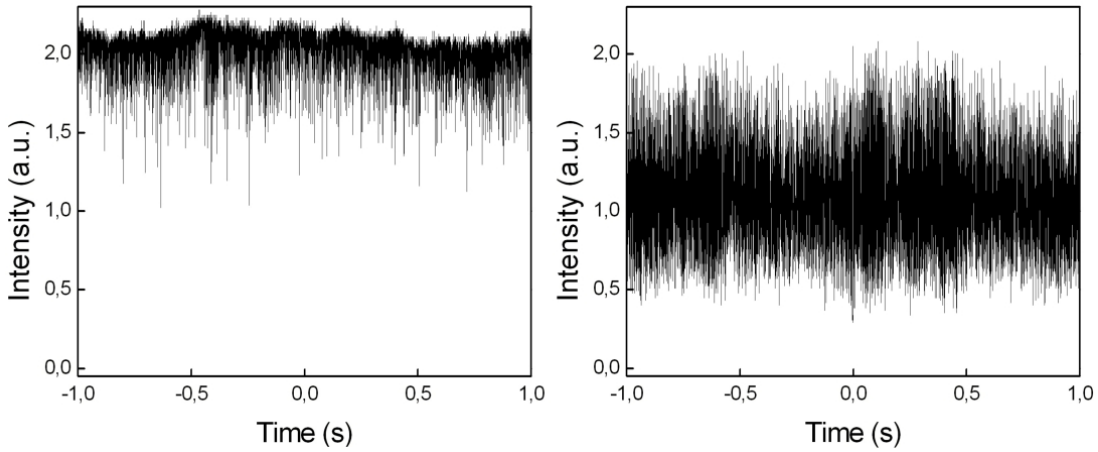

Figure 5-11 Sum-frequency signals at the cross-correlation peak (a) and half its peak value (b).

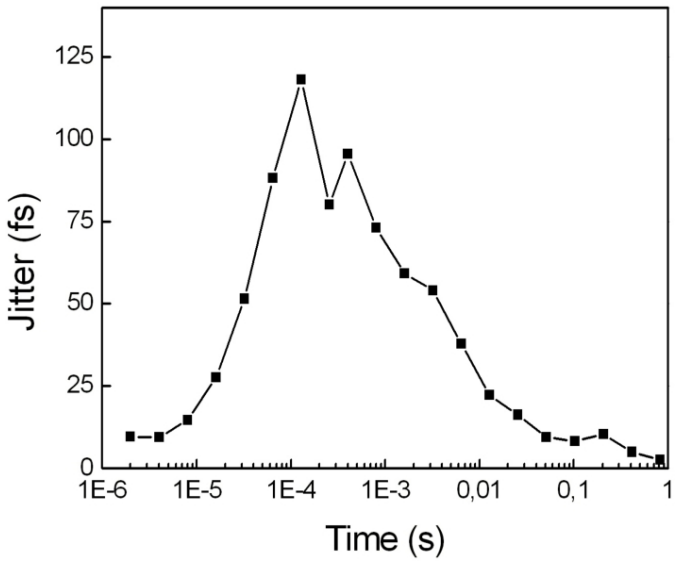

Figure 5-12 Allan variance of the timing jitter

This measurement shows that the main contribution to the timing jitter lies around 100 µs. As in most passively mode-locked laser systems, the main source of timing jitter has frequency components around the relaxation oscillation frequency of the laser f_{RO} [134], given by

$$f_{RO} = \frac{1}{2\pi}\sqrt{\frac{l}{\tau_r}\frac{P_{int}}{E_{sat}} - \frac{1}{4}\left(\frac{1}{\tau_g} + \frac{P_{int}}{E_{sat}}\right)}, \tag{5-5}$$

where l are the total cavity losses, τ_r is the cavity round-trip time, τ_g is the laser material upper state life time, P_{int} is the intracavity power, and $E_{L,sat}$ is the saturation fluence of the laser material. For solid-state lasers, $\tau_g >> \tau_r$, the expression can be simplified to

$$f_{RO} = \frac{1}{2\pi}\sqrt{\frac{l}{\tau_r}\frac{P_{int}}{E_{sat}}}. \tag{5-6}$$

Parameters	Ti:Sapphire oscillator	Yb:YAG oscillator
l	10%	13%
τ_r	14.5 ns	87 ns
P_{int}	2.5W	500 W
E_{sat}	0.3 J/cm^2	0.3 J/cm^2
f_{RO}	140 kHz	6.5 kHz

Table 5-1 Oscillator parameters.

From table 5-1, the relaxation oscillation frequencies of the Ti:Sapphire and Yb:YAG lasers are estimated to be 140 kHz and 6.5 kHz, respectively. The second value is very close to the highest component of the timing jitter located around 5 kHz. Most likely, the relaxation oscillations of the Yb:YAG are the main source of jitter in our system. This coupling of intensity noise into timing noise has been thoroughly investigated in the case of passively mode-locked lasers [132]. In the presence of a saturable absorber, the damping of the relaxation oscillations tend to be reduced. This can lead to a timing noise originated from the intensity modulation of the pulse train produced by the relaxation oscillations.

The synchronisation would certainly benefit from an optimisation of the SBR parameters and the cavity design to improve the stability performances of the oscillator. Another improvement of the timing precision could be obtained by increasing the feedback bandwidth of our active control loop to a few kHz. This would require using a faster PZT but also minimising the mass of the mirror attached to it to obtain a faster response. The feedback loop used in this locking scheme was originally designed for compensation of large timing drift rather than fast timing drift. In this perspective, a PZT with a large scanning range (50 µm) was implemented in the Ti:Sapphire oscillator.

With this combined electronic-optical locking scheme, a timing jitter of ∼120 fs was demonstrated for the synchronisation between a broadband seed oscillator and a high energy pump

oscillator. This residual jitter is still within approximately 10% of the pump pulse width. Tight phase-locking can be maintained continuously for several hours without readjustment of the locking parameters. These results allow for first parametric amplification experiments of the Ti:Sapphire pulses pumped by the frequency-doubled output of the Yb:YAG laser at MHz repetition rate.

6 MHz optical parametric chirped pulse amplifier

Current rapid advancement in the fields of extreme nonlinear optics relies on the availability of high peak intensity few-cycle lasers. Optical parametric chirped pulse amplification offers a promising route towards few-cycle high-intensity laser systems. However, optical parametric amplifiers are most commonly operated at sub-Hz to few kHz due to power scaling issues of the pump sources at increasing repetition rates [28, 29, 135]. Only recently, the availability of MHz-pump sources with energy beyond the microjoule level has made the development of ultrafast amplifiers possible [34, 136, 137]. Such repetition rates allow for the observation and characterisation of ultrafast phenomena within a fraction of the previously necessary data recording time simultaneously with improved signal-to-noise ratios. This would be particularly beneficial for the study of processes with low probability or low conversion efficiency, for which integration times over several hours are often necessary. In this regard, pushing amplifiers towards MHz repetition rate for the generation of carrier-envelope phase stabilised few-cycle pulses could open novel fields of investigation.

6.1 Preliminary considerations

The realisation of a high-power few-cycle optical noncollinear optical parametric amplifier requires a careful optimisation of the nonlinear crystal, the beam geometry and the pump-seed pulse duration. Especially the design of our amplifier has to be adjusted to the large optical bandwidth (400 nm) of the seed, the relatively low pump energy (µJ rather than mJ or J) and short pump pulse duration (1 ps rather than tens of ps or ns).

6.1.1 Choice of a nonlinear crystal

First, the crystal should exhibit a large effective non-linear optical coefficient to permit high conversion efficiencies. Due to the noncollinear geometry the pump and the seed pulse propagate under different directions inside the crystal, which for small beam diameters leads to a shortening of the interaction length. Therefore broadband phase-matching requires a small noncollinear angle in order to minimise this spatial walk-off. Second, in high-power OPAs even minor absorption of the pump, seed or idler become particularly problematic as it would cause a substantial heating inside the crystal. In extreme case, this could lead to a thermal fracture of the material. Consequently, the crystal should have a large transparency range covering the spectral region of the interacting pulses. The parametric amplification of our 400-nm bandwidth Ti:Sapphire seed is accompanied by the generation of an idler stretching from 1060 nm to 3.6 µm, when pumped at 515 nm. Such broadband amplification necessitates therefore a transparent medium between 515 nm and 3.6 µm. Finally, the crystal should be of high optical quality with high damage threshold to allow high pumping intensities.

Over the past decades, beta barium borate (BBO), lithium triborate (LBO) and potassium

dideuterium phosphat (KD*P) have established themselves as materials of first choice for the amplification of ultrashort pulses. KD*P is a good candidate for high-power applications because of the availability of large-aperture crystals. However, its higher absorption losses towards the infrared would hinder the amplification of the shorter wavelengths from our seed. Bismuth triborate (BiBO) is a relatively new nonlinear material with unique optical properties, making it an potential new competitor to BBO and LBO [138]. The major properties of the above mentioned crystals are listed in table 6-1. BiBO is very attractive because of its high nonlinear coefficient and non-hygroscopic property in contrast to BBO and to some extent LBO. On the other hand, the transparency range of BiBO is slighly too short for our Ti:Sapphire seed. LBO offers a good compromise between LBO and BiBO with its broad phase-matching range and highest damage threshold [139], which compensates for its lower nonlinear coefficient.

Material	KD*P	BBO	LBO	BiBO
NLO coefficient	0.23	2.02	0.85	2.97
Damage threshold(GW/cm^2)	0.5	0.5	10	0.3
Peak intensity used (GW/cm^2)	> 60 [140]	> 100 [34]		> 40 [141]
Transparency range (nm)	180-2000	190-3500	160-3200	290-2500
Hygroscopicity	high	low	very low	none

Table 6-1 Comparison of nonlinear crystals. The damage threshold for KD*P, BBO and LBO are given by the supplier Eksma for 10 ns pulses at 1064 nm. For BiBO, the value is given by the company Castech for the same pulse parameters.

To select a nonlinear crystal, their phase-matching bandwidths are compared after optimisation of the phase-matching angle θ and α using the Sandia National Laboratories Nonlinear Optics software [142]. We define the phase-matching deviation as the difference between the perfect phase-matching angle at a given wavelength and the optimised angle for broadest phase-matching around the centre wavelength. Figure 6-1 compares this deviation for LBO, BiBO and BBO. From these simulations, it can be seen that BBO is better suited than LBO for amplification of our seed pulses through its flatter phase-matching curve in the blue. Because of the larger spectral overlap between our Ti:Sapphire source and the phase-matching curve of the BBO, BBO will be exclusively used in this near-infrared OPA system.

6.1.2 Parametric gain and bandwidth

Thin crystals are crucial for broadband parametric amplification because the group velocity mismatch between the seed and idler waves leads to a narrowing of the amplification bandwidth, which becomes stronger with increasing crystal lengths. On the other hand, thinner crystals require higher pumping intensities to compensate for their lower gain, which is ultimately limited by the damage threshold of the nonlinear material and the onset of incompressible parametric superfluorescence.

Figure 6-2 shows the parametric gain for different BBO crystal lengths. The gain is estimated from equation **(2-9)** using the dispersive properties of BBO given in reference [143]. The pump

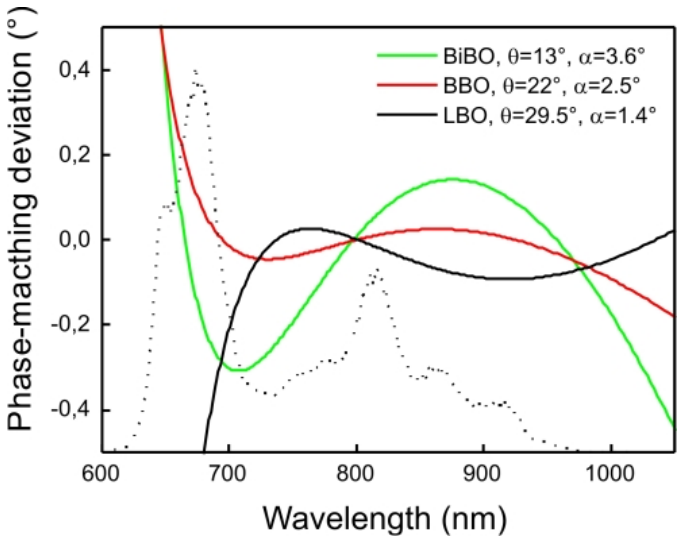

Figure 6-1 Phase-matching deviation and optical spectrum of the Ti:Sapphire seed source (dotted line). The phase matching are all calculated for type-I frequency mixing, in the XZ plane for LBO and YZ plane for BiBO.

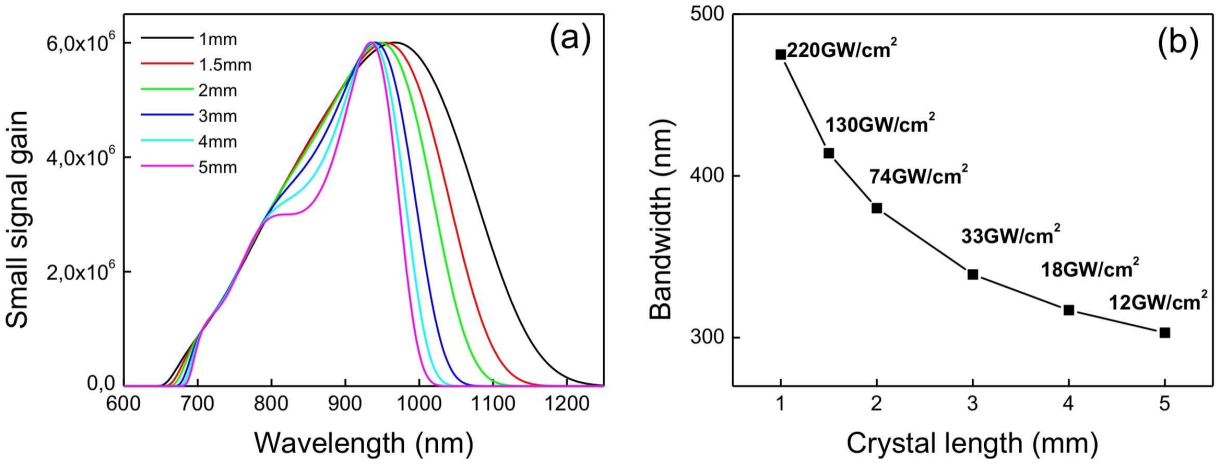

Figure 6-2 (a) Calculated small signal gain for different BBO crystal lengths. The pump wavelength is 515 nm, α and θ are set to 2.5° and 22° respectively. (b) Calculated -10-dB bandwidth.

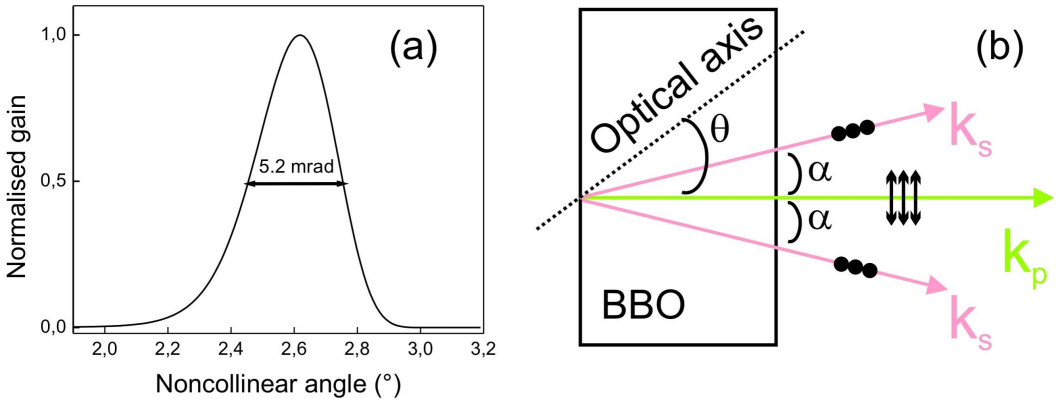

Figure 6-3 (a) Gain acceptance angle at 800 nm with 33-W incident pump power, 100-μm beam radius and $\theta = 22°$ in a 4 mm BBO. (b) Type-I phase matching in NOPA.

power is kept constant to 33 W and the beam diameter is adjusted to keep the same maximum parametric gain. From 5-mm to 1-mm crystals the bandwidth is remarkably extended, mostly to the infrared, but the necessary intensity is dramatically increased (almost 20 times).

Tight focusing rises additional issues in a OPCPA system. For smaller beam diameters the interaction length is shortened in a noncollinear geometry, due to the different propagation directions between the pump, seed and idler. Furthermore the parametric gain becomes more sensitive to the adjustment of the seed-pump beam overlap inside the crystal.

Another yet critical parameter is the beam divergence. Indeed, tighter focusing results in a stronger angular spread of the wave-vectors, which can decrease the parametric gain and cause a degradation of the amplified beam through spatial chirp. Thus broadband amplification requires a careful optimisation of the crystal length and beam radius to maximise the efficiency. This is particularly important for our MHz repetition rate OPA, where the pump pulse energy is "only" of a few microjoules. The acceptance angle for the seed can be evaluated by calculating the parametric gain as a function of α. In figure 6-3, the dependence of the gain on α is plotted for a beam waist of 100 µm. Based on these beam parameters, the Rayleigh range of the Ti:Sapphire seed is close to 40 mm. Within a 4-mm crystal, the divergence is then kept very small around the focus with an almost flat wave-front, ensuring negligible effects on the gain and beam profile. From these first estimations, longer crystals (3 mm to 5 mm) offer a good compromise between large gain at moderate intensities and amplification bandwidth.

In a noncollinear parametric amplifier, two different beam geometries may be used as depicted in figure 6-3b. The seed beam can either propagate between the direction of the optical axis and the pump, or it can propagate at a larger angle than the pump with respect to the optical axis. These geometries are referred as tangential phase-matching and Poynting vector walk-off compensation, respectively. Earlier work showed that the Poynting vector walk-off compensation configuration leads to a lower gain and a stronger second-harmonic generation [43]. Therefore, the amplifier will be preferably built in a tangential phase-matching geometry.

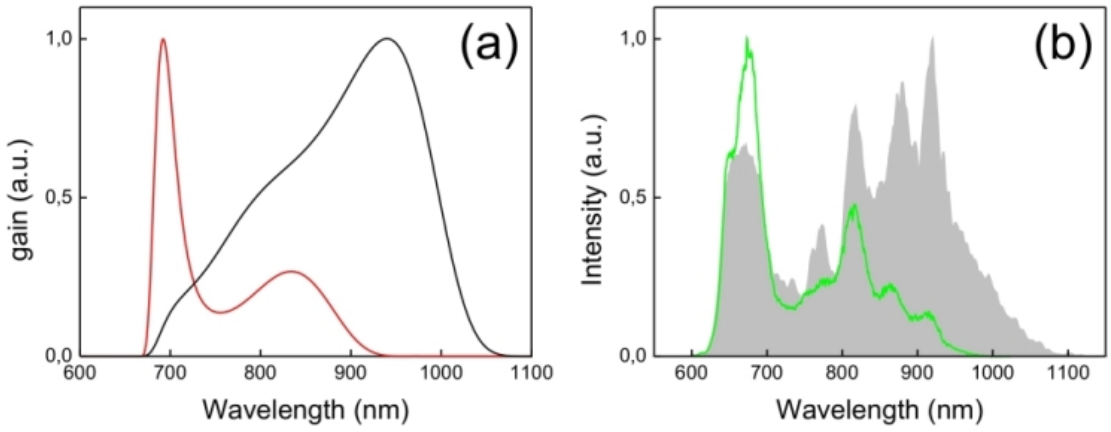

Figure 6-4 **(a) Detuned gain spectrum with $\alpha = 2.63°$ and $\theta = 22.14°$ (red line) and optimised spectrum for broadband gain. (b) Ti:Sapphire seed source used in our experiments (green line) and an infrared-enhanced spectrum (shaded grey area).**

From figure 6-2b, it can be seen that amplification of the shortest Ti:Sapphire wavelengths (< 700 nm) is difficult to achieve from a single BBO crystal pumped at 515 nm. Since the seed is typically stretched, one could adjust the delay between the pump and the seed in order to overlap the shortest wavelengths with the central part of the pump. These wavelengths would experience a larger pump intensity, and hence a larger gain. On the other hand, higher sensitivity to the timing jitter is expected and some distortions of the amplified seed pulses may occur. Another option is to use a second stage with different angles α and θ, so that the amplification gain is enhanced for the blue region in one stage, as illustrated in figure 6-4a.

Rather than extending the parametric bandwidth to shorter wavelength, one can tune the spectrum of the seed towards the infrared. This can be relatively easily done without modifying the oscillator layout. Through adjustment of the stability range and the intracavity dispersion, the longer spectral components of the Ti:Sapphire oscillator can be enhanced. In figure 6-4b, the seed spectrum is extended almost 100 nm further in the infrared.

6.2 Experimental realisation

6.2.1 Ti:Sapphire seed

The seed laser consists of a Kerr-lens mode-locked Ti:Sapphire oscillator operating in the soliton regime [59]. The necessary negative dispersion for stable operation is introduced by a set of ultrabroadband low-loss chirped multilayer dielectric mirrors. Fine tuning of the intracavity dispersion is achieved through a pair of wedges. The oscillator set-up is represented in figure 6-5. The laser delivers about 280 mW of mode-locked power resulting in 4-nJ pulses at 69 MHz. These pulses can be additionally phase-stabilised using the carrier-envelope offset beat signal generated between self-phase modulation and difference-frequency generation in a nonlinear crystal [12].

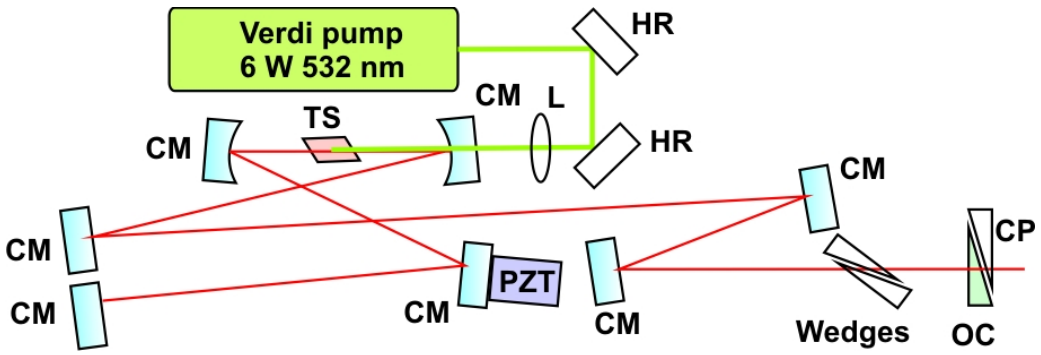

Figure 6-5 **Ti:Sapphire oscillator optical lay-out. TS: Ti:Sapphire crystal, CM: chirped mirror, HR: high reflector for 532 nm, OC: output coupler, CP: compensating plate, L: focusing lens, PZT: piezoelectric transducer.**

Typically, the oscillator is operated with a narrower spectrum (figure 6-6a). The corresponding transform-limited pulses are calculated to be 5.6 fs. The measurement of the pulse interferometric autocorrelation indicates a recompression down to ~ 7 fs (figure 6-6b). Under these

conditions the laser is less sensitive to thermal fluctuations in the laboratory. In order to control the repetition rate of the laser, one of the intracavity mirror is mounted on a piezoelectric transducer. The synchronisation scheme uses the combined electronic-optical loop described in chapter 5.

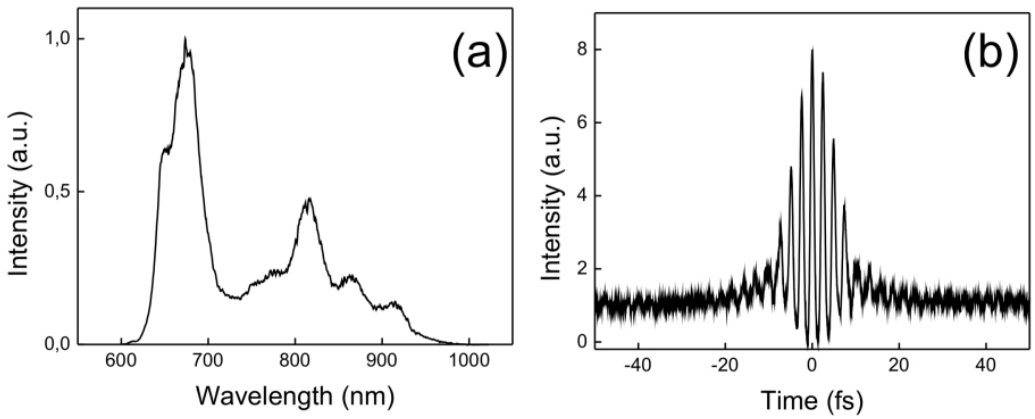

Figure 6-6 **Optical spectrum (a) and interferometric autocorrelation of the seed laser (b).**

After propagation through the different optical elements, the seed pulses are substantially lengthened before amplification. The total dispersion is estimated to be approximately $\sim 500\ \text{fs}^2$ from 6 m of air, 6 mm of fused silica (beam splitters and oscillator output coupler) and 3 mm of BK7 (focusing lens). It follows a pulse duration of ~ 220 fs on the OPA crystal.

6.2.2 Amplification results

The experimental set-up of the 11.5MHz is schematically presented in figure 6-7.

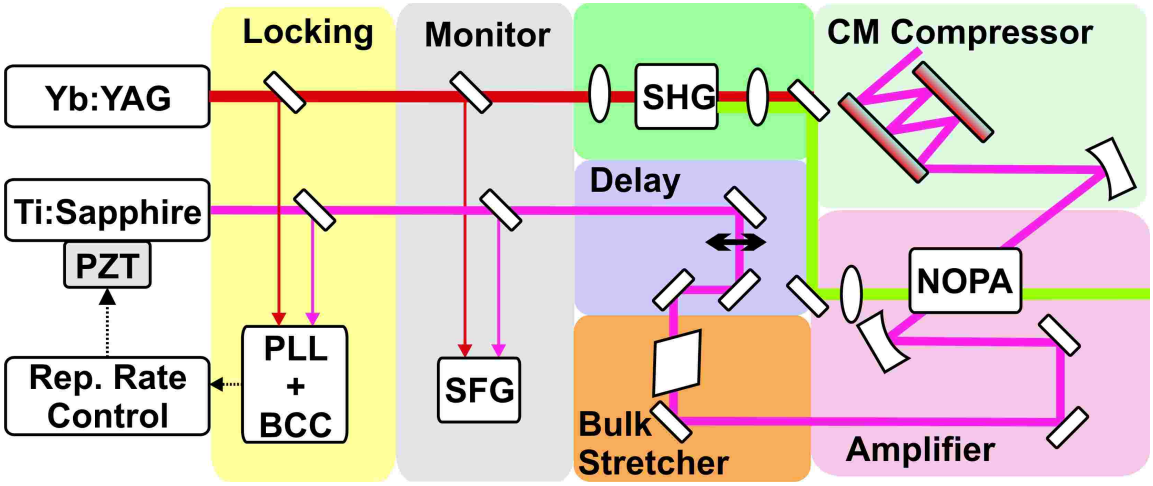

Figure 6-7 **Schematic set-up of the OPCPA. PLL: Phase-lock-loop, BCC: Balanced cross-correlator, SHG: Second-harmonic generation, SFG: Sum-frequency generation.**

It consists of a single-stage NOPA, optimised according to the previous section. The seed power at the front of the OPA crystal was measured to be only 100 mW due to beam delivery losses from 20 reflections on silver mirrors and two 10% beam splitters. The parametric amplifier is driven by the frequency-doubled output of the Yb:YAG thin-disk oscillator. The pump is

focused with a 400-mm lens to a beam diameter of $\sim$ 200 µm, slightly larger than the seed. The two focused beams are shown in figure 6-8. Pump and seed are crossed at an internal angle $\alpha \approx 2.5°$ inside a 4-mm BBO crystal cut at $\theta = 24°$ for type-I phase-matching. For these beam diameters and crossing angle, the interaction length is longer than the crystal, ensuring good conversion efficiency and uniform amplification. In this configuration, the o-seed is horizontally polarised, while the e-pump is vertically polarised and orthogonal to the crystal face. Under these conditions, the optical plane, defined by the angles θ-α, is vertical.

The beam spatial overlap can be optimised using a camera, placed above the crystal. A sum-frequency stage was built in front of the OPA to control the locking stability by monitoring the intensity fluctuations of the generated signal (see figure 6-7).

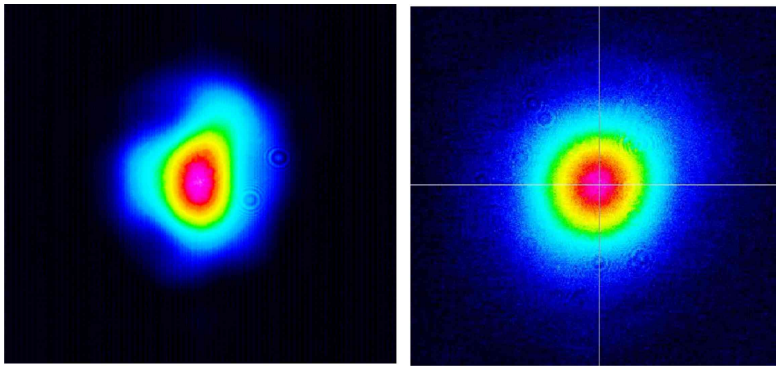

Figure 6-8 Seed beam (left) and pump beam (right) at focus.

The parametric amplifier delivers up to 5.6 W of output power when the crystal is pumped with 34 W of average power. With our focusing parameters, this corresponds to a pump intensity of about 18 GW/cm^2. At this pumping level, no superfluorescence ring could be observed. The seed is amplified to approximately 490 nJ at 11.5 MHz, leading to a pump-to-signal conversion efficiency of 17%. For an initial seed energy of 1.4 nJ, the amplication factor is 340. This is relatively low, since single-pass gain up to six orders of magnitude are not uncommon in OPCPA systems. The seeding level is indeed quite high for this OPA driven by a microjoule pump. The amplified spectra at different pump intensities are plotted in figure 6-9. The differences in the amplified spectral profiles essentially originate from intermediate readjustments of the OPA. Despite the lower gain of the parametric amplifier at shortest wavelength, the transformed-limited pulses corresponding to these spectra are not significantly longer than the original seed. Their pulse widths range from 6 to 6.2 fs, while it is calculated to be 5.8 fs for the unamplified seed. This originates from an enhancement of the infrared part, which is clearly visible using a logarithmic scale in figure 6-9.

Using 1-ps pump pulses, the stretcher for the seed can consist of only a few centimetres of bulk material. Two uncoated fused silica substrates are simply placed at the output of the Ti:Sapphire oscillator to lengthen the seed pulses. The additional dispersion from 16 mm of fused silica chirps the pulses to about 500 fs. After reoptimisation of the spatial and temporal overlap, the seed average power increases to 8 W. This corresponds to a pulse energy of 700 nJ

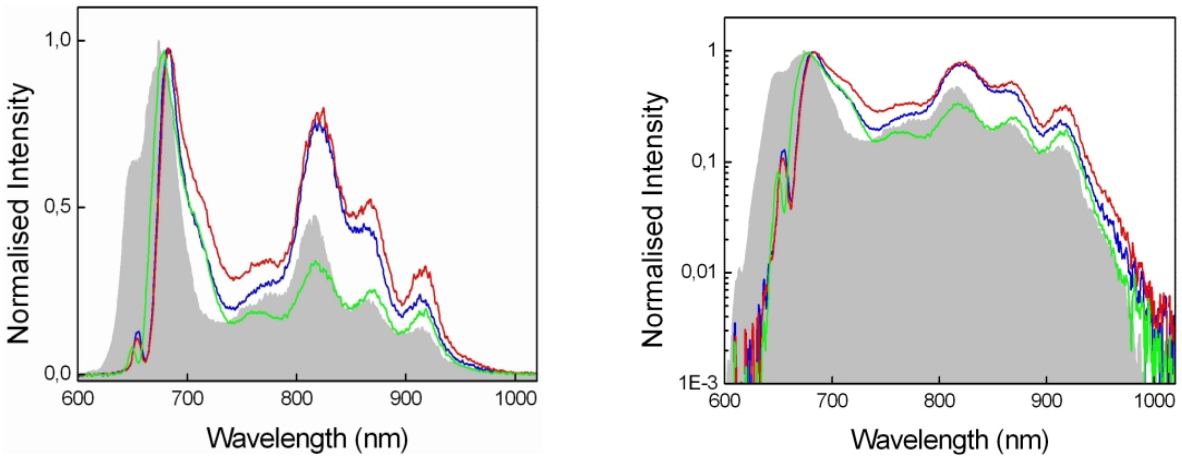

Figure 6-9 **Seed spectrum (grey shaded ared) and amplified spectra for 27 W (blue line), 32 W (red line) and 34 W (green line) of pump power, on linear scale (left) and logarithmic scale (right).**

and a conversion efficiency of 24.3%. In this case, the amplified spectrum becomes narrower, as shown on figure 6-10. Yet, the bandwidth still supports sub-7fs pulses assuming a flat spectral phase.

The superfluorescence background could not be measured with the powermeter available to us. The superfluorescence ring was only visible using a CCD camera and removing the neutral density filter in front of it. With an optical density of 4.3, this means a superfluorescence-to-signal ratio in the range of 0.1%.

Though the mode profile does not substantially degrade at higher pumping intensities, the seed beam becomes elliptical after amplification. We pictured the beams with and without amplification but under identical pumping conditions to maintain the same thermal stress on the crystal. The two beams in the far field are compared in figure 6-11. From this, it can be seen that the beam becomes larger in the horizontal plane, while it is almost unchanged in the other direction. In the presence of a Gaussian pump profile, the amplified pulse may experience a certain narrowing since the edges of the beam will experience a lower gain. This could result in a spatial widening of the seed observed in the far field. However, this should affect both directions. In the optical (vertical) plane, the spatial walk-off would on the contrary lead to a spatial widening of the seed. The origins of this ellipticity are still not explained. Operating the parametric amplifier with an efficiency of 15%, a pulse-to-pulse stability below 2% is measured, which is equivalent to the stabililty of the pump pulses. Figure 6-12 shows the amplified pulse train.

At this level of amplified seed average power, multiple bulk damages were observed in the crystal. Typically the crystal heated up and thermal fracture occurred. Despite the absence of energy storage in the crystal inherent to the instantaneous parametric amplification process, thermal effects are not completely absent. Even minor absorption losses will create a thermal load inside the crystal, which can become critical for such a high-power system.

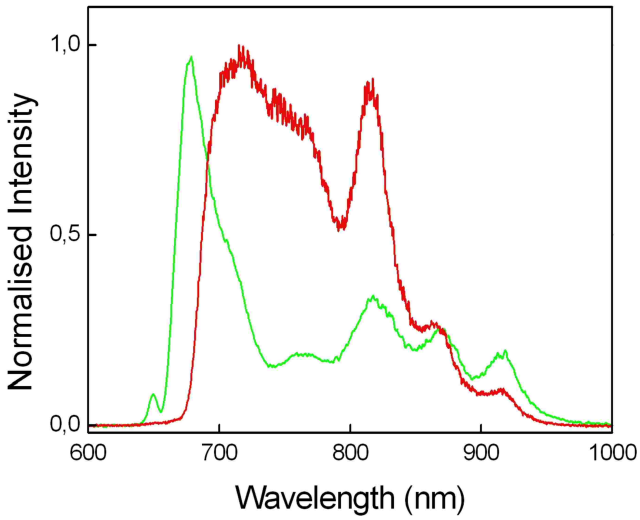

Figure 6-10 Amplified spectra for 220-fs (green line) and 500-fs seed (red line) for a pump intensity of 18 GW/cm^2.

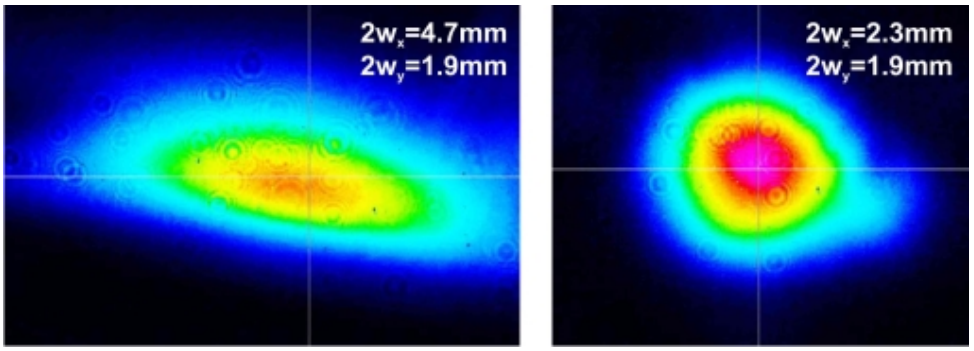

Figure 6-11 Amplified (left) and non-amplified seed (right).

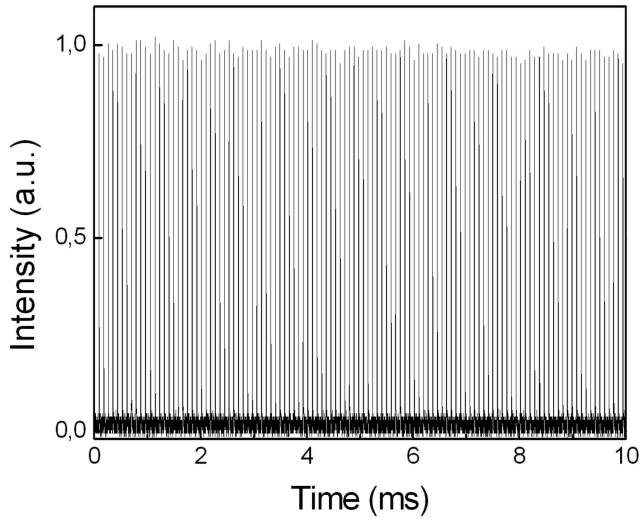

Figure 6-12 Pulse train with 5 W of amplified seed power.

One reason for this heating may be the relative increase of absorption losses above 2 µm in BBO, where still a significant part of the idler is generated. The transparency range of BBO is plotted in figure 6-13. It should be additionally mentioned that the only crystals available at that time were relatively old, with some evidence of previous bulk damages and coating defects. These could be a further source of power dissipation. In high-power OPA systems, cooling of the nonlinear crystal would be beneficial to reduce thermal effects. Indeed, a temperature increase of the crystal gives also rise to a modification of the refractive index, thereby altering the phase-matching relation between the pump, seed and idler waves. Ultimately, this will cause a decrease of the conversion efficiency and a deterioration of the amplified seed characteristics.

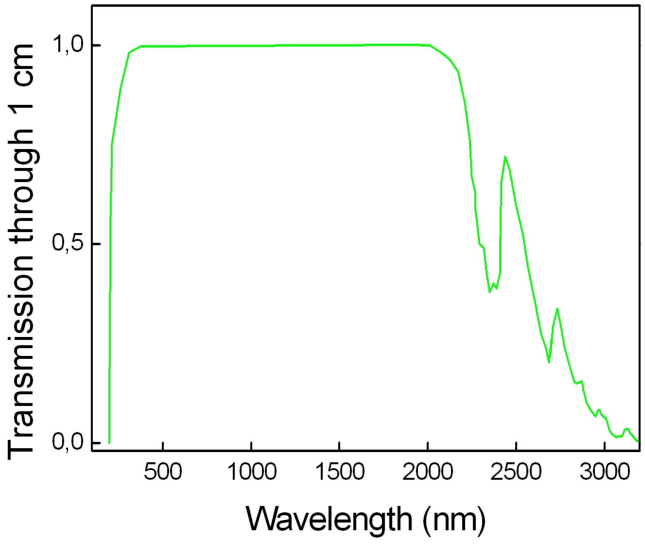

Figure 6-13 BBO transparency curve.

6.3 Pulse compression

6.3.1 Compressor design

An all-chirped-mirror compressor was favoured in this system because of its compactness and simplicity of alignment. Yet, designing and producing chirped mirrors with smooth dispersive curve over such large bandwidths is not a trivial issue. In our compressor, double-angle multilayer mirrors are used to reduce the spectral oscillations [145]. The characteristics of the complementary pair of mirrors are presented in figure 6-14. These ultra-broadband mirrors were originally produced for pulse compression after nonlinear broadening in a gas-filled hollow fibre. This system required much less group delay dispersion compensation than in the case of our OPCPA system. These mirrors support sub-4 fs pulse duration and were optimised for less than 10 bounces. The average dispersion level is thus relatively low with only approximately 35 fs^2 per bounce at 800 nm.

In our first experiments, the seed beam was shaped using spherical and cylindrical lenses before

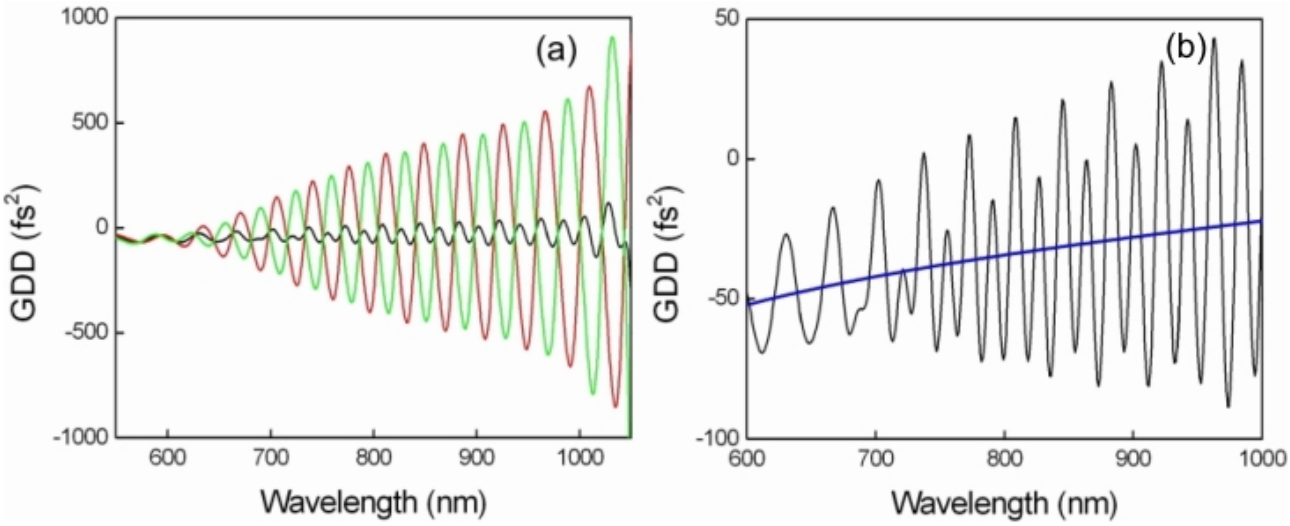

Figure 6-14 **(a) Dispersive characteristics of the double-angle mirrors PC34 under 5° (red line) and 20° (green line) incident angle after one bounce. The black line is the combined dispersion. (b) Residual oscillations for a double-angle mirror pair. For better readability, the averaged dispersion is also plotted (blue line).**

and after amplification as shown in figure 6-15. These transmissive optics introduced additional chromatic dispersion after the OPA, which needed to be compensated. As a result, pulse compression required over 30 bounces on the chirped mirrors. Furthermore, a deterioration of the pulse temporal characteristics was observed with apparent side-wings due to chromatic aberrations. Figure 6-16 shows the improvement of the autocorrelation traces when reflective optics were used instead of lenses. In these measurements, the amplifier was not pumped in order to discard possible pulse distortions from thermal aberrations inside the crystal. The final NOPA set-up using a 3 mm BBO and curved mirrors is represented in figure 6-17.

Due the limited choice of focusing optics, the lower gain of the 3-mm BBO crystal could not be compensated by reducing the pump diameter for increased pumping intensity. The pump and seed are focused using a lens and a mirror with both 500 mm of focal length. In this set-up, the pump intensity is consequently reduced to 12 GW/cm^2. At this pumping level, the seed pulses are only amplified to 2.8 W, resulting in a pulse energy of 250 nJ. The compressor consists of six 1-inch-diameter chirped mirrors with three bounces on each, compensating for approximately -630 fs^2 of GDD at 800 nm.

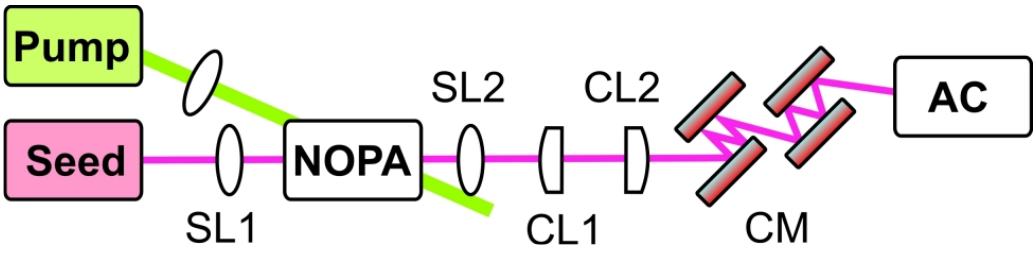

Figure 6-15 **Schematic set-up of the NOPA with lenses and chirped mirror compressor. SL1 and SL2: spherical lenses, CL1 and CL2: cylindrical lenses, CM: chirped mirror, AC: autocorrelator.**

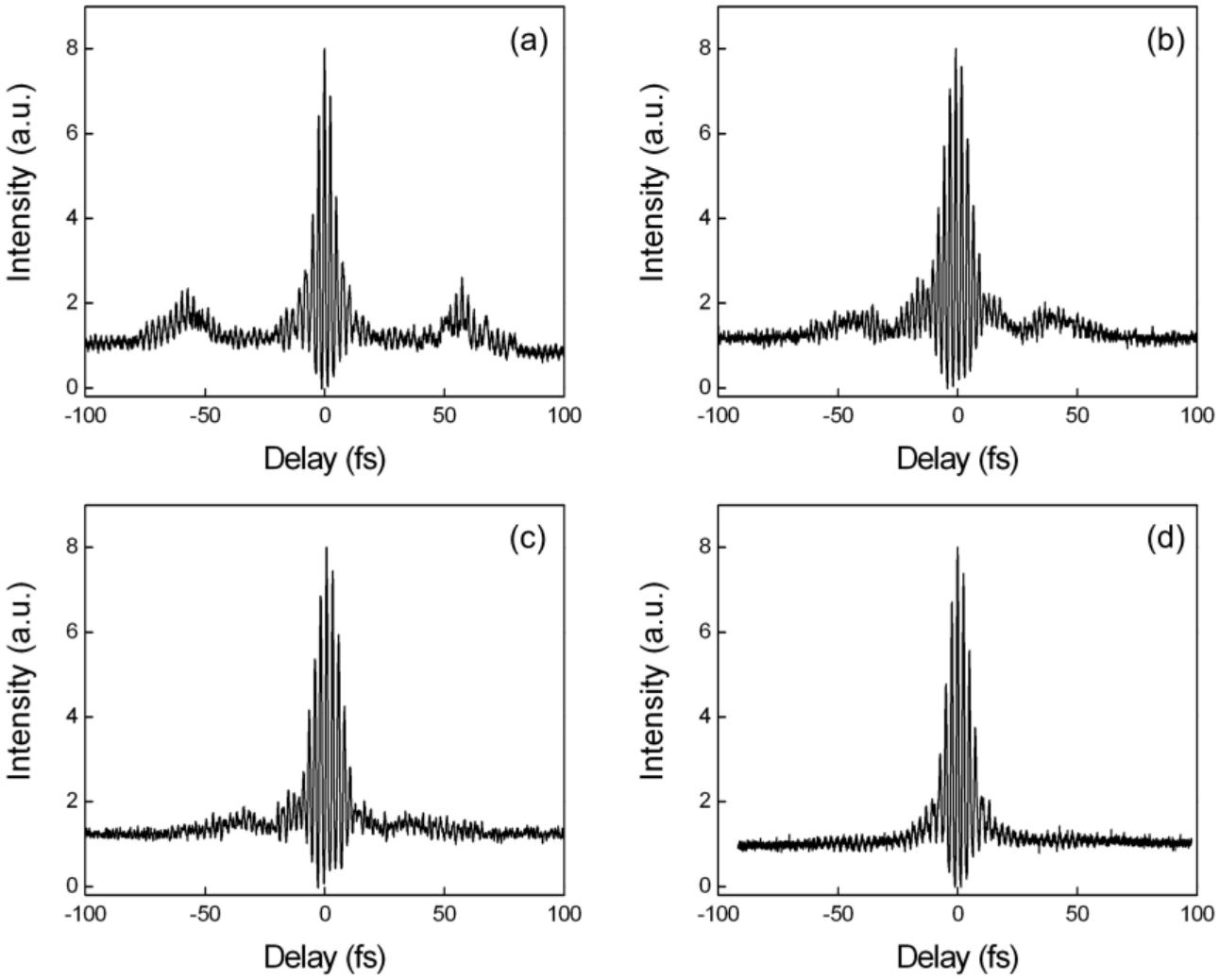

Figure 6-16 **Interferometric autocorrelations of the non-amplified seed.**
(a) With SL1, SL2, CL1, CL2 and 32 bounces.
(b) With SL1, SL2 and 24 bounces.
(c) With SL1, SL2 replaced by a spherical mirror and 20 bounces.
(d) With SL1 and SL2 replaced by spherical mirrors and 18 bounces
SL1, SL2, CL1, CL2 are the lenses represented in figure 6-15.

The calculated residual GDD after 18 bounces is given in figure 6-18a, assuming 6 mm of fused silica, 3 mm of BBO and a total path in the air of 8 m. From figure 6-18b, it is apparent that there will be uncompensated third-order dispersion. This will be confirmed by the results of the pulse characterisation presented in the next section. This higher-order dispersion can be in principal minimised by playing between different combinations of materials of different length and dispersive characteristics, while adjusting the number of bounces on the compressor. A more elegant but challenging approach consists in measuring this residual dispersion and producing mirrors of exactly the opposite value.

Despite the high number of reflections on the mirrors, the compressor is still relatively efficient with a throughput of approximately 80%. From 18 bounces on the dispersive mirrors and six on the silver mirrors (reflectivity of 98%), the losses of the dispersive mirrors can be estimated to be 0.5% per bounce.

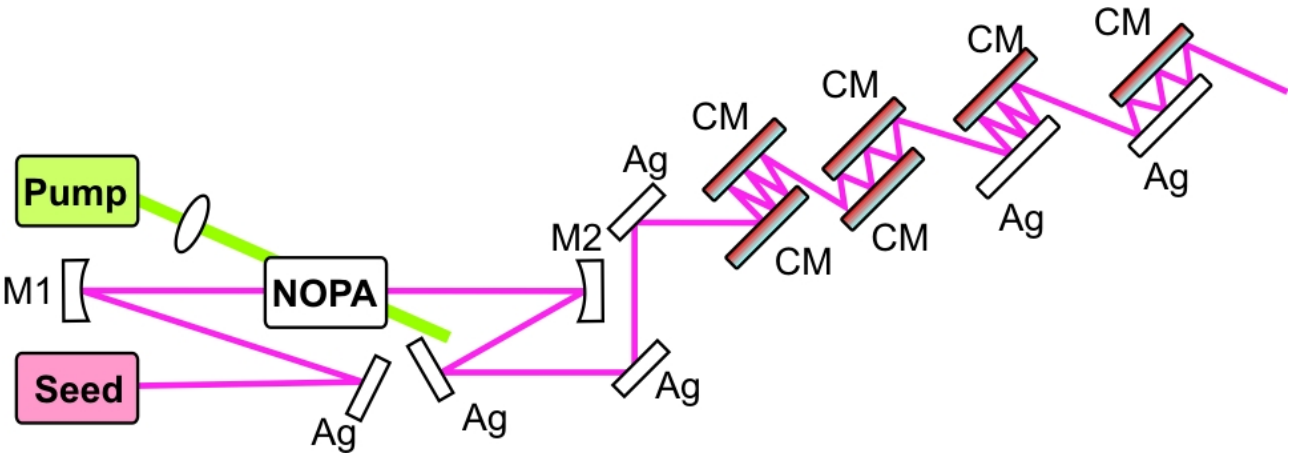

Figure 6-17 **Schematic set-up of the NOPA with reflective optics and chirped mirror compressor. M1, M2: ROC−1000 mm, Ag: flat silver mirror, CM: chirped mirror.**

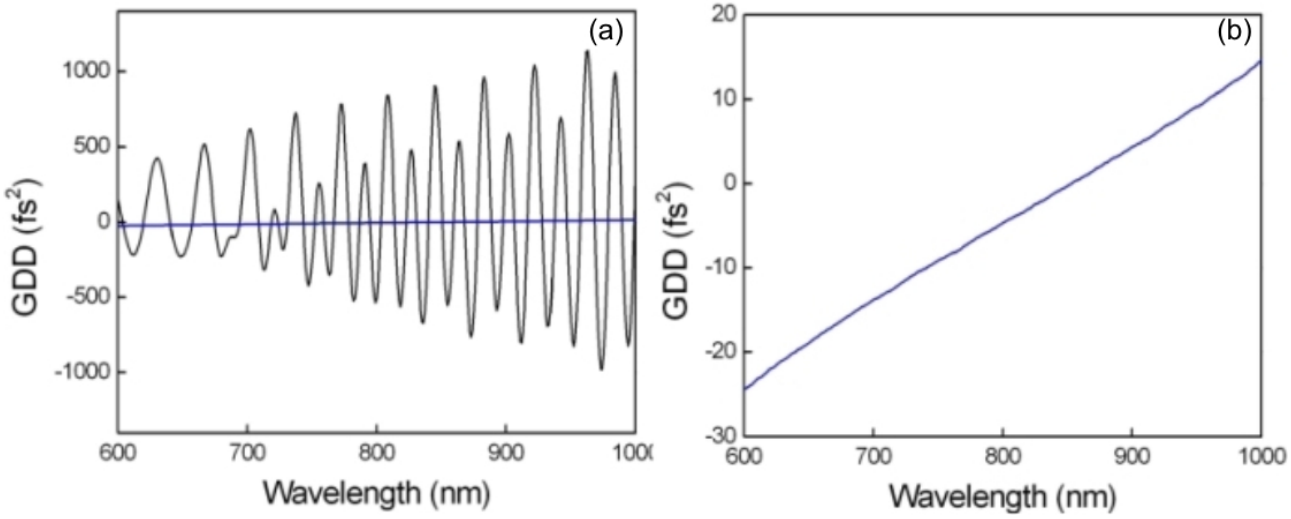

Figure 6-18 **(a) Calculated residual GDD (black line) and its averaged value (blue line) after compression. (b) Calculated residual average GDD (note the change of scale). The mirrors do not compensate for third-order dispersion.**

6.3.2 FROG measurement

Due to some remaining laser instabilities, it was not possible to measure a clear interferometric autocorrelation trace of the amplified pulses. Since this measurement is based on a multi-shot acquisition, high pulse stability is a prerequisite to resolve the interference fringes. Autocorrelation techniques can give some qualitative information about the phase, for a quantitative measurement of the phase other characterisation techniques are usually used such as SPIDER or FROG (see section 2.3.3). Grenouille is a powerful tool for the single-shot measurement of low-energy pulses. Indeed, this concept uses a thicker nonlinear crystal which allows for the generation of an intense second-harmonic signal. Unfortunately, our commercial Grenouille is not able to handle the average power broadband pulses. The residual fundamental light after frequency doubling is not attenuated sufficiently, so that the second-harmonic signal is not distinguishable from the background noise of the fundamental light.

Pulse characterisation was thus performed with a home-made second-harmonic generation FROG. The set-up uses a 10-µm-thick BBO crystal cut at $\theta = 29°$ for type-I phase-matched SHG. The second-harmonic signals are recorded for different delays by a UV-spectrometer. Despite an acquisition time of a few minutes, a coherent FROG trace could be measured, as shown in figure 6-19.

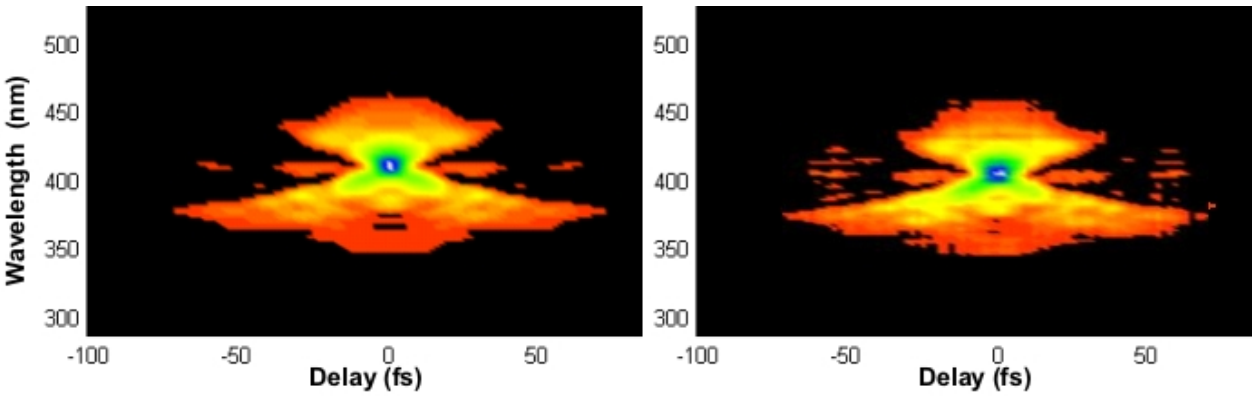

Figure 6-19 Measured (left) and retrieved FROG trace (right).

Figure 6-20a presents the retrieved temporal profile of the amplified pulses. The duration of the main pulse is 9.8 fs, while the transform-limited pulse is calculated to be 6.8 fs. High-order dispersion terms from the different optical elements could not be compensated over the entire spectral range in this chirped mirror compressor (figure 6-20b). The uncompensated quadratic chirp, especially in the blue, is clearly visible in figure 6-19. Such chirp leads to the formation of satellite pulses, which is confirmed by the pulse retrieval shown in figure 6-20a [146].

6.4 Summary of results

A broadband near-infrared high-power OPCPA system was demonstrated based on two passively mode-locked pump and seed lasers. The amplifier is seeded with 1.5-nJ pulses from a

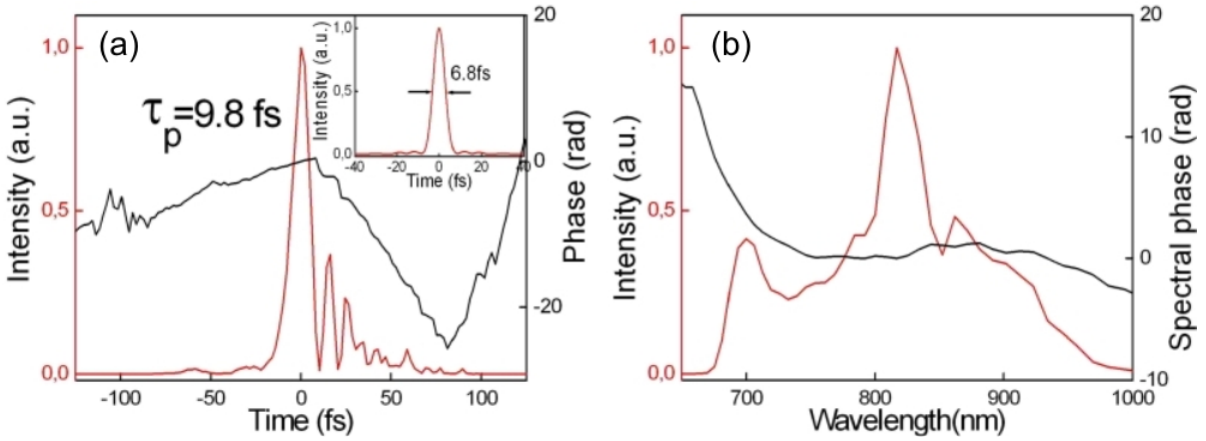

Figure 6-20 **(a) FROG retrieval in the time domain and transformed-limited pulse (inset). (b) FROG retrieval in the spectral domain.**

Ti:Sapphire oscillator, while pumped with 2.9-μJ pulses from the frequency-doubled output of an Yb:YAG thin-disk oscillator The two independent lasers are actively synchronised using a combined electronic and optical control loop. In this preliminary work, up to 700 nJ pulses are generated from a single-stage parametric amplifier. At 11.5 MHz, this corresponds to an average power of 8 W. The calculated transformed-limited pulses have a duration of 7 fs. Despite the relatively low pump pulse energy, a pump-to-signal conversion efficiency as high as 24% is obtained when the seed pulses are stretched to about half the pump pulse width. First compression experiments were undertaken at a lower pulse energy of 250 nJ and resulted in 9.8 fs pulses. The deviation from the transformed-limited pulse duration of approximately 7 fs originates from essentially uncompensated quadratic chirp.

The recent multiplication of parametric amplifiers operating between 100 kHz and few MHz shows the need for high-peak-power pulses at higher repetition rates. Some of these results are summarised in table 6-2. Finer compression and increased compressor output should be possible through new tailored chirped mirrors with higher average GDD values and higher-order dispersion compensation. Further increase of the amplified seed energy could be easily obtained by reducing the beam delivery losses of the pump. Overall, 1-μJ pulses with 7-fs duration seem to be in reach resulting in unprecedented peak powers > 100 GW/cm^2 at MHz repetition rates.

Reference	λ	E_p	τ_p	Rep. Rate
[147]	800 nm	16 μJ	51 fs	80 kHz
[148]	800 nm	37 μJ	52 fs	97 kHz
[149]	3.5μm	1 μJ	92 fs	100 kHz
[150]	3.2μm	1.2 μJ	96 fs	100 kHz
[151]	620 nm	140 nJ	20 fs	500 kHz
[30]	800 nm	30 nJ	16 fs	1 MHz
[34]	800 nm	500 nJ	16 fs	2 MHz
This work	**800 nm**	**200 nJ**	**10 fs**	**11.5 MHz**

Table 6-2 **Comparison bewteen high-repetition-rate OPCPA systems**

6.5 Applications

Numerous application in physics, chemistry, biology or medicine require high-peak-power ultrashort pulses and would benefit from MHz repetition rate laser sources by allowing faster measurements or treatments. This OPCPA system could be used to drive both an electron gun for the generation of tens of keV electron pulses and excite targets in pump-probe experiments with few-cycle pump pulses in the microjoule level [152]. Diffraction experiments based on this electron source could be be applied to the characterisation of structural changes in chemical reactions by resolving molecular reaction dynamics induced by an intense laser pulse.

Another application of this OPCPA could be the study of nanostructures (from material science to biology) in operation with a scattering-type scanning near-field optical microscope (s-SNOM) [153]. Through different frequency generation between the generated idler (1.4 μm) and the residual 1030-nm radiation, it could be possible to obtain a broadband light source in the mid-infrared. In particular the region between 5 to 10 μm is of major interest, as biological molecules and living tissues exhibit characteristic absorption fingerprints. The s-SNOM technology combined with this laser source would provide a unique tool capable of topographic imaging with spectroscopic analysis with 10-nm spatial resolution.

In extreme nonlinear phenomena, the carrier-envelope phase plays a determinant role in the interaction between the medium an the intense few-cycle light pulse. The CEP-stabilisation of our laser source could be easily done by implementation of a highly efficient monolithic CEP-locking scheme to the femtosecond seed oscillator [12]. This would extend the applications possibilities of the laser system to CEP-sensitive experiments.

Nowadays, femtosecond laser systems are routinely used to generate attosecond pulses by means of high-harmonic generation in a noble gas. However, this technique requires extremely intense light sources with energy in the millijoule range [154] typically obtained from Ti:Sapphire-based amplifiers operating at a few kHz repetition rate. Recently, extreme ultraviolet (XUV) radiations were produced from few hundreds of nanojoule pulses using highly efficient hollow-core gas-filled photonic crystal fibres [155]. Combined with this technology, our OPCPA system could open the way to attosecond spectroscopy at MHz repetition rates.

A further development for this system is the amplification of infrared pulses around 2 μm. Through frequency mixing of the low and high frequency wings of the Ti:Sapphire pulse spectrum, a difference-frequency signal centred around 2 μm can be generated and used as a seed for a NOPA pumped directly by the Yb:YAG oscillator pulses. Simultaneously, the difference-frequency generation scheme ensures self-stabilisation of the pulse carrier-envelope phase, which is faithfully preserved in the parametric amplification process. Using intense pulses at longer wavelengths, the cut-off energy of the high-harmonic spectrum can be significantly extended allowing for the generation of shorter coherent extreme ultraviolet radiations and novel experiments in high-field physics [156].

7 Conclusion and outlook

Intense few-cycle-pulse laser sources are readily available using chirped pulse amplification and post-amplification spectral broadening schemes. Based on these technologies sub-femtosecond time scale could be accessed for the first time, leading to the emergence of attosecond science. So far, most of the significant results in this field were obtained using a CPA approach. Over the past decade, great efforts were put into the development of optical parametric chirped pulse amplifiers because of their extreme amplification bandwidths and energy-power scaling possibilities. Unlike gain media with inversion storage, parametric amplification poses nevertheless a severe challenge of ensuring strict synchronisation between the pump and seed pulses. This perennial problem of synchronisation has somewhat hindered the establishment of the OPCPA technology based on two-colour sources for the realisation of high average power systems with ultrashort pulse durations.

In this thesis, two high-repetition rate parametric amplifiers driven by stand-alone pump sources were presented with their synchronisation schemes. The all-optical synchronisations presented in chapter 3 offer a substantial reduction of the complexity and cost in the design of an amplifier-based pump source. Soliton-self-frequency-shift in PCFs is a powerful approach for synchronising a laser amplifier to a femtosecond seed oscillator in the absence of spectral overlap between the two lasers. In this scheme, a fraction of the seed is injected in a PCF to obtain a spectrally-shifted signal inside the gain region of the amplifier medium. Provided a sufficiently broadband seed oscillator, direct seeding of the amplifier yields to a radical simplification of the entire OPCPA systems. Both approaches were successfully demonstrated in this work. Since our first results in 2005, various OPCPA systems were realised using our proposed solutions [28, 31, 34, 151, 157, 158] confirming their reliability and versatility. The PCF approach is ideally suited for parametric amplifiers pumped by ytterbium-doped fibre systems, as it can be directly spliced to the fibre amplifier. Further developments could resolve in robust turn-key all-fibre pump lasers for OPCPA.

The ultrafast laser detailed in chapter 4 based on the power-scalable passively mode-locked thin-disk concept has demonstrated its ability to drive parametric amplifiers at MHz repetition rates with unprecedented average amplified output powers. The elaboration of highly dispersive dielectric mirrors with reduced losses enabled the operation in ambient air of such a high-energy oscillator despite the enhanced Kerr-nonlinearity. Stable single-pulse soliton regime could be obtained with energies up to 6 μJ. Further increase of the thin-disk pulse energy should be possible based on the recent advances in the conception of active multipass resonator cavities [32] and the reduction of the intracavity nonlinearity [109]. Such developments would permit the direct scaling of the parametric amplifier output. Earliest experimental results presented in chapter 6 showed that amplification of 7 fs pulses to the microjoule level is achievable with our current pump source. Tight focusing of these pulses can lead to intensities in the range of 10^{14} GW/cm^2, which are sufficiently high for the generation of soft X-rays by high-order

harmonics in gas-jet targets and hollow-core photonic crystal fibres [155] or by plasmon field enhancement in nanostructures [159]. This would open the way to new extreme ultraviolet sources in the multi-MHz regime with accordingly increased photon flux.

Both OPCPA schemes developed in the framework of this thesis allow for the amplification of carrier-envelope phase stabilised few-cycle pulses. With the implementation of CEP-stabilisation methods, new experiments in high-field physics are conceivable taking full advantage of these high-repetition-rates. Time-resolved attosecond spectroscopy in the kHz and MHz regimes would allow faster acquisition times and improved signal-to-noise ratios for accurate tracing of electron dynamics.

A List of acronyms

AC	Autocorrelation
ASE	Amplified spontaneous emission
BBO	Beta barium borate
BiBO	Bismuth borate crystal
BK7	Type of borosilicate crown glass
CEP	Carrier-envelope phase
CPA	Chirped pulse amplification
CW	Continuous wave
FROG	Frequency-resolved optical gating
FWHM	Full-width at half-maximum
GD	Group delay
GDD	Group dispersion delay
GRENOUILLE	Grating-eliminated no-nonsense observation of ultrafast incident laser light E-fields
GVD	Group velocity dispersion
KD*P	Potassium dideuterium phosphate
LBO	Lithium borate
Lu_2O_3	Lutetium oxide
Nd	Neodymium
NIR	Near-infrared
NOPA	Noncollinear optical parametric amplification
OPA	Optical parametric amplification
OPCPA	Optical parametric chirped pulse amplification
OPO	Optical parametric oscillator
PCF	Photonic crystal fibre
PLL	Phase-locked loop
PZT	Piezo transducer
RF	Radio frequency
RMS	Root mean square
ROC	Radius of curvature
RTP	Rubidium titanyle phosphate
SBR	Semiconductor Bragg reflector
Sc_2O_3	Scandium oxide
SFG	Sum-frequency generation
SHG	Second harmonic generation
SNOM	Scanning near-field microscope
SPIDER	Spectral phase interferometry for direct electric field reconstruction
SPM	Self-phase modulation
SSFS	Soliton self-frequency shift
TEM_{00}	Transverse electromagnetic mode 00
TOD	Third-order dispersion
TL	Transform-limited
UV	Ultraviolet
VCO	Voltage controlled oscillator
XUV	Extreme ultraviolet
YAG	Yttrium aluminum garnet
Yb	Ytterbium
YLF	Yttrium lithium fluoride

B List of physical symbols

α	Noncollinear seed-pump angle
β	Noncollinear idler-pump angle
d_{eff}	Effective second order nonlinear coefficient
Δk	Wave vector mismatch
Δk_{FWHM}	FWHM phase-matching bandwidth
ΔR	Modulation depth
Δ_{ns}	Nonsaturable losses
E_p	Pulse energy
f	focal length
$F_{A,sat}$	Fluence of the saturable absorber
$F_{L,sat}$	Fluence of the laser medium
f_{RO}	Frequency of the relaxation oscillation
γ_{SPM}	Nonlinear phase-shift
I_p	Pump intensity
I_s	Seed intensity
I_{s0}	Initial seed intensity
k_i	Idler wave vector
k_p	Pump wave vector
k_s	Seed wave vector
l	Cavity losses
L	Length
M^2	Beam quality factor
n	Refractive index
n_e	Extraordinary refractive index
n_i	Idler refractive index
n_{ie}	Idler extraordinary refractive index
n_{io}	Idler ordinary refractive index
n_o	Ordinary refractive index
n_p	Pump refractive index
n_{pe}	Pump extraordinary refractive index
n_s	Seed refractive index
n_{so}	Seed ordinary refractive index
n_2	Nonlinear refractive index
ω_i	Idler angular frequency
ω_p	Pump angular frequency
ω_s	Seed angular frequency
P_{int}	Intracavity power
σ_j	RMS timing jitter
τ_a	Recovery time of the absorber
τ_g	Laser material upper state life time
τ_i	Timing jitter
τ_p	Pulse duration
τ_r	Cavity round-trip time
v_{gi}	Group velocity of the idler
v_{gs}	Group velocity of the seed
w	$1/e^2$ intensity mode radius
Z_0	Vacuum impedance

C Dispersion and ultrashort pulses

$$\text{with} \quad \omega = 2\pi f, \quad f = \frac{c_0}{\lambda}, \quad k = n\frac{2\pi}{\lambda} = n\frac{\omega}{c_0}, \quad \varphi = \omega t$$

Phase velocity: $$v_\phi = \frac{\omega}{k} = \frac{c_0}{n}$$

Group velocity: $$v_g = \frac{d\omega}{dk} = v_\phi \frac{1}{1 + \frac{\omega}{n}\frac{dn}{d\omega}} = v_\phi \frac{1}{1 - \frac{\lambda}{n}\frac{dn}{d\lambda}}$$

Group velocity dispersion (GVD): $$GVD = \frac{d^2k}{d\omega^2} = \frac{d}{d\omega}\left(\frac{1}{v_g}\right) = \frac{\lambda^3}{2\pi c_0^2}\frac{d^2n}{d\lambda^2}$$

Third order dispersion (TOD): $$TOD = \frac{d^3k}{d\omega^3} = -\frac{\lambda^4}{(2\pi)^2 c_0^3}\left(3\frac{d^2n}{d\lambda^2} + \lambda\frac{d^3n}{d\lambda^3}\right)$$

Group delay: $$GD = \frac{d\varphi}{d\omega} = \frac{L}{v_g}$$

Group delay dispersion (GDD): $$GDD = \frac{d^2\varphi}{d\omega^2} = GVD \cdot L$$

For an initial transformed limited pulse of duration τ_{TL}, dispersion lengthened to pulse to:

$$\tau_p(GDD) = \tau_{TL} \cdot \sqrt{1 + (4\ln 2 \cdot \frac{GDD}{\tau_{TL}^2})^2}$$

For the calculation of the GDD, the following expressions of the Sellmeier equation were used.

Material	Reference
Air	[160]
FS	[161]
BK7	[162]
BBO	[143]

D Bibliography

[1] H. Mainam, "Stimulated optical radiation in ruby," Nature **187**, 493 (1960).

[2] S. Nolte, C. Momma, H. Jacobs, A. Tunnemann, B. N. Chichkov, B. Wellegehausen, and H. Welling, "Ablation of metals by ultrashort laser pulses," J. Opt. Soc. Am. B **14**, 2716 (1997).

[3] A. Heisterkamp, H. Lubatschowski, F. Will, A. Singh, J. Sebrin, A. Ostendorf, O. Kermani, R. Heermann, H. Welling, W. Ertmer, "Medical applications for ultrafast laser pulses," RIKEN Rev. **50** (2003).

[4] M. Dantus, M.J. Rosker, and A.H. Zewail, "Real-Time Femtosecond Probing of Transition-States in Chemical-Reactions," J. Chem. Phys. **87**, 2395 (1987).

[5] A.H. Zewail, "Femtochemistry: Atomic-scale dynamics of the chemical bond,"nbJ. Phys. Chem. A **104**, 5660 (2000).

[6] E. Goulielmakis, M. Schultze, M. Hofstetter, V.S. Yakovlev, J. Gagnon, M. Uiberacker, A.L. Aquila, E.M. Gullikson, D.T. Attwood, R. Kienberger, F. Krausz and U. Kleineberg, "Single-Cycle Nonlinear Optics," Science **320**, 1614 (2008).

[7] P.F. Moulton, "Spectroscopic and laser characteristics of Ti:Al_2O_3," J. Opt. Soc. Am. B **3**, 125 (1986).

[8] D. Strickland and G. Mourou, "Compression of amplified chirped optical pulses," Opt. Commun. **56**, 219 (1985).

[9] A. Dubietis, G. Jonusauskas, and A. Piskarskas, "Powerful femtosecond pulse generation by chirped and stretched pulse parametric amplification in BBO crystal," Opt. Commun. **88**, 437 (1992).

[10] H.R. Telle, G. Steinmeyer, A.E. Dunlop, J. Stenger, D.H. Sutter, and U. Keller, "Carrier-envelope offset phase control: A novel concept for absolute optical frequency measurement and ultrashort pulse generation," Appl. Phys. B **69**, 327 (1999).

[11] A. Baltuska, T. Fuji, and T. Kobayashi, "Controlling the carrier-envelope phase of iltrashort light pulses with optical parametric amplifiers," Phys. Rev. Lett. **88**, 133901 (2002).

[12] T. Fuji, J. Rauschenberger, A. Apolonski, V.S. Yakovlev, G. Tempea, T. Udem, C. Gohle, T. W. Hänsch, W. Lehnert, M. Scherer, and F. Krausz, "Monolithic carrier-envelope phase-stabilization scheme," Opt. Lett. **30**, 332 (2005).

[13] A. Baltuska, T. Udem, M. Uiberacker, M. Hentschel, E. Goulielmakis, C. Gohle, R. Holzwarth, V.S. Yakovlev, A. Scrinzi, T.W. Hänsch, and F. Krausz, "Attosecond control of electronic processes by intense light fields," Nature **421**, 611 (2003).

[14] R. Kienberger, M. Hentschel, M. Uiberacker, Ch. Spielmann, M. Kitzler, A. Scrinzi, M. Wieland, Th. Westerwalbesloh, U. Kleineberg, U. Heinzmann, M. Drescher and F. Krausz, "Steering attosecond electron wave packets with light," Science **297**, 1144 (2002).

[15] F. Grüner, S. Becker, U. Schramm, T. Eichner, M. Fuchs, R. Weingartner, D. Habs, J. Meyer-ter-Vehn, M. Geissler, M. Ferrario, L. Serafini, B. van der Geer, H. Backe, W. Lauth and S. Reiche, "Design considerations for table-top, laser-based VUV and X-ray free electron lasers," Appl. Phys. B **86**, 431 (2007).

[16] M.D. Perry, D. Pennington, B.C. Stuart, G. Tietbohl, J.A. Britten, C. Brown, S. Herman, B. Golick, M. Kartz, J. Miller, H. T. Powell, M. Vergino, and V. Yanovsky, "Petawatt laser pulses," Opt. Lett. **24**, 160 (1999).

[17] A.A. Eilanlou, Y. Nabekawa, K. L. Ishikawa, H.Takahashi, and K. Midorikawa, "Direct amplification of terawatt sub-10-fs pulses in a CPA system of Ti:sapphire laser," Opt. Express **16**, 13431 (2008).

[18] C.P. Hauri, P. Schlup, G. Arisholm, J. Biegert, and U. Keller, "Phase-preserving chirped-pulse optical parametric amplification to 17.3 fs directly from a Ti:sapphire oscillator," Opt. Lett. **29**, 1369 (2004).

[19] E. Mével, O. Tcherbakoff, F. Salin, and E. Constant, "Extracavity compression technique for high-energy femtosecond pulses," J. Opt. Soc. Am. B **20**, 105 (2003).

[20] A.J. Verhoef, J. Seres, K. Schmid, Y. Nomura, G. Tempea, L. Veisz and F. Krausz, "Compression of the pulses of a Ti:sapphire laser system to 5 femtoseconds at 0.2 terawatt level," Appl. Phys. B **82**, 513 (2006).

[21] Z. Major, S.A. Trushin, I. Ahmad, M.Siebold, C. Wandt, S. Klingebiel, T. Wa, J. Fülop, A. Henig, S. Kruber, R. Weingartner, A. Popp, J. Osterhoff, R. Hörlein, J. Hein, V. Pervak, A. Apolonski, F. Krausz and S. Karsch, "Basic Concepts and Current Status of the Petawatt Field Synthesizer – A New Approach to Ultrahigh Field Generation," Laser Rev. **37**, 431 (2009).

[22] J. Zhou, C. Huang, M.M. Murnane, and H. C. Kapteyn, "Amplification of 26-fs, 2-TW pulses near the gain-narrowing limit in Ti:sapphire," Opt. Lett. **20**, 64 (1995).

[23] D. Herrmann, L. Veisz, R. Tautz, F. Tavella, K. Schmid, V. Pervak, and Ferenc. Krausz, "Generation of sub-three-cycle, 16 TW light pulses by using noncollinear optical parametric chirped-pulse amplification," Opt. Lett. **34**, 2459 (2009).

[24] S. Witte, R.T. Zinkstok, W. Hogervorst, and K.S.E. Eikema, "Generation of few-cycle terawatt light pulses using optical parametric chirped pulse amplification," Opt. Express **13**, 4903 (2005).

[25] N. Ishii, L. Turi, V.S. Yakovlev, T. Fuji, F. Krausz, A. Baltuska, R. Butkus, G. Veitas, V. Smilgevicius, R. Danielius, and A. Piskarskas, "Multimillijoule chirped parametric

amplification of few-cycle pulses," Opt. Lett. **30**, 567 (2005).

[26] Z.Y. Wei, Y. Kobayashi, Z.G. Zhang, and K. Torizuka, "Generation of two-color femtosecond pulses by self-synchronizing Ti : sapphire and Cr : forsterite lasers," Opt. Lett. **26**, 1806 (2001).

[27] G. Cerullo, M. Nisoli, S. Stagira, and S. De Silvestri, "Sub-8-fs pulses from an ultrabroadband optical parametric amplifier in the visible," Opt. Lett. **23**, 1283 (1998).

[28] F. Tavella, A. Marcinkevicius, and F. Krausz, "90 mJ parametric chirped pulse amplification of 10 fs pulses," Opt. Express **14**, 12822 (2006).

[29] V.V. Lozhkarev, G.I. Freidman, V.N. Ginzburg, E.V. Katin, E.A. Khazanov, A.V. Kirsanov, G.A. Luchinin, A.N. Malshakov, M.A. Martyanov, O.V. Palashov, A.K. Poteomkin, A.M. Sergeev, A.A. Shaykin, S.G. Garanin, S. Sukharev, N.N. Rukavishnikov, V. Charukhchev, R.R. Gerke, V.E. Yashin and I.V. Yakovlev, "200 TW 45 fs laser based on optical parametric chirped pulse amplification," Opt. Express **14**, 446 (2006).

[30] A. Killi, Andy Steinmann, G. Palmer, U. Morgner, H. Bartelt, and J. Kobelke, "Megahertz optical parametric amplifier pumped by a femtosecond oscillator," Opt. Lett. **31**, 125 (2006).

[31] T. Metzger, A. Schwarz, C.Y. Teisset, D. Sutter, A. Killi, R. Kienberger, and F. Krausz, "High-repetition-rate picosecond pump laser based on a Yb:YAG disk amplifier for optical parametric amplification," Opt. Lett. 34, 2123 (2009).

[32] J. Neuhaus, D. Bauer, J. Kleinbauer, A. Killi, S. Weiler, D.H. Sutter and T. Dekorsy, "Pulse energies exceeding twenty microjoule directly from a femtosecond Yb:YAG oscillator," XVI International Conference on Ultrafast Phenomena, Stresa, Italy (2008).

[33] P. Russbueldt, T. Mans, G. Rotarius, J. Weitenberg, H.D. Hoffmann, and R. Poprawe, "400 W Yb:YAG Innoslab fs-Amplifier," Opt. Express **17**, 12230 (2009).

[34] J. Rothhardt, S. Hädrich, D.N. Schimpf, J. Limpert, and A. Tünnermann, "High repetition rate fiber amplifier pumped sub-20 fs optical parametric amplifier," Opt. Express **15**, 16729, (2007).

[35] R.A. Bartels, A. Paul, H. Green, H.C. Kapteyn, M.M. Murnane, S.Backus, I.P. Christov, Y. Liu, D. Attwood, and C. Jacobsen, "Generation of Spatially Coherent Light at Extreme Ultraviolet Wavelengths," Science **297**, 376 (2002).

[36] C.Y. Teisset, N. Ishii, T. Fuji, T. Metzger, S. Köhler, R. Holzwarth, A. Baltuska, A.M. Zheltikov and F. Krausz, "Soliton-based pump-seed synchronization for few-cycle OPCPA," Opt. Express. **13**, 6550 (2005).

[37] C. Y. Teisset, H. Fattahi, A. Sugita, L. Turi, X. Gu, O. Pronin, V. Pervak, F. Krausz and A. Apolonski, "700 nJ Broadband MHz Optical Parametric Amplifier," Conference on ultrafast optics, Arcachon, France (2009).

[38] R.W. Boyd, "Nonlinear Optics", Academic Press, 3rd edition (2008).

[39] A. Fragemann, V. Pasiskevicius, G. Karlsson, and F. Laurell, "High-peak power nanosecond optical parametric amplifier with periodically poled KTP," Opt. Express **11**, 1297 (2003).

[40] M.E. Fermann, A. Galvanauskas, and G. Sucha, "Ultrafast Lasers: Technology and Applications," CRC Press (2007).

[41] J.A. Fülöp, ZS. Major, B. Horvat, F. Tavella, A. Baltuska and F. Krausz, "Shaping of picosecond pulses for pumping optical parametric amplification," Appl. Phys. B **87**, 79 (2007).

[42] Y. Park, M. Kulishov, R. Slavik, and J. Azaña, "Picosecond and sub-picosecond flat-top pulse generation using uniform long-period fiber gratings," Opt. Express **14**, 12670 (2006).

[43] N. Ishii, "Development of optical parametric chirped-pulse amplifiers and their applications," Ph.D-Thesis, Ludwig-Maximilians-Universität München, Department für Physik, (2006).

[44] T. Clausnitzer, J. Limpert, K. Zöllner, H. Zellmer, H.-J. Fuchs, E.-B. Kley, A. Tünnermann, M. Jupé, and D. Ristau, "Highly Efficient Transmission Gratings in Fused Silica for Chirped-Pulse Amplification Systems," Appl. Opt. **42**, 6934 (2003).

[45] Robert Szipöcs, Kárpát Ferencz, Christian Spielmann, and Ferenc Krausz, "Chirped multilayer coatings for broadband dispersion control in femtosecond lasers," Opt. Lett. **19**, 201 (1994).

[46] FEMTOSOURCE^{TM}RAINBOW^{TM}, http://www.femtolasers.com/.

[47] I. Ahmad, V. Pervak, S.A. Trushin, Zs. Major, S. Karsch and F. Krausz, "Implementation of all-dispersive-mirror compressor for mJ-scale sub-20-fs chirped pulse amplifier," Conference on ultrafast optics, Arcachon, France (2009).

[48] J.-C. Diels and W. Rudolph, "Ultrashort laser pulse phenomena: fundamentals, techniques, and applications on a femtosecond time scale," Academic Press (2006).

[49] F. Tavella, Y. Nomura, L. Veisz, V. Pervak, A. Marcinkevicius, and F. Krausz, "Dispersion management for a sub-10-fs, 10 TW optical parametric chirped-pulse amplifier," Opt. Lett. **32**, 2227 (2007).

[50] C. Iaconis and I. A. Walmsley, "Self-referencing spectral interferometry for measuring ultrashort optical pulses," IEEE J. QE. **35**, 501 (1999).

[51] D. Kane and R. Trebino, "Characterization of arbitrary femtosecond pulses using frequency-resolved optical gating", IEEE J. QE. **29**, 571 (1993).

[52] P. O'Shea, M. Kimmel, X. Gu, and R. Trebino, "Highly simplified ultrashort pulse measurement," Opt. Lett. **26**, 932 (2001).

[53] B. C. Stuart, M.D. Feit, S. Herman, A. M. Rubenchik, B.W. Shore, and M.D. Perry, "Nanosecond-to-femtosecond laser-induced breakdown in dielectrics," Phys. Rev. B **53**, 1749 (1996).

[54] F. Tavella, K. Schmid,N. Ishii, A. Marcinkevicius, L. Veisz, and F.Krausz, "High-dynamic range pulse-contrast measurements of a broadband optical parametric chirped-pulse amplifier," Appl. Phys. B **81**, 753 (2005).

[55] J. Dörring, A. Killi, U. Morgner, A. Lang, M. Lederer, and D. Kopf, "Period doubling and deterministic chaos in continuously pumped regenerative amplifiers," Opt. Express **12**, 1759 (2004).

[56] A. E. Siegman, "Lasers," University Science Books, (1986).

[57] A. J. DeMaria, D. A. Stetser, and H. Heynau, "Self mode-locking of lasers with saturable absorbers," Appl. Phys. Lett. **8**, 174 (1966).

[58] T. Brabec, C. Spielmann, P. F. Curley, and F. Krausz, "Kerr lens mode locking," Opt. Lett. **17**, 1292 (1992).

[59] T. Fuji, A. Unterhuber, V.S. Yakovlev, G. Tempea, A. Stingl, F. Krausz, and W. Drexler, "Generation of smooth, ultra-broadband spectra directly from a prism-less Ti:sapphire laser," Appl. Phys. B **77**, 125 (2003).

[60] C. Hönninger, R. Paschotta, F. Morier-Genoud, M. Moser, and U. Keller, "Q-switching stability limits of continuous-wave passive mode locking," J. Opt. Soc. Am. B **16**, 46 (1999).

[61] U. Keller, K.J. Weingarten, F. X. Kartner, D. Kopf, B. Braun, I. D. Jung, R. Fluck, C. Honninger, N. Matuschek, and J. Aus der Au, "Semiconductor saturable absorber mirrors (SESAM's) for femtosecond to nanosecond pulse generation in solid-state lasers," IEEE J. QE. **2**, 435 (1996).

[62] M. Haiml, R. Grange, and U. Keller, "Optical characterization of semiconductor saturable absorbers," Appl. Phys. B **79**, 331 (2004).

[63] F.X. Kärtner, and U. Keller, "Stabilization of solitonlike pulses with a slow saturable absorber," Optics Lett. **202**, 16 (1995).

[64] W. Seitz, T.R. Schibli, U. Morgner, F.X. Kärtner, C.H. Lange, W. Richter, and B. Braun, "Passive synchronization of two independent laser oscillators with a Fabry-Perot modulator," Opt. Lett. **27**, 454 (2002).

[65] G. Banfi, P. Di Trapani, R. Danielius, A. Piskarskas, R. Righini, and I. Santa, "Tunable femtosecond pulses close to the transform limit from traveling-wave parametric conversion," Opt. Lett. **18**, 1547 (1993).

[66] T. Sosnowski, P.B. Stephens, and T.B. Norris, "Production of 30-fs pulses tunable

throughout the visible spectral region by a new technique in optical parametric amplification," Opt. Lett. **21**, 140 (1996).

[67] A. Shirakawa, I. Sakane, M. Takasaka, and T. Kobayashi, "Sub-5-fs visible pulse generation by pulse-front-matched noncollinear optical parametric amplification," Appl. Phys. Lett. **74**, 2268 (1999).

[68] E. Riedle, M. Beutter, S. Lochbrunner, J. Piel, S. Schenkl, S. Spoerlein, and W. Zinth, "Generation of 10 to 50 fs pulses tunable through all of the visible and the NIR," Appl. Phys. B. **71**, 457 (2000).

[69] Fully integrated broadly tunable femtosecond Ytterbium system "Pharos" http://www.lightcon.com.

[70] C. Manzoni, G. Cerullo, and S. De Silvestri, "Ultrabroadband self-phase-stabilized pulses by difference-frequency generation," Opt. Lett. **29**, 2668 (2004).

[71] D.J. Jones, S.A. Diddams, J.K. Ranka, A. Stentz, R.S.Windeler, J.L. Hall, and S.T. Cundiff, "Carrier-envelope phase control of femtosecond mode-locked lasers and direct optical frequency synthesis," Science **288**, 635 (2000).

[72] A. Apolonski, A. Poppe, G. Tempea, C. Spielmann, T. Udem, R. Holzwarth, T.W. Hänsch, and F. Krausz, "Controlling the Phase Evolution of Few-Cycle Light Pulses," Phys. Rev. Lett. **85**, 740 (2000).

[73] T. Brabec and F. Krausz, "Intense few-cycle laser fields: Frontiers of nonlinear optics," Rev. Mod. Phys **72**, 545 (2000).

[74] I.N. Ross, P. Matousek, M. Towrie, A.J. Langley, and J.L. Collier, "The prospects for ultrashort pulse duration and ultrahigh intensity using optical parametric chirped pulse amplifiers," Opt. Commun. **144**, 125 (1997).

[75] X. Yang, Z. Xu, Y. Leng, H. Lu, L. Lin, Z. Zhang, R. Li, W. Zhang, D. Yin, and B. Tang, "Multiterawatt laser system based on optical parametric chirped pulse amplification," Opt. Lett **27**, 1135 (2002).

[76] R. Butkus, R. Danielius, R. Dubietis, A. Piskarskas, and A. Stabinis, "Progress in chirped pulse optical parametric amplifiers," Appl. Phys. B **79**, 693 (2004).

[77] R.T. Zinkstok, S. Witte, W. Hogervorst,and K.S.E. Eikema, "High-power parametric amplification of 11.8-fs laser pulses with carrier-envelope phase control," Opt. Lett. **30**, 78 (2004).

[78] M.J.W. Rodwell, D.M. Bloom, and K.J. Weingarten, "Subpicosecond laser timing stabilization," IEEE J. Quantum Electron. **25**, 817 (1989).

[79] W.F. Krupke, "Ytterbium solid-state lasers- the first decade," IEEE J. Sel. Top. in Quantum Electron. **6**, 1287 (2000).

[80] A. Baltuska, T. Fuji, and T. Kobayashi, "Self-Referenced 200 MHz octave-spanning Ti:Sapphire laser with 50 attosecond carrier envelope phase jitter," Opt. Lett. **27**, 306 (2002).

[81] H. Zheng, J. Wu, H. Xu, K. Wu, and E. Wu, "Generation of accurately synchronized pump source for optical parametric chirped pulse amplification," Appl. Phys. B **79**, 837 (2004).

[82] G.P. Agrawal, "Nonlinear Fiber Optics," Academic Press, San Diego (2001).

[83] F.M. Mitschke and L.F. Mollenauer, "Discovery of the soliton self-frequency shift," Opt. Lett. **11**, 659 (1986).

[84] E.M. Dianov, A.Y. Karasik, P.V. Mamyshev, A.M. Prokhorov, V.N. Serkin, M.F. Stel'makh, and A.A. Fomiche, "Stimulated-Raman conversion of multisoliton pulses in quartz optical fibers," JETP Lett. **41**, 294 (1985).

[85] P. Russell, "Photonic Crystal Fibers," Science **299**, 358 (2003).

[86] X. Liu, C. Xu, W.H. Knox, J.K. Chandalia, B.J. Eggleton, S.G. Kosinski, and R.S. Windeler, "Soliton self-frequency shift in a short tapered air-silica microstructure fiber," Opt. Lett. **26**, 358 (2001).

[87] W.H. Reeves, D.V. Skryabin, F. Biancalana, J.C. Knight, P.S.J. Russell, F.G. Omenetto, A. Efimov, and A.J. Taylor, "Transformation and control of ultra-short pulses in dispersion-engineered photonic crystal fibres," Nature **424**, 511 (2003).

[88] E.E. Serebryannikov, A.M. Zheltikov, N. Ishii, C.Y. Teisset, S. Köhler, T. Fuji, T. Metzger, F. Krausz, and A. Baltuska, "Soliton self-frequency shift of 6-fs pulses in photonic-crystal fibers," Appl. Phys. B **81**, 579 (2005).

[89] T.M. Fortier, D.J. Jones, and S.T. Cundiff, "Phase stabilization of an octave-spanning Ti:sapphire laser," Opt. Lett. **28**, 2198 (2003).

[90] O.D. Mücke, R. Ell, A. Winter, J.-W. Kim, J.R. Birge, L. Matos, and F.X. Kärtner, "Self-Referenced 200 MHz Octave- Spanning Ti:Sapphire Laser with 50 Attosecond Carrier-Envelope Phase Jitter," Opt. Express **13**, 5163 (2005).

[91] A. Poppe, L. Xu, F. Krausz, and C. Spielmann, "Noise Characterization of Sub-10-fs Ti:Sapphire Oscillators," IEEE J. Sel. Top. in Quantum Electron. **4**, 179 (1998).

[92] A. Giesen, H. Hügel, A. Voss, K. Wittig, U. Brauch, and H. Opower, "Scalable Concept for Diode-Pumped High-Power Solid-State Lasers," Appl. Phys. B **58**, 363 (1994).

[93] K. Contag, M. Karszewski, C. Stewen, A. Giesen, H. Hügel, "Theoretical modelling and experimental investigations of the diode-pumped thin disk Yb:YAG laser," IEEE J. Quantum Electron. **29**, 697 (1999).

[94] A. Giesen and J. Speiser, "Fifteen years of work on thin-disk lasers: Results and scaling

laws," IEEE J. QE. **13**, 598 (2007).

[95] A. Killi, I. Zawischa, D. Sutter, J. Kleinbauer, S. Schad, J. Neuhaus, and C. Schmitz, "Current status and development trends of disk laser technology," Proceedings of SPIE, **6871**, 68710 (2008).

[96] F. Brunner, E. Innerhofer, S.V. Marchese, T. Südmeyer, R. Paschotta, T. Usami, H. Ito, S. Kurimura, K. Kitamura, G. Arisholm, and Ursula Keller, "Powerful red-green-blue laser source pumped with a mode-locked thin disk laser", Opt. Lett. **29**, 1921 (2004).

[97] V. Pervak, C. Teisset, A. Sugita, S. Naumov, F. Krausz, A. Apolonski, "High-dispersive mirrors for femtosecond lasers," Opt. Express **16**, 10220 (2008).

[98] U. Griebner, V. Petrov, K. Petermann, and V. Peters, "Passively mode-locked Yb:Lu_2O_3 laser," Opt. Express **12**, 3125 (2004).

[99] S. Uemura and K. Torizuka, "Kerr-Lens Mode-Locked Diode-Pumped Yb:YAG Laser with the Transverse Mode Passively Stabilized," Appl. Phys. Express **1**, 012007 (2008).

[100] H. Bruesselbach and D.S. Sumida, "A 2.65-kW Yb:YAG single-rod laser," IEEE J. QE. **11**, 600 (2005)

[101] T. Taira, "RE3+ -Ion-Doped YAG Ceramic Lasers," IEEE J. QE. **13**, 798 (2007).

[102] A. Ikesue and Y. L. Aung, "Ceramic laser materials," Nat. Photon. **2**, 721 (2008).

[103] G. Palmer, M. Schultze, M. Siegel, M. Emons, U. Bünting, and U. Morgner, "Passively mode-locked Yb:$KLu(WO_4)_2$ thin-disk oscillator operated in the positive and negative dispersion regime," Opt. Lett. **33**, 1608 (2008)

[104] S.V. Marchese, C.R.E. Baer, R. Peters, C. Kränkel, A.G. Engqvist, M. Golling, D.J H.C. Maas, K. Petermann, T. Südmeyer, G. Huber, and U. Keller, "Efficient femtosecond high power Yb:Lu_2O_3 thin disk laser," Opt. Express **15**, 16966 (2007).

[105] K. Petermann, G. Huber, L. Fornasiero, S. Kuch, E. Mix, V. Peters, S. A. Basun, "Rare-earth-doped sesquioxides," J. Lumin. **87**, 973 (2000).

[106] V. Magni, "Multielement stable resonators containing a variable lens," J. Opt. Soc. Am. A **4**, 1962 (1987).

[107] H. Kogelnik and T. Li, "Laser Beams and Resonators," Appl. Opt. **5**, 1550 (1966).

[108] R. Paschotta, and U. Keller, "Passive mode locking with slow saturable absorbers," Appl. Phys. B **73**, 653 (2001).

[109] S.V. Marchese, T. Südmeyer, M. Golling, R. Grange, and U. Keller, "Pulse energy scaling to 5 μJ from a femtosecond thin disk laser," Opt. Lett. **31**, 2728 (2006).

[110] E.T.J. Nibbering, G. Grillon, M.A. Franco, B.S. Prade, and A. Mysyrowicz, "Determination of the inertial contribution to the nonlinear refractive index of air, N_2, and O_2 by use

of unfocused high-intensity femtosecond laser pulses," J. Opt. Soc. Am. B **14**, 650 (1997).

[111] S.V. Marchese, C.R.E. Baer, A. G. Engqvist, S. Hashimoto, D. J. H. C. Maas, M. Golling, T. Südmeyer and U. Keller "Femtosecond thin disk laser oscillator with pulse energy beyond the 10-microjoule level," Opt. Express **16**, 6397 (2008).

[112] E. Innerhofer, T. Südmeyer, F. Brunner, R. Häring, A. Aschwanden, R. Paschotta, U. Keller, C. Hönninger, and M. Kumkar, "60 W average power in 810-fs pulses from a thin-disk Yb:YAG laser," Opt. Lett. **28**, 367 (2003).

[113] D. von der Linde, "Characterization of the noise in continuously operating mode-locked lasers," Appl. Phys. B **39**, 201 (1986).

[114] A. Poppe, L. Xu, F. Krausz, and C. Spielmann, "Noise characterization of sub-10-fs Ti:sapphire oscillators," IEEE J. QE. **4**, 179 (1998).

[115] E. Innerhofer, "High average power Yb:YAG thin disk laser and its application for an RGB laser source," Series in Quantum Electronics, **37** (2005).

[116] C. Hönninger, I. Johannsen, M. Moser, G. Zhang, A. Giesen and U. Keller, "Diode-pumped thin-disk Yb:YAG regenerative amplifier," Appl. Phys. B **65**, 423 (1997).

[117] U. Griebner, V. Petrov, K. Petermann, and V. Peters, "Passively mode-locked Yb:Lu2O3 laser," Opt. Express **12**, 3125 (2004).

[118] C.R.E. Baer, C. Kränkel, C.J. Saraceno, O.H. Heckl, M. Golling, T. Südmeyer, R. Peters, K. Petermann, G. Huber, and U. Keller, "63-W Average Power from Femtosecond Yb:Lu_2O_3 Thin Disk Laser," Conference on Lasers and Electro-Optics (Europe), Munich, Germany (2009).

[119] C.R.E. Baer, C. Kränkel, O.H. Heckl, M. Golling, T. Südmeyer, R. Peters, K. Petermann, G. Huber, and U. Keller, "227-fs pulses from a mode-locked? Yb:$LuScO_3$ thin disk laser," Opt. Express 17, 10725 (2009).

[120] K. Takaichi, H. Yagi, A. Shirakawa, K. Ueda, S. Hosokawa, T. Yanagitani, and A. A. Kaminskii, "Lu_2O_3: Yb^{3+} ceramics - a novel gain material for high-power solid-state lasers," Phys. Stat. Sol. (a) **202**, R1 (2005).

[121] V.E. Kisel, N.A. Tolstik, A.E. Troshin, N.V. Kuleshov, V. N. Matrosov, T.A. Matrosova, M.I. Kupchenko, F. Brunner, R. Paschotta, F. Morier-Genoud, and U. Keller, "Spectroscopy and femtosecond laser performance of Yb^{3+}:$Gd_0.64Y_0.36VO_4$ crystal", Appl. Phys. B, **85**, 581 (2006).

[122] M. Tokurakawa, A. Shirakawa, K. Ueda, H. Yagi, M. Noriyuki, T. Yanagitani and A. A. Kaminskii, "Diode-pumped ultrashort-pulse generation based on Yb^{3+}:Sc_2O_3 and Yb^{3+}:Y_2O_3 ceramic multi-gain-media oscillator," Opt. Express **17**, 3334 (2009).

[123] S. Matsubara, M. Fukuda, Y. Tsujioka, S. Takasaki,S. Kawato and T. Kobayashi, "Kerr-

lens mode-locking of directly LD pumped Yb:YAG laser," Proceedings of SPIE **4831**, (118) (2003).

[124] A. Fernandez, T. Fuji, A. Fürbach, A. Poppe, A. Stingl, F. Krausz and A. Apolonski, "Chirped-pulse oscillators: a route to high-power femtosecond pulses without external amplification," Opt. Lett. 29, 1366 (2004).

[125] V.L. Kalashnikov, and A. Apolonski, "Chirped-pulse oscillators: A unified standpoint," Phys. Rev. A **79**, 043829 (2009).

[126] S.H. Cho, B.E. Bouma, E.P. Ippen, and J.G. Fujimoto, "Low-repetition-rate highpeak-power Kerr-lens mode-locked $TiAl_2O_3$ laser with a multiple-pass cavity", Opt. Lett. **24**, 417 (1999).

[127] D. Herriott, H. Kogelnik and R. Kompfner, "Off-axis paths in spherical mirror interferometers," Appl. Opt. **3**, 523 (1964).

[128] A. Sennaroglu and J. Fujimoto, "Design criteria for Herriott-type multi-pass cavities for ultrashort pulse lasers," Opt. Express **11**, 1106 (2003).

[129] T. Miura, H. Nagaoka, K. Takasago, K. Kobayashi, A. Endo, K. Torizuka, M. Washio and F. Kannari,"Active synchronization of two mode-locked lasers with optical cross correlation," Appl. Phys. B **75**, 19 (2002).

[130] T.R. Schibli, J. Kim, O. Kuzucu, J.T. Gopinath, S.N. Tandon, G.S. Petrich, L A. Kolodziejski, J.G. Fujimoto, E.P. Ippen, and F.X. Kaertner, "Attosecond active synchronization of passively mode-locked lasers by balanced cross correlation," Opt. Lett. **28**, 947 (2003).

[131] L.-S. Ma, R.K. Shelton, H.C. Kapteyn, M.M. Murnane, and J. Ye, "Sub-10-femtosecond active synchronization of two passively mode-locked Ti:sapphire oscillators," Phys. Rev. A, **64**, 021802 (2001).

[132] R. Paschotta, "Noise of mode-locked lasers (Part II): timing jitter and other fluctuations," Appl. Phys. B **79**, 163 (2004).

[133] D.W. Allan, "Statistics of Atomic Frequency Standards," Proc. IEEE **54**, 221 (1966).

[134] J. Son, J.V. Rudd, and J.F. Whitaker, "Noise characterization of a self-mode-locked Ti:sapphire laser," Opt. Lett. **17**, 733 (1992).

[135] N. Ishii, C.Y. Teisset, T. Fuji, S. Köhler, K. Schmid, L. Veisz, A. Baltuska and F. Krausz, "Seeding of an eleven femtosecond optical parametric chirped pulse amplifier and its Nd3+ picosecond pump laser from a single broadband Ti:sapphire oscillator,"IEEE Journ. Select. Top. Quantum Electron. **12**, 173 (2006).

[136] A. Steinmann, A. Killi, G. Palmer, T. Binhammer, and U. Morgner, "Generation of few-cycle pulses directly from a MHz-NOPA," Opt. Express **14**, 10627 (2006).

[137] M. Marangoni, R. Osellame, R. Ramponi, G. Cerullo, A. Steinmann, and U. Morgner, "Near-infrared optical parametric amplifier at 1 MHz directly pumped by a femtosecond oscillator," Opt. Lett. **32**, 1489 (2007).

[138] M. Ghotbi, M. Beutler, V. Petrov, A. Gaydardzhiev, and F. Noack, "High-energy, sub-30 fs near-IR pulses from a broadband optical parametric amplifier based on collinear interaction in BiB_3O_6," Opt. Lett. **34**, 689 (2009).

[139] H. Yoshida, H. Fujita, M. Nakatsuka, M. Yoshimura, T. Sasaki, T. Kamimura and K. Yoshida, "Dependences of Laser-Induced Bulk Damage Threshold and Crack Patterns in Several Nonlinear Crystals on Irradiation Direction," Jpn. J. Appl. Phys, **45**, 766 (2006).

[140] K. Ogawa, K. Sueda, Y. Akahane, M. Aoyama, K. Tsuji, K. Fujioka, T. Kanabe, K. Yamakawa, and N. Miyanaga, "Controlling the phase matching conditions of optical parametric chirped-pulse amplification using partially deuterated KDP," Opt. Express **17**, 7744 (2009).

[141] V. Petrov, F. Noack, P. Tzankov, M. Ghotbi, M. Ebrahim-Zadeh, I. Nikolov, and I. Buchvarov, "High-Power Femtosecond Optical Parametric Amplifier in the Near-IR Based on BiB3O6," Conference on Lasers and Electro-Optics, Baltimore, USA (2007).

[142] A. V. Smith, "How to select nonlinear crystals and model their performance using SNLO software," Proc. SPIE **4972**, 50 (2003).

[143] Zhang, Y. Kong and J.-Y. Zhang, "Optical parametric properties of 532-nm-pumped beta-bariumborate near the infrared absorption edge," Opt. Commun. **184**, 485 (2000).

[144] T. Fuji, N. Ishii, C.Y. Teisset, X. Gu, T. Metzger, A. Baltuska, N. Forget, D. Kaplan, A. Galvanauskas, and F. Krausz, "Parametric amplification of few-cycle carrier-envelope phase-stable pulses at 2.1 μm," Opt. Lett. **31**, 1103 (2006).

[145] V. Pervak, I. Ahmad, M. K. Trubetskov, A.V. Tikhonravov, and F. Krausz, "Double-angle multilayer mirrors with smooth dispersion characteristics,"Opt. Express **17**, 7943 (2009).

[146] R. Trebino, "Frequency-resolved optical gating: the measurement of ultrashort laser pulses," Kluwer Academic Publishers (2002).

[147] J. Rothhardt, S. Hädrich, J. Limpert, and A. Tünnermann, "80 kHz repetition rate high power fiber amplifier flat-top pulse pumped OPCPA based on BIB_3O_6," Opt. Express **17**, 2508 (2009).

[148] J. Rothhardt, S. Hädrich, F. Röser, J. Limpert, and A. Tünnermann, "500 MW peak power degenerated optical parametric amplifier delivering 52 fs pulses at 97 kHz repetition rate," Opt. Express **16**, 8981 (2008).

[149] C. Erny, C. Heese, M. Haag, L. Gallmann, and U. Keller, "High-repetition-rate optical parametric chirped-pulse amplifier producing 1-μJ, sub-100-fs pulses in the mid-infrared," Opt. Express **17**, 1340 (2009).

[150] O. Chalus, P.K. Bates, M. Smolarski, and J. Biegert, "Micro-Joule energy, mid-IR pulses with 9-cycle duration from a 100 kHz OPCPA source," Conference on ultrafast optics, Arcachon, France (2009).

[151] C. Homann, C. Schriever, P. Baum, and E. Riedle, "Octave wide tunable UV-pumped NOPA: pulses down to 20 fs at 0.5 MHz repetition rate," Opt. Express **16**, 5746 (2008).

[152] D. Wytrykus, M. Centurion,P. Reckenthaeler, F. Krausz, A. Apolonski and E. Fill, "Ultrashort pulse electron gun with a MHz repetition rate," Appl. Phys. B **96**, 309 (2009).

[153] M. Brehm, A. Schliesser, and F. Keilmann, "Spectroscopic near-field microscopy using frequency combs in the mid-infrared," Opt. Express **14**, 11222 (2006).

[154] E. Goulielmakis, V.S. Yakovlev, A. L. Cavalieri, M. Uiberacker, V. Pervak, A. Apolonski,R. Kienberger, U. Kleineberg, and F. Krausz, "Attosecond control and measurement: lightwave electronics," Science **317**, 769 (2007).

[155] O.H. Heckl, C.R.E. Baer, C. Kränkel, S.V. Marchese, F. Schapper, M. Holler, T. Südmeyer, J.S. Robinson, J.W.G. Tisch, F. Couny, P. Light, F. Benabid, P. St. J. Russell and U. Keller, "High Harmonic Generation (HHG) in a Kagome-type Hollow-Core Photonic Crystal Fiber (HC-PCF)," Conference on Lasers and Electro-Optics (Europe), Munich, Germany (2009).

[156] P. Colosimo, G. Doumy, C. I. Blaga, J. Wheeler, C. Hauri, F. Catoire, J. Tate, R. Chirla, A.M. March, G.G. Paulus, H.G. Muller, P. Agostini, and L.F. Dimauro, "Scaling strong-field interactions towards the classical limit," Nature Phys. **4**, 386 (2008).

[157] D.A. Akimov, T. Siebert, A.M. Zheltikov, and W. Kiefer, "A double-pass optical parametric amplifier seeded by a blue-shifted output of a photonic-crystal fiber," Appl. Phys. B **83**, 185 (2006).

[158] Y. Tzeng, Y. Lin, C. Huang, J. Liu, H. Chui, H. Liu, J.M. Stone, J.C. Knight, and S. Chu, "Broadband tunable optical parametric amplification from a single 50 MHz ultrafast fiber laser," Opt. Express **17**, 7304 (2009).

[159] S. Kim, J. Jin, Y.-J. Kim, I.-Y. Park, Y. Kim, and S.-W. Kim, "High-harmonic generation by resonant plasmon field enhancement," Nature **453**, 757 (2008).

[160] P.E. Ciddor, "Refractive index of air: new equations for the visible and near infrared," Appl. Optics **35**, 1566 (1996).

[161] I.H. Maliston, "Interspecimen Comparison of the Refractive Index of Fused Silica," J. Opt. Soc. Am. **55**, 1205 (1965).

[162] SCHOTT Optical Glass Data Sheets, 2008-02-26, www.schott.com.

Acknowledgements

I would first and foremost like to thank Prof. Ferenc Krausz for giving me the opportunity to work in his group. This work would not have been possible without his support and encouragement. I am deeply grateful to Prof. Heinz Lehr and Dr. Alexander Binder for accepting to be the reviewers of this thesis and for their assistance in the final process of this work. Many thanks to Dr. Alexander Apolonskiy for his supervision but also his direct support in the lab every time I needed it.

I am also thankful to Xun Gu for his advice and trouble-shooting services on the parametric amplifier. Thanks to my best office mate and team mate Roswitha Graf for sharing coffee, bruises and my chaotic office. I am particularly indebted to Thomas Metzger for his invariable support and letting me know that everything will be all right.

For the pleasant working atmosphere at the LMU, I especially thank Ioachim Pupeza for its musical lab, Oleg Pronin for his immediate help when needed and Hanieh Fattahi for the difficult task of overtaking my laser system. Further I gratefully acknowledge the help of Zsuzsanna Major, Yunpei Deng, László Veisz, Daniel Hermann, Takao Fuji, Sergei Naumov, László Turi, Atsushi Sugita, Volodymyr Pervak, Nobuhisa Ishii, Andrius Baltuska, Matt Mac Eckett, Siegfried Herbst, the MPQ-LMU administrative staff, technicians and workshop and many many others.

The author acknowledges the funding of this work by the German "Bundesministerium für Bildung, Wissenschaft, Forschung und Technologie" (BMBF) in the frame of the FEMTONIK research program FULMINA, project no. (FKZ): 13N8724.

Finally, thanks to my parents for supporting me from the other side of the world ...

[0] Onions?